12-2022

Improving Building CFD Peak Pressure Computation Using LES with a Focus on Inflow Turbulence Methods and Grid Spacing Size.

Zahra Mansouri
University of Arkansas, Fayetteville

Improving Building CFD Peak Pressure Computation Using LES with a Focus on Inflow Turbulence Methods and Grid Spacing Size.

A dissertation submitted in partial fulfillment
of the requirements for the degree of
Doctor of Philosophy in Engineering

by

Zahra Mansouri
Shahrekord University
Bachelor of Science in Civil Engineering, 2013
K. N. Toosi University of Technology
Master of Science in Civil Engineering, 2016

December 2022
University of Arkansas

This dissertation is approved for recommendation to the Graduate Council.

_____
R. Panneer Selvam, Ph.D.
Dissertation Director

_____
Mark E. Arnold, Ph.D.
Committee Member

_____
Ernie Heymsfield, Ph.D.
Committee Member

_____
Cameron Murray, Ph.D.
Committee Member

Abstract

Structural failures by extreme winds often leads to economic losses and even deaths. Proper design of buildings requires accurate estimation of wind loads to prevent structural damage. Using routine guidelines generally leads to the underestimation of buildings' peak pressures, in which most failures occur. To estimate wind loads more accurately three different methods (i.e., field measurement, wind tunnel (WT), and computational fluid dynamics (CFD)) are in use. A well-validated CFD provides more flow field details at lower costs compared to field measurements and WT. As strong winds are extremely turbulent, the effects of turbulence in wind should be incorporated into CFD using various turbulence modeling methods. Among these turbulence modeling methods, Large Eddy Simulation (LES) is more reliable and applicable in the industry compared to other methods. However, in LES simulations, a proper turbulent flow field at the inlet as an inflow boundary condition is required to apply and predict peak pressure correctly. Otherwise, CFD underestimates peak pressure coefficients.

The turbulent flow behavior in the computational domain is extremely dependent on the type of inflow generators. Inflow turbulence generation methods are categorized to (a) precursor database, (b) recycling method, and (c) synthetic turbulence methods. Synthetic inflow turbulence is a more applicable approach, as it does not require expensive prior flow simulations. In this study, different types of synthetic turbulence generator methods are considered to investigate their performance in wind engineering applications by plotting pressures and wind spectrums. The velocity spectrum at the inlet and building location is compared to the Von Karman spectrum for different inflow methods to determine how well the inflow field is representative of the real wind flow and how well the energy is carried from the inlet to the building location. Furthermore, spurious pressures

are introduced and different methods are evaluated to see whether they produce spurious pressures in the domain. It is concluded that spurious pressure exists in all the considered methods except Synthetic Eddy Method (SEM) method with the Gaussian shape function (SEM-G). In addition, SEM-G is found to be a suitable method for peak pressure prediction on buildings with the upmost 30% error. Furthermore, for the considered Random Fourier Generation (RFG) Method (i.e., Consistent Discrete Random Flow Generator (CDRFG)) an approach is suggested to control spurious pressure and improve computed peak pressures on buildings.

Keywords: Computational fluid dynamics, Synthetic inflow turbulence, Peak pressure, Large eddy simulation, Synthetic Eddy Method (SEM), Random Fourier Generation (RFG).

Preface

This thesis improves peak pressure computation using the large eddy simulation (LES) method with a focus on inflow turbulence generation methods and grid spacing size. The thesis is based on the following papers and reports:

Paper 1. Mansouri, Z., Selvam, R. P., and Chowdhury, A. G. (2021), High Frequency Effect on Peak Pressure Computation on the TTU Building Using Synthetic Inflow Turbulence Generator. Presented and published summary paper, *6th American Association for Wind Engineering (AAWE) Workshop*, Clemson University, Clemson, May 2021. https://tigerprints.clemson.edu/cgi/viewcontent.cgi?article=1048&context=aawe

Paper 2. Verma, S., **Mansouri, Z.**, and Selvam, R. P. (2021), Incorporating Two Weeks Open-Source Software Lab Module in CFD and Fluids Courses, *In 2021 ASEE Midwest Section Conference*, https://peer.asee.org/38325.pdf

Paper 3. Mansouri, Z., Verma, S., and Selvam, R. P. (2021), Teaching Modeling Turbulent Flow Around Building Using LES Turbulence Method and Open-source Software OpenFOAM, *In 2021 ASEE Midwest Section Conference*, https://peer.asee.org/teaching-modeling-turbulent-flow-around-building-using-les-turbulence-method-and-open-source-software-openfoam.pdf

Paper 4. Mansouri, Z., Selvam, R. P., and Chowdhury, A. G. (2022). Maximum grid spacing effect on peak pressure computation using inflow turbulence generators. *Results in Engineering*, 100491. https://www.sciencedirect.com/science/article/pii/S259012302200161X

Paper 5. Mansouri, Z., Selvam, R. P., and Chowdhury, A. G. (2022). Performance of Different Inflow Turbulence Methods for Wind Engineering Applications. Submitted for Publication in *Journal of Wind Engineering and Industrial Aerodynamics*.

Report 1. Mansouri, Z., and Selvam, R. P. (2021). Incorporating Three Weeks Open-Source Software Lab Module in CFD and Fluids Courses, report, https://github.com/rpsuark/ASEE21-OpenFOAM-LES/blob/main/ASEE-LES.pdf

Papers 2 and 3, and report 1 were prepared to educate students and practicing engineers to be able to set up CFD models for evaluating wind loads on buildings. These papers' relevant case files are provided on the Github webpage, https://github.com/rps, for readers to download and learn along the way by reading the paper. These papers explain the preparation steps of the numerical model in paper 5.

This thesis's chapter-wise development is presented in the following. The subject (i.e., improves peak pressure computation using large eddy simulation (LES) method with a focus on inflow turbulence generation methods and grid spacing) is introduced first in Chapter - 1, followed by a literature review in Chapter - 2. In Chapter - 3, the numerical case file preparation for OpenFOAM is provided and paper-4 is used for the contents of this chapter. In Chapter - 4, the effect of grid spacing size on peak pressure results is provided and paper-4 is used for the contents of this chapter. In Chapter - 5, the performance of different inflow methods is evaluated for wind engineering application and paper-5 is used for the contents of this chapter. Finally, in Chapter - 6, this study conclusions are summarized, the present study contribution is pointed out, and the future research directions are outlined.

Division of work between authors

For Paper 3, the numerical implementation of the flow around the TTU building and OpenFOAM case file preparation was done by Zahra Mansouri (ZM). The first draft writing was done by ZM. Editing and writing were done by ZM, Sumit Verma, and R. Panneer Selvam (RPS).

For Paper 4, the MATLAB code developed originally by Aboshosha et al. (2015) is used to generate the inflow turbulence field. This MATLAB code was modified by ZM to be implemented in the CFD code developed by RPS. The numerical implementation of the flow around the TTU building was done in collaboration between RPS and ZM. The first draft writing was done by ZM. Editing and writing were done by ZM and RPS.

For Paper 5, using the Turbulence Inflow (TInF) Tool to generate inflow methods and developing the CFD model of flow with and without building using OpenFOAM was done by ZM. The first draft writing was done by ZM. Editing and writing were done by ZM and RPS.

The wind tunnel data used in papers 4 and 5 for comparing the CFD results were provided by M. Moravej and A. G. Chowdhury (AGC) from FIU.

Acknowledgment

Firstly, I would like to express my sincerest gratitude to my advisor, Prof. R. Panneer Selvam, for his mentorship over the last three years. He has always been available and helpful. His guidance was the key driving force that kept me going with research. I would also like to thank my dissertation committee members, Prof. Mark E. Arnold, Prof. Ernie Heymsfield, and Prof. Cameron Murray for serving on my dissertation committee and providing me with valuable comments to improve the quality of this work.

I would also like to take the opportunity to acknowledge the financial support from the James T. Womble Professorship from the University of Arkansas. Lastly, I would like to acknowledge the member of my research group, Dr. Sumit Verma, for all his help. Finally, I would also like to thank my family for their supports during this journey.

Table of Contents

List of published papers

List of published papers that are used in this thesis:

1. Mansouri, Z., Verma, S., and Selvam, R. P. (2021), Teaching Modeling Turbulent Flow Around Building Using LES Turbulence Method and Open-source Software OpenFOAM, *In 2021 ASEE Midwest Section Conference*, https://peer.asee.org/teaching-modeling-turbulent-flow-around-building-using-les-turbulence-method-and-open-source-software-openfoam.pdf

2. Mansouri, Z., Selvam, R. P., and Chowdhury, A. G. (2022). Maximum grid spacing effect on peak pressure computation using inflow turbulence generators. *Results in Engineering*, 100491. https://www.sciencedirect.com/science/article/pii/S259012302200161X

3. Mansouri, Z., Selvam, R. P., and Chowdhury, A. G. (2022). Performance of Different Inflow Turbulence Methods for Wind Engineering Applications. Submitted for Publication in *Journal of Wind Engineering and Industrial Aerodynamics*.

In Chapter – 3 of the current work, the numerical case file preparation for OpenFOAM is provided and paper-4 is used for the contents of this chapter. In Chapter - 4, the effect of grid spacing size on peak pressure results is provided and paper-4 is used for the contents of this chapter. In Chapter - 5, the performance of different inflow methods is evaluated for wind engineering application and paper-5 is used for the contents of this chapter.

Figure Captions

Nomenclature

The following symbols are used in this dissertation*:*

C_p = Mean pressure coefficient

C_{pmin} = Minimum pressure coefficient

C_{pmax} = Maximum pressure coefficient

dt = Non-dimensional time step

dT = Dimensional time step

f = Non-dimensional frequency= $nH/U_H = H/L$

f_{LES} = Maximum frequency cutoff for LES

f_{grid} = Maximum frequency transported by the grid spacing *h* using FDM

f_{max} = Maximum frequency provided for MATLAB code for inflow computation

f_{min} = Minimum frequency provided for MATLAB code for inflow computation

f_{maxe} = Maximum frequency from the field or WT velocity spectrum

f_{mine} = Minimum frequency from the field or WT velocity spectrum

H = Building height

h = Maximum grid spacing

I_u = Turbulence intensity in x direction

I_v = Turbulence intensity in y direction

I_w = Turbulence intensity in z direction

L = Wavelength for a given frequency n

L_u = Turbulence length scale in x direction

L_v = Turbulence length scale in y direction

L_w = Turbulence length scale in z direction

M = Number of random frequencies in one segment for CDRFG

N = The number of frequency segments for CDRFG

n = Dimensional frequency

n_{max} = Maximum dimensional frequency

n_{min} = Minimum dimensional frequency

Re = Reynolds number = $U_H H/\nu$

T_{ref} = Reference time

U_{ave} = Average velocity

U_H = Average velocity at building height

λ = Non-dimensional wavelength = $L/H = U_H/nH$

Chapter 1- Introduction

1.1. Introduction

When wind interacts with structures, as shown in Fig. 1.1(a), positive and negative (i.e., suction) pressure occurs on buildings concurrently. Buildings should be strong enough to resist these winds. Otherwise, buildings cannot withstand wind loads and can be damaged as indicated in Fig. 1.1(b). During 2017–2018, disaster damages caused by winds led to encounter more than 345 billion USD economic loss in Maria, Florence, and Michael (Aon, 2019 and Klotzbach et. al., 2020). National Weather Service (NWS) reported 38 fatalities, 202 injuries, and damage resulting in costs of 187.67 million dollars caused by severe thunderstorm wind in 2019. Based on this report, the number of fatalities and damages increased by 14 people and 31.81 million dollars in 2019 compared to 2018. Because wind flows have higher intensity compared to those in the past and are expected to be higher in the future (Woods, 2019), a better understanding of wind load and peak pressures on buildings is required for the adequate design of structures.

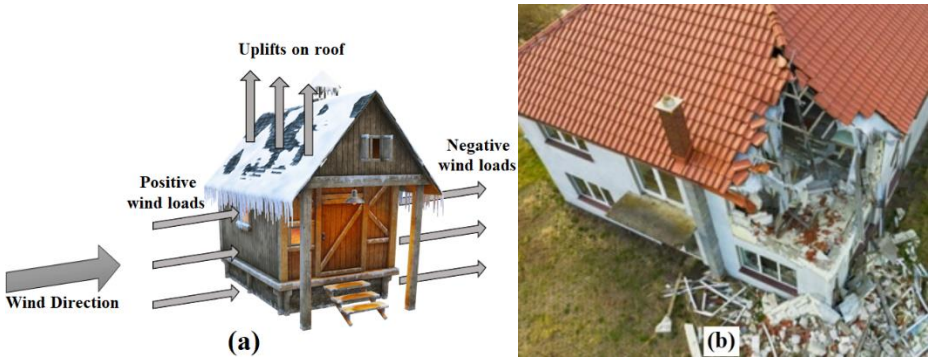

Fig.1.1 (a) Schematic of wind pressures on a building (b) A building's roof damaged by the strong wind (FStockLuk).

1.1.1. Turbulent Flow

High-speed winds are the predominant cause of the most of these catastrophic failures, and as flow speed increases, the flow becomes more chaotic and unstable. This class, known as turbulent flow, includes most natural flows. The plot shown in Fig. 1.2(a) is for a turbulent flow in which the velocity is recorded in time at a particular point in space. In Fig. 1.2(a), the instantaneous velocity is given by $u = U + u'$, where U is the time-averaged velocity and u' is the velocity fluctuation over time. As the variation in time does not follow any specific pattern, hence, such these random and chaotic flows are called turbulent flows. Eddies, which are circular fluid movements associated with turbulent flow, are depicted in Fig. 1.2.(b). There is a wide range of eddy diameters fluctuating at various frequencies in a typical turbulent flow (i.e., large eddies have large velocity fluctuations of low frequency and vice versa).

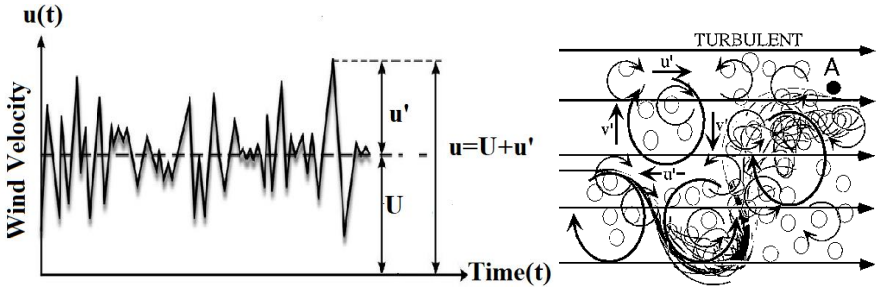

Fig. 1.2. (a) Wind velocity in time at one point, (b) Turbulent flow structures

1.1.2. Different Methods for Estimating Peak Pressure on Buildings

In the literature, three different methods—(a) field measurements, (b) wind tunnel measurements, and (c) Computational Fluid Dynamics (CFD)—have been employed to estimate wind loads on structures due to strong winds. For instance, the maximum peak pressure coefficient (*Cp*) determined by ASCE 7-16 for components and cladding is -3.2 for a low-rise building. However, field measurements have reported that the maximum peak *Cp* on a low-rise building can be even

lower than -8 (Richards et al., 2007). According to Fig. 1.3, Mooneghi et al. (2016) reported the Wind Tunnel (WT) and field maximum peak *Cp* of -7 and -18 respectively at the corner of the Texas Tech University (TTU) building. The disparity between the WT and field measurements is rooted in that large scales WT cannot produce the wind spectrum's low-frequency part as shown in Fig. 1.3(b) and it can influence the pressure distributions and peak *Cp* estimation (Moravej, 2018).

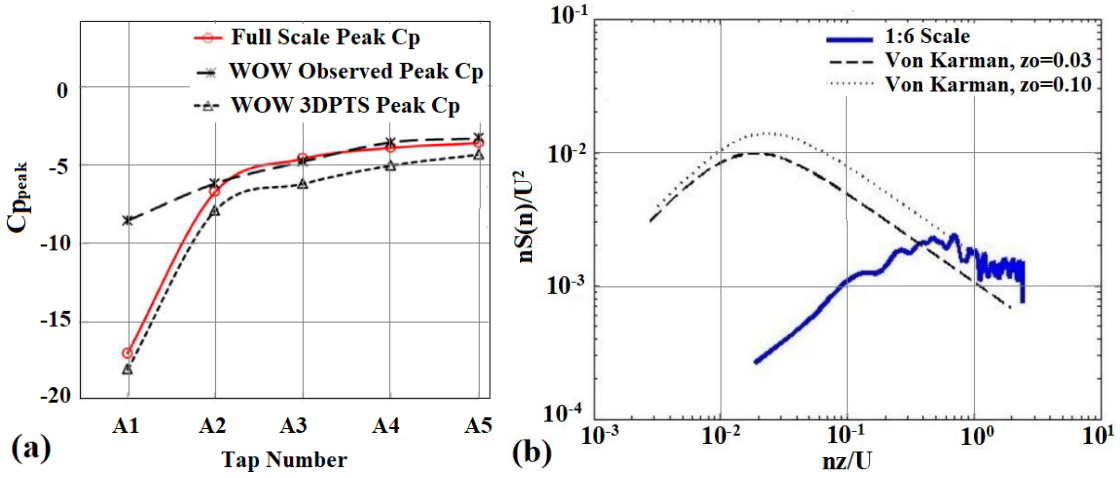

Fig. 1.3. (a) TTU Roof peak *Cp* values (Mooneghi et al., 2016). (b) Comparison of Turbulence Spectra between WT and full-scale for the low-rise building of 4m height (Moravej, 2018).

Strong winds are highly turbulent, and the computed wind loads would not be accurate for structure design purposes if wind turbulence is not appropriately taken into consideration. Various turbulence modeling techniques can be used in CFD to incorporate the effects of wind turbulence. In comparison to other turbulence modeling techniques, LES is more effective and practical in the industry. To accurately predict peak pressure in LES simulations, an appropriate turbulent flow field at the inlet is needed to apply as an inflow boundary condition. According to Fig. 1.4, CFD without inflow turbulence field underestimated pressure coefficients compared to WT 1:6 because

the CFD without inflow cannot simulate low-frequency turbulences. Hence, the turbulent flow behavior in the domain interior is extremely dependent on this inflow physical quality.

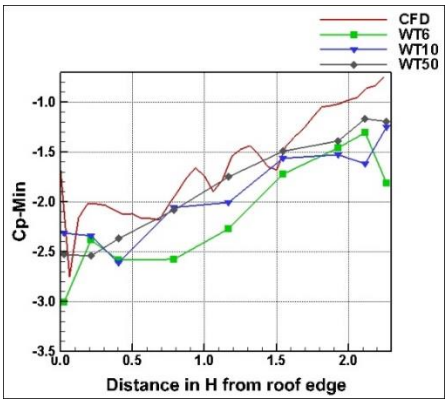

Fig. 1.4. Minimum Pressure coefficient diagram without inflow turbulence boundary condition

1.1.3. Inflow Methods

Thus, choosing the appropriate inflow turbulence boundary conditions (BCs) is a critical element of the numerical LES investigation. According to Selvam (1997), insufficient grid resolution and inflow BC are to blame for at least a 30% inaccuracy in CFD peak Cp compared to field measurements. Modern advances in computer resources have enabled the use of higher grid resolution and the development of computational models with a promise of becoming adaptable, accessible, and reliable means of wind load estimations (Ding, 2019). Inflow boundary condition issues, however, are still unresolved.

The main divisions of the inflow turbulence generation techniques are (a) precursor databases, (b) recycling techniques, and (c) synthetic turbulence (Keating et al., 2004). The first and second approaches' drawbacks are that they require databases, which increases their computational cost. As synthetic inflow turbulence does not require pricey prior flow simulations, it is a more applicable approach (Aboshosha et al., 2015; Ding et al., 2019). Synthetic turbulence methods

include a wide range of methods that can be classified into a) Random Flow Generation Methods (RFG), b) Digital filter methods (DFM), and c) Synthetic Eddy Method (SEM). In chapter 2 a summary of each method is provided.

1.1.4. LES Maximum Grid Spacing and Its Corresponding Maximum Possible Frequency

The Fourier spectral approach can transport waves in the form of sine or cosine functions with a minimum wavelength L of $2h$ for a given grid spacing of h. (Orszag, 1979). In spectrum analysis, the corresponding frequency is known as the Nyquist frequency. Even though transport of Nyquist frequency is possible with the spectral method, the amount of error using the finite difference method (FDM) is very high. Consequently, to have fewer errors for finite difference or control volume method, Ferziger and Peric (2002) and Kravchenko and Moni (1997) suggested $L=4h$, which its corresponding frequency is f_{grid}. Selvam (2017) recommended using $L=10h$ even to have more than 90% accuracy, but this level of the refined grid is impractical. To make it clear, appendix 3.B provides a detailed example of transporting a sine wave with wavelengths of $2h$ and $4h$. This example illustrates a sine wave with a $2h$ wavelength being transported with an inaccuracy of nearly 100%, which is unacceptable. For the wavelength of $4h$, it is around 25%. Consequently, $L=4h$ can transport a wave with a reasonable error. This wavelength's corresponding dimensional and non-dimensional frequency is n_{grid} and f_{grid}. As the relation between frequency and wavelength is $L = U_H/n$, f_{grid} *in* terms of L is calculated by Eq. 1.

$$f = \frac{1}{\lambda} = \frac{H}{L} = \frac{nH}{U_H} \tag{1.1}$$

Where λ is the non-dimensional wavelength, H is the building height, and U_H is the mean velocity at the building height. As a result, the highest non-dimensional frequency can be carried by the grid in the flow using the FDM and LES is approximated using Eqn. 1.1 as $f_{grid}=H/4h$. As an

example, f_{grid} is calculated as $f_{grid} = H/(4H/16) = 4$ for L=4h and h=H/16 grid. This study aims to demonstrate the impact of frequency selections beyond f_{grid} on peak pressure results.

1.1.5. Velocity Spectrum at the Inlet and Building Location

Turbulent flow contains eddies, which are circular movements of fluid. Typical turbulent flow is three-dimensional (3D), unsteady, and has a wide range of eddy sizes fluctuating at different frequencies (i.e., large eddies fluctuate at low frequencies and vice versa) that need to be resolved. Hence, it is required to construct the inflow velocity fields appropriate for various scale features. The range of eddies produced by the inflow method is depicted in the wind velocity spectrum, which also displays the frequency distribution of turbulent wind flow. Since the Von Karman spectrum describes the frequency distribution of the actual turbulent wind flow, the velocity spectrum generated by the inflow method should first be comparable to it. Additionally, the energy should not be lost in the building location compared to the inlet location to get more precise numerical results. According to Rana et al. (2011), if the grid maximum frequency is violated, DFM turbulent inflow data immediately dissipates in the computational domain. Therefore, the amount of similarity between the inlet and building location velocity spectrums could be affected by the maximum frequency selection, and that is what this study is focused on.

1.1.6. Definition of Spurious Pressure

Many of the inflow turbulence generator methods produce spurious pressure, according to Rigall et al. (2021), Haywood (2019), and Lebovitz (2017). Rigall et al. (2021) used the adapted RFG method and Lebovitz (2017) used DFM. In all of these publications, the mentioned spurious pressure occurs when the frequency of the pressure is greater than the frequency of the velocity. In this study, spurious pressures are defined as pressures with frequencies higher than the Nyquist frequency since velocity frequency cannot be higher than this frequency. As an instance, the inflow

turbulence field is calculated for the f_{max}=10 and the grid spacing of $h=H/16$ using the Consistent Discrete Random Flow Generator (CDRFG). The Nyquist frequency is $H/2h=H/2(H/16)$ =8 for the grid spacing of $h=H/16$. In Fig. 1.5, the pressure is plotted at the inlet and building location for this case. According to Fig. 1.5, the pressure frequency is about 9 to 10 for this case if frequencies are taken as the number of peaks or cycles per unit time. As pressure frequency (i.e., 9-10) is greater than Nyquist frequency (i.e., 8), this case has spurious pressures.

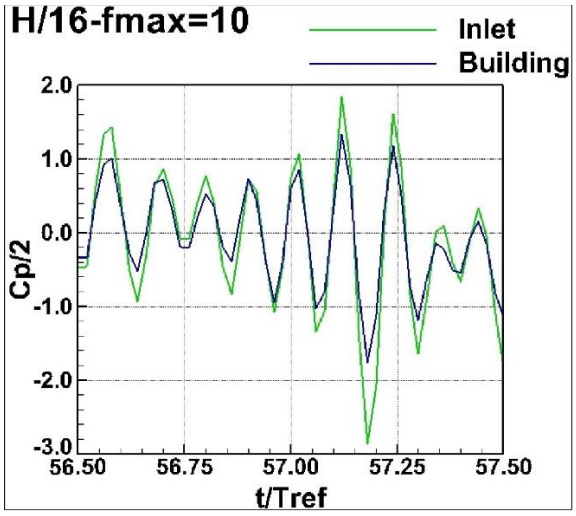

Fig. 1.5. Non-dimensional velocity at the inlet and the building location and pressures coefficient at the building location without building *for* $h=H/16$, f_{max}=10, and for 1 time unit.

1.1.7. Thesis Objectives

In this study, different types of synthetic turbulence generator methods are considered to investigate their performance in wind engineering applications. The considered methods are a) Consistent Discrete Random Flow Generator method (CDRFG) under RFG, b) Digital filter methods (DFM), c) Synthetic Eddy Method (SEM) with three different shape functions, d) Divergence Free Synthetic Eddy Method (DFSEM), and e) two types of Anisotropy Turbulent Spot Method (ATSM). For the RFG method, this study investigates the effects of maximum

frequency selection regardless of the grid spacing size on spurious pressure productions in the domain. Afterward, the effects of these spurious pressures on the peak pressure results are studied.

Objective-1: Suggesting a proper approach to use the RFG method (i.e., the Consistent Discrete Random Flow Generator (CDRFG)) based on maximum frequency selection regarding the computational grid used in the flow direction to reduce spurious pressures and its effects on peak pressure results.

O-1.1. Investigating the maximum frequency selection effects on spurious pressures in a domain.

O-1.2. To understand the effect of these spurious pressures on peak pressure results, the peak pressures on the 1:6 scale TTU building are calculated using CFD and CDRFG inflow method and compared with WT measurement results reported by Moravej (2018).

Objective-2: Suggesting the most proper method for wind engineering application.

O-2.1. Comparing the Von Karman spectrum with the velocity spectrum at the inlet and building location for two different grid spacing sizes. This determines how well the energy is carried from the inlet location to the building location.

O-2.2. Plotting the pressure over time at the inlet and building location to see how much spurious pressure is produced by various inflow methods.

O-2.3. Finally, the flow with the building is modeled for inflow methods concluded are appropriate for wind engineering, and the resulted peak pressure is compared to WT measurements reported by Moravej (2018) to evaluate the inflow methods performance in predicting peak pressures.

References

Aboshosha, H., Elshaer, A., Bitsuamlak, G. T., and El Damatty, A. (2015). Consistent inflow turbulence generator for LES evaluation of wind-induced responses for tall buildings. *Journal of Wind Engineering and Industrial Aerodynamics*, 142, 198-216

American Society of Civil Engineers. (2017). Minimum design loads and associated criteria for buildings and other structures. *American Society of Civil Engineers*.

Aon. (2019). Weather, climate, and catastrophe insight. 2018 Annual Aon Report, Chicago, Illinois, 86. https://www.weather.gov/media/hazstat/sum19.pdf

Ding, F., Kareem, A., and Wan, J. (2019). Aerodynamic tailoring of structures using computational fluid dynamics. *Structural Engineering International*, 29, 26-39.

Ferziger, J. H., and Perić, M. (2002). Computational methods for fluid dynamics. Berlin: Springer, 3, 196-200.

FStockLuk, https://www.shutterstock.com/image-photo/aerial-view-on-damaged-red-single-1378621508

Haywood, J. S. (2019). Turbulent inflow generation methods for Large Eddy Simulations, Mississippi State University.

Lebovitz, L. (2017). Modeling and time-resolved numerical simulations of urban turbulent wind flows around buildings, Master's thesis, ETH Zurich.

Keating, A., Piomelli, U., Balaras, E., and Kaltenbach, H. J. (2004). A priori and a posteriori tests of inflow conditions for large-eddy simulation. *Physics of fluids*, 16, 4696-4712.

Kravchenko, A. G., and Moin, P. (1997). On the effect of numerical errors in large eddy simulations of turbulent flows, *Journal of Computational Physics*, 131, 310-322.

Mooneghi, M. A., Irwin, P., and Chowdhury, A. G. (2016). Partial turbulence simulation method for predicting peak wind loads on small structures and building appurtenances. *Journal of Wind Engineering and Industrial Aerodynamics*, 157, 47–62.

Moravej, M. (2018). Investigating scale effects on analytical methods of predicting peak wind loads on buildings. Ph.D. thesis, Florida International University, Miami, Florida.

Orszag, S. A. (1979). Spectral methods for problems in complex geometrics. Numerical methods for partial differential equations, 273-305. Academic Press.

Rana, Z. A., Thornber, B., and Drikakis, D. (2011). On the importance of generating accurate turbulent boundary condition for unsteady simulations, *Journal of Turbulence*, 12, N35.

Richards, P. J., Hoxey, R. P., Connell, B. D., and Lander, D. P. (2007). Wind-tunnel modelling of the Silsoe Cube. *Journal of Wind Engineering and Industrial Aerodynamics*, 95, 1384–1399.

Rigall, T., Cotté, B., and Lafon, P. (2021). Low-noise synthetic turbulence tailored to lateral periodic boundary conditions, *Fluids*, 6, 193.

Selvam, R. P. (1997). Computation of pressures on Texas Tech University building using large eddy simulation. *Journal of Wind Engineering and Industrial Aerodynamics*, 67, 647–657.

Woods, J. (2019). Turbulent Effects on Building Pressure using a Two-Dimensional Finite Element Program. Master's thesis, Department of Civil Engineering, University of Arkansas.

Chapter 2- Literature Review

2. Literature Review

2.1.Wind Load Estimation Difficulties and Benefits

Three main methods have been used to estimate wind loads on structures due to severe winds: (a) field measurements; (b) wind tunnel measurements; and (c) numerical modeling using computational fluid dynamics (CFD). Each method offers the following benefits and drawbacks for design purposes:

2.1.1. Field Measurements Difficulties

The most precise method for determining wind peak pressures would be through field measurements, which also capture the true complexity of wind flow. However, because to the inherent variability of the wind characteristics, such as the wind speed, direction, and so on it cannot be completely controlled (Blocken, 2015). Furthermore, data collection in strong winds could be dangerous and even fatal. In field measurements, the accuracy of velocity or pressure data is constrained by the accuracy of the measuring equipment, and data can only be collected at a restricted number of places. For instance, in the Texas Tech University (TTU) building field measurements, Levitan et al. (1991) collected pressures at 11 places, wind speeds at four heights, and wind direction at one height. Field measurements are expensive and time-consuming to undertake due to the factors listed, hence, it cannot be used for designing purposes.

2.1.2. Wind Tunnel Measurements Method's Difficulties

Another method to estimate wind loads due to severe winds in a controlled environment within the lab is utilizing WT. This method avoids the uncertainty of field measurements and the life-

threatening risks involved. For instance, in numerous model and full-scale experiments, Cochran and Cermak (1992) validated pressure measurements on the TTU experimental building. However, in most cases just point measurements are carried out, as in field and wind tunnel measurements. Although methods like Laser-Induced Fluorescence (LIF) and Particle Image Velocimetry (PIV) can provide 2D plans or even complete 3D data, their costs are significantly higher, and applying them to complex geometries is challenging since model obstacles can block laser light (Blocken, 2015). Another drawback of WT testing is that, when it conducted at smaller scales, match criteria must be fulfilled. To eliminate scale effects, model scales for low-rise structures can be in the range of 1:5 to 1:30, whereas it is 1:200 to 1:500 for high-rise buildings. The derived velocity power spectrum and the Von Karman spectrum are compared for various scales in Fig. 2.1. Von Karman, which is spectral densities of velocities, describes the statistics of turbulent wind flow and its frequency distribution. Fig. 2.1 shows that large scales WT model difficulty can simulate the entire wind turbulence spectrum. Because the largest possible size for turbulent eddies (i.e., the minimum turbulence frequency) that may be simulated is constrained by the WT working section size. As a result, the low-frequency portion of the wind spectrum is not appropriately simulated, which can have an impact on the pressure distributions and subsequently peak pressure prediction (Moravej, 2018).

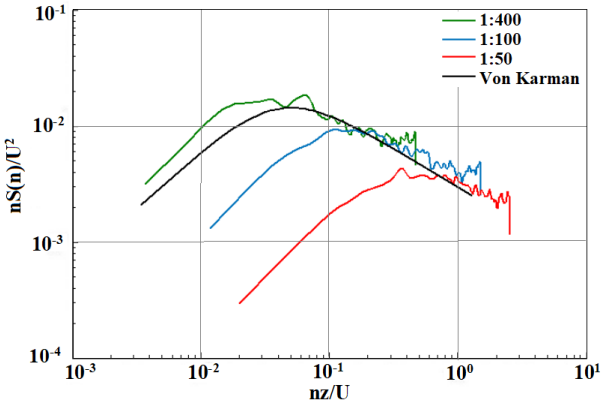

Fig. 2.1. Comparison of Turbulence Spectra between different model scales and full-scale for the tall building of 61 m height (Moravej, 2018)

2.1.3. Computational Fluid Dynamics (CFD) Method's Benefits

Selvam (1997) conducted a numerical model using Large Eddy Simulation (LES) to compute the peak pressure on the TTU building, whereas prior CFD studies typically reported mean and Root Mean Square (RMS) pressures. Selvam (1997) stated that low grid resolution and inflow boundary conditions may be the cause of the discrepancy between CFD peak pressures and field measurements. Nowadays, cutting-edge advancements in computer resources and concurrent developments in CFD have led to the creation of computational simulations that promise to become flexible, accessible, and trustworthy methods of evaluating the effects of wind load (Ding, 2019). In contrast to WT, which is restricted to just sensor locations in wind tunnels, CFD may offer complete information on the wind flow variables at any place in the domain. A skilled CFD engineer can run the simulation, conduct analysis, and create reports, whereas field measurement and WT cannot be completed by one person, hence CFD requires fewer human resources. As a result, structural engineering is becoming increasingly interested in CFD, which can be a powerful and affordable option to determine precise wind pressures on buildings in well-controlled conditions and without similarity restrictions. Nevertheless, the accuracy of CFD is a crucial topic of attention. This accuracy is closely related to the choice of turbulence modeling techniques. The effects of turbulence in wind can be included by employing a variety of turbulence modeling techniques, despite the fact that the irregularity of turbulence makes it appear impossible to describe the turbulent flow as a function of space and time.

2.2.Turbulence Modeling

Turbulent flow is irregular, and because of this irregularity, it seems challenging to express turbulent flow as a function of space and time. We should employ turbulence modeling to simulate turbulent flow. A mathematical approximation used to simulate the physical behavior of turbulent flows is called turbulence modeling. In tensorial notation, Eqn. 2.1 and Eqn.2.2 provide the Navier Stokes (NS) equations for incompressible flow.

$$\frac{\partial u_i}{\partial t} + u_j \frac{\partial u_i}{\partial x_j} = -\frac{1}{\rho}\frac{\partial p}{\partial x_i} + \frac{\partial}{\partial x_j}\left(\nu \frac{\partial u_i}{\partial x_j}\right) \tag{2.1}$$

$$\frac{\partial u_i}{\partial x_i} = 0 \tag{2.2}$$

If we average the NS equation in time or space and consider $u_i = U_i + u'$ we have:

$$U_j \frac{\partial U_i}{\partial x_j} = -\frac{1}{\rho}\frac{\partial p}{\partial x_i} + \frac{\partial}{\partial x_j}\left((\nu + \nu_t)\frac{\partial U_i}{\partial x_j}\right) \tag{2.3}$$

$$\frac{\partial U_i}{\partial x_i} = 0 \tag{2.4}$$

Versteeg and Malalasekera (2007) provide the derivation's details. In order to account for turbulence, turbulence modeling techniques attempt to approximate the equivalent viscosity or directly solve NS equations. Three techniques can be used to model turbulence:

1. Reynolds-averaged Navier–Stokes (RANS) based models: Eddy viscosity, which resembles molecular viscosity, is thought to roughly resemble turbulence quantities in this model. Two-equation models like the *k*- ε model are an illustration of this approach. In the *k*- ε model, transport equations for k and ε and must be solved in addition to the time-averaged NS

equations. The use of time-averaged equations prevents the capturing of time-dependent effects.

2. Direct Numerical Simulation (DNS) solves the equations for all eddies. Applying for practical problems is exceedingly tough given the current computer resources.
3. Large-eddy Simulation (LES): In LES, smaller eddies are described by Subgrid Scale Stress (SGS) model, which is similar to RANS approaches, and larger eddies that can be captured by mesh are calculated directly. The SGS model utilized under this study is the Smagorinsky-Lilly SGS model, which Smagorinsky (1963) developed. SGS model using Eqn. 2.5 estimates the equivalent viscosity for the turbulence of smaller eddies.

$$\nu_{SGS} = \sqrt{\frac{C_k^3}{C_e}}\Delta^2\sqrt{2\overline{S_{ij}}.\overline{S_{ij}}}\,, \quad \overline{S_{ij}} = \frac{1}{2}\left(\frac{\partial u_i}{\partial x_j} + \frac{\partial u_j}{\partial x_i}\right) \tag{2.5}$$

Where Δ is the grid size and C is constant. This method for small scales assumes that the energy production and dissipation are in equilibrium.

These three turbulence modeling methods are depicted also in Fig. 2.2 in relation to eddy size variation in the wind spectrum. In Fig. 2.2, an eddy is illustrated as a circular vortex. As can be observed, while the effects of all the eddies with various length scales are modeled in RANS, all eddy sizes are resolved in DNS. LES, on the other hand, resolves large eddies and models the impact of smaller eddies. Because RANS utilizes the time-averaging Navier-Stokes (NS) equations, it is unable to account for time-dependent effects. Given the limited computer resources, it is exceedingly challenging to apply DNS to real-world issues as DNS solves the NS equations for all eddies (i.e., a circular circulation of fluid). Therefore, compared to other turbulence modeling techniques, Large Eddy Simulation (LES) is more efficient and applicable in the industry.

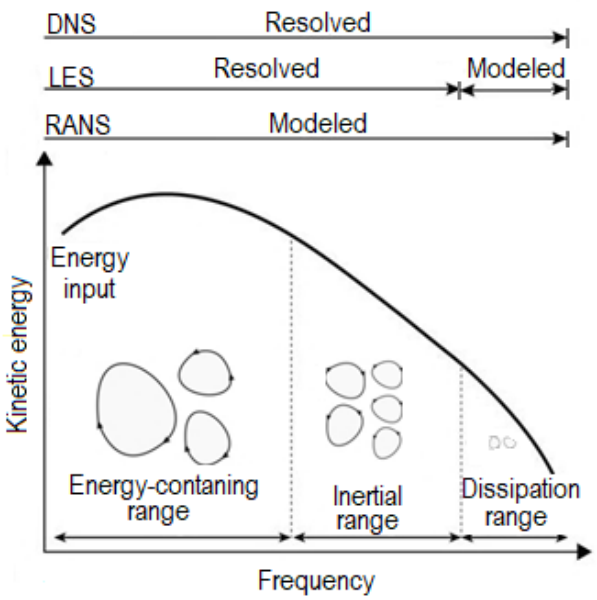

Fig. 2.2. Comparing different turbulence models with respect to eddy size variation in the wind spectrum.

2.3. Inflow Turbulence Generation Methods

Determining the appropriate inflow turbulence boundary condition for an LES model that satisfies particular spectra and correlations is a crucial part of the numerical investigation. At all determined temporal and spatial scales, the turbulent inflow generation method should produce time-varying fluctuations. These fluctuations should have the appearance of turbulence and be consistent with the Navier-Stokes equations. Turbulent flow is made up of coherent structures or eddies across a wide range of length scales. Deformation, direction, stretching, and fluid bursting are further characteristics of these structures that are critical for the produced inflow to accurately represent a realistic turbulent flow. Furthermore, the method should take into account a wide variety of given turbulence data as inputs in addition to be effective and simple to implement (Tabor and Baba-Ahmadi, 2010). Finally, the method also should be unaffected by the inflow geometry or grid spatial discretization (Dhamankar, 2015).

2.3.1. Precursor Method

By running a separate simulation of an equilibrium flow, the precursor method creates a database of turbulent flow. The main computation can then use this database of turbulent flow fields as the inflow conditions. Therefore, the inflow should have many of the essential properties, including correlated temporal and spatial fluctuations with a proper energy spectrum, as turbulent flow fields applied at an inlet are realistic solutions to the Navier-Stokes equations. This library can be created using a variety of methods, such as cyclic channel flow computations or periodic boxes of turbulence. They still need a unique database to be created and stored, though. Data mapping from a precursor simulation of a cyclic channel to the main simulation of a related channel was studied by Chung and Sung (1997) using a number of different techniques. These consist of a temporal database and a spatial database produced by using Taylor's hypothesis and moving the cutting plane across a single timestep of the precursor simulation. The most realistic turbulent inflow condition is produced via accurate precursor methods, despite the added expense of a separate simulation. This method is computationally expensive since building the precursor database requires a lot of processing time. The precursor database method can only be practical if the precursor database is already available due to this flaw.

2.3.2. Recycling Method

To create inflow turbulence on smooth surfaces, Lund et al. (1998) created the Recycling Method, which is similar to the precursor database. There are two computational domains in the recycling method: the driver domain and the computational domain (Aboshosha et al. 2015). The flow is repeated across a short domain in the driver domain until it becomes statistically stable, and flow characteristics on a mapping plane are saved and utilized as the inflow condition for the calculation domain. Following that, Nozawa et al. (2002) employed Lund's method to create turbulent inflow

data for rough surfaces as well. This method's shortcoming is that it requires a lot of processing time, making it computationally expensive, while also being vulnerable to surface roughness.

2.3.3. Synthetic Methods

Developed synthetic methods are generally categorized into a) Random Fourier Turbulence Generation Methods (RFG), b) Digital filter methods (DFM), and c) Synthetic Eddy Method (SEM).

2.3.3.1. Random Fourier Generation Methods

Kraichnan (1970) used the summing of random Fourier modes to create a divergence-free synthetic homogeneous isotropic turbulence (HIT) approximation. Kraichnan's approximation was soon acknowledged as a helpful tool for inflow turbulence generation of wind past buildings and other structures. To create random turbulent fluctuations, the simplest method is to add separate random fields with a mean of zero and a variance of one to a mean velocity profile. Using the turbulent kinetic energy (k), these random fields can be scaled. Then, this method was developed by Lund et al. in 1998, however instead of scaling by turbulent kinetic energy, the random fields are transformed by the Cholesky decomposition of the Reynolds stress tensor. Although the field produced by this method agrees well with a given Reynold's stress tensor, the flow field is uncorrelated in space and time and violates the real turbulence energy spectrum. Additionally, the anisotropic field might not satisfy the continuity equation as a result of the alteration mentioned above. For the purpose of creating a turbulent velocity field with turbulent spectra that closely resemble the desired atmospheric boundary layer (ABL) flow characteristics, Huang et al. (2010) proposed the discrete random flow generation (DRFG) method. To get velocity fields that more closely matched the target spectra, Castro et al. (2011) suggested modifying the DRFG approach. In general, the DRFG method can simply be implemented in a parallel computer environment, can

produce turbulent spectra close to the target, and can retain the spatial velocity correlations. The Consistent Discrete Random Flow Generator (CDRFG) was then created by Aboshosha et al. (2015) to maintain both the coherency function and the turbulent spectra. This method only examined the spatial correlation generated flow field in one direction. Then, Yu et al. (2018) created a novel technique called the narrowband synthesis random flow generator (NSRFG) to spatially correlate in three directions.

2.3.3.2. Synthetic Eddy Methods

Perry & Chong (1982) and Marusic & Perry (1995) serve as the foundation for Jarrin (2006) Synthetic Eddy Method (SEM) concept. They claimed that their representative coherent eddy structures could be directly superimposed to recreate their boundary layer. SEM uses synthetic eddies, or three-dimensional synthetic coherent structures, to create oscillations in all three dimensions. Jarrin et al. (2006) used a one-dimensional flow example to show the mathematical steps involved in SEM (Kornev and Hassel, 2007). According to the SEM, the flow is made up of randomly dispersed turbulent spots, and each turbulent spot is represented by a three-dimensional form function with compact support and complies with the necessary normalizing requirements. The Taylor hypothesis is then used to assume that the spots are transformed through an inlet plane at a reference velocity. To restore the appropriate statistical properties and take into consideration the inhomogeneity and anisotropy conditions, the resulting inflow turbulence is then rebuilt using the procedure that has been suggested. Since the two-point autocorrelation function and, in turn, the power spectrum of the synthetic turbulence are closely related, the shape function selection is crucial in the SEM. In order to create a divergence-free technique, Poletto et al. (2013) proposed applying the original SEM methodology to the vorticity field, which is then translated back to the velocity field by taking its curl. The new method name is Divergence Free Synthetic Eddy Method

(DFSEM). Based on the superposition of vortical structures (there denoted as vortons), Kroger and Kornev (2018) presented the Anisotropy Turbulent Spot Method (ATSM). Such a technique allows us to directly regulate the three turbulence intensities as well as the three integral length scales. It is a quality that inflow generators would find highly desirable.

2.3.3.3. Digital Filter Methods (DFM)

By filtering a random velocity field, DFM creates coherent structures in space and time. In order to prevent inaccurate pressure fluctuations, corrections must be made because it does not automatically produce a velocity that is divergence-free. For this method, OpenFoam offers the gaussian and exponential filtering functions. Since it has been previously empirically proven that correlation functions have a form more like exponential than Gaussian, Xie and Castro (2008) employed the exponential velocity correlation function. The Xie and Castro technique (XC) is two-dimensional and satisfied the spatial correlation, but they employed the idea that adding a new slice of random data to the inflow data at the next time step is somewhat equal to adding a fully new slice of random data at the next time step. Overall, it therefore comes close to being the same as the whole three-dimensional digital filter process. Particularly when the longitudinal length scale is large, this method is significantly more cost-effective than computing two-dimensional slices for each slice in the longitudinal direction. In the modified XC technique, the calculated velocity is multiple to the prescribed bulk velocity divided by the instantaneous bulk velocity derived from the uncorrected velocities, which corrects the instantaneous velocity at the inlet boundary with just a single correction. The XC method does not satisfy the divergence-free condition, which results in producing unreal large pressure fluctuations in direct numerical and large-eddy simulations. For this reason, Kim et al. (2013) developed the XC divergence-free (XCDF) method, in which they used a straightforward correction to maintain the constant mass

flux in inflow in addition to inserting generated turbulence inflow on the plane near the inlet during the procedure. The velocity-pressure coupling process is then used to adjust the velocities. They employed the two-step Pressure-Implicit with Splitting of Operators (PISO) algorithm. Based on the pressure at the prior time level, an intermediate velocity (the second velocity) is computed, denoted by the symbol $u*$. The second stage of correction will correct the velocity and pressure again since the intermediate velocity typically does not meet the divergence-free requirement. Finally, the corrected pressure $p**$ can be determined if the further corrected velocities $u***$ are divergence-free.

2.4. LES Maximum Grid Spacing and Its Corresponding Maximum Possible Frequency

Turbulent flow contains eddies, which are circular movements of fluid. There is a wide range of eddy sizes fluctuating at various frequencies in a typical turbulent flow (i.e., large eddies have low frequency fluctuations and vice versa). As demonstrated in Fig. 2.3(a), a minimum of four CFD meshes are needed to capture each eddy in LES. Mesh can resolve eddies of various sizes, as illustrated in Fig. 2.3(b). Because each eddy fluctuates at a unique frequency, the maximum grid spacing in LES can only transfer frequencies within a specified frequency range (Sagaut et al., 2003; Chow and Moin, 2003). According to Fig. 2.3(d), the greatest frequency that a grid can resolve is known as f_{LES}. In addition, in the current LES modeling, the filter length (Δ) is taken into account to be equal to the grid spacing size (h) (i.e., $\Delta/h=1$). This is done to avoid the impacts of LES filtering. Accordingly, eddies with wavelengths (L) less than filter lengths (Δ), which in this case matches mesh size (Fig. 2.3(c)), cannot be resolved and are instead approximated using sub-grid scale models like the Smagorinsky model. In Fig. 2.3(d), the non-dimensional maximum and minimum frequency from field measurements, or WT, are denoted by the letters f_{maxe} and f_{mine}.

Moreover, the non-dimensional maximum frequency (f_{max}) and minimum frequency (f_{min}) are employed as inputs to the inflow turbulence models.

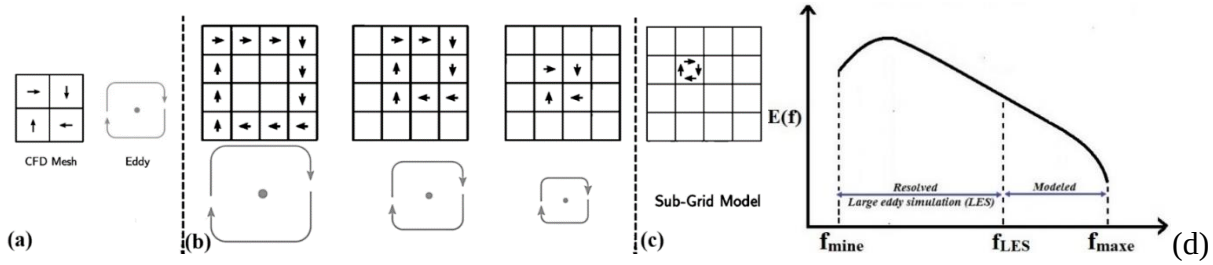

Fig. 2.3. (a), (b), and (c) Different eddy sizes compared to the mesh size, (d) Frequency region resolved and modeled by LES

The minimum wavelength L of a wave in the form of a sine or cosine function transported by the Fourier spectral method is $2h$ for a certain grid spacing of h (Orszag, 1979). In spectral analysis, the corresponding frequency is known as the Nyquist frequency. Nyquist frequency transport is possible using the spectral method, however using the finite difference method (FDM), it has a very high percentage of errors. Consequently, Ferziger and Peric (2002) and Kravchenko and Moni (1997) recommended $L=4h$ with the equivalent frequency of f_{grid} for finite difference or control volume approach in order to have less errors. Selvam (2017) suggested employing $L=10h$ even if the accuracy was over 90%, but this level of the improved grid is impractical. To make it clear, Fig. 2.4 and appendix 4.B present a detailed example of transferring a sine wave with the wavelengths of $2h$ and $4h$. Fig. 2.4 shows a sine wave with a wavelength of $2h$ being transported with an inaccuracy of nearly 100%, which is unacceptable. It is about 25% for the $4h$ wavelength.

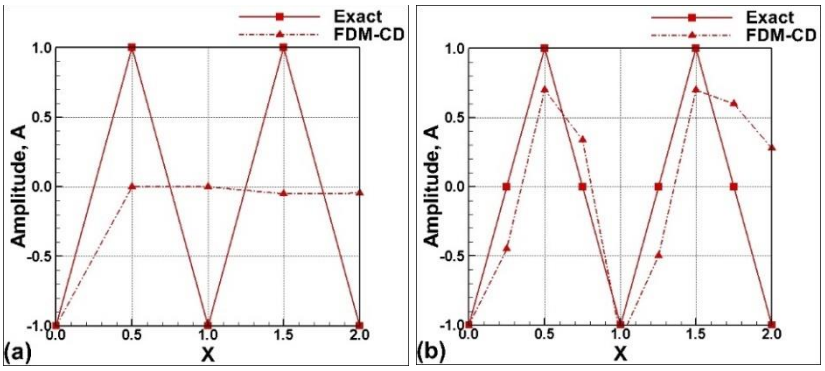

Fig. 2.4. Comparison of an exact sine wave transport with the FDM after 2.25 time units for (a) h=L/2=0.5 and (b) h=L/4=0.25 units

As mentioned, the greatest frequency that the grid can carry is f_{grid}, which is equal to f_{LES} in the LES studies. As a result, the equation f_{LES}=f_{grid}=H/4h is used to calculate the suggested maximum non-dimensional frequency can be transported in the flow using the FDM and LES.

2.5. Spurious Pressure

According to Rigall et al. (2021), Haywood (2019), and Lebovitz (2017), numerous input turbulence generator methods result in spurious pressure. Rigall et al. (2021) employed the modified RFG method, while Lebovitz (2017) used DFM. In all of these publications, the mentioned spurious pressure occurs when the frequency of the pressure is greater than the frequency of the velocity. In this study, spurious pressures are defined as pressures with frequencies greater than the Nyquist frequency. It should be highlighted that previous studies recognized pressure fluctuations and provided some justifications for these unwanted pressures. For instance, according to Patruno and Ricci (2017), pressure fluctuations occur when an inflow fails to respect mass conservation or retain momentum for each spatial direction. In addition to the previously described causes, Patruno and Ricci (2018) provide a detailed explanation of how boundary condition mismatches result in undesirable pressure productions close to boundaries. A solution to reduce unwanted pressures brought on by violations of mass and momentum

conservation was invented by Patruno and Miranda (2020). However, they simply employed a sine wave that adhered to the LES frequency, and they claimed that pressure fluctuation decreased while it was further away from the inlet (Fig. 2.5). However, the magnitude of pressure fluctuations, and not their frequency, is reduced (Fig. 1.5). In Fig. 1.5, pressure is plotted at the building height at the inlet and the building location. This figure illustrates how the pressure amplitude changes from the inlet location to the building location. The pressure's frequency, however, is unaltered.

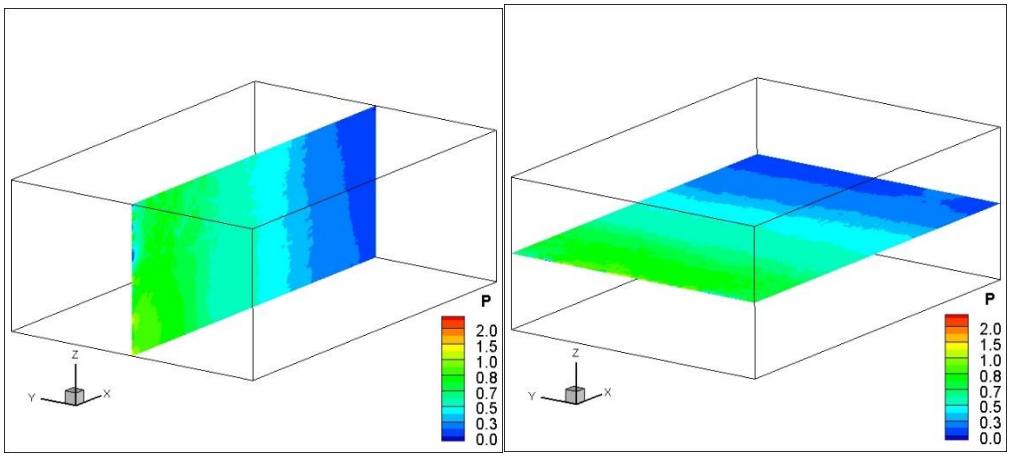

Fig. 2.5. Pressures coefficient contour without building for $h=H/16$, $f_{max}=10$

References

Aboshosha, H., Elshaer, A., Bitsuamlak, G. T., and El Damatty, A. (2015). Consistent inflow turbulence generator for LES evaluation of wind-induced responses for tall buildings. *Journal of Wind Engineering and Industrial Aerodynamics*, 142, 198-216

Castro, H. G., and Paz, R. R. (2013). A time and space correlated turbulence synthesis method for Large Eddy Simulations. *Journal of Computational Physics*, 235, 742-763.

Chung, Y. M., and Sung, H. J. (1997). Comparative study of inflow conditions for spatially evolving simulation. *AIAA Journal*, 35, 269-274.

Ding, F., Kareem, A., and Wan, J. (2019). Aerodynamic tailoring of structures using computational fluid dynamics. *Structural Engineering International*, 29, 26-39.

Dhamankar, N., Blaisdell, G. A., and Lyrintzis, A. S. (2015). An overview of turbulent inflow boundary conditions for large eddy simulations (Invited), *AIAA Journal*, 3213.

Dyrbye, C., and Hansen, S. O. (1997). Wind loads on structures. Wiley, Chichester, UK.

Ferziger, J. H., and Perić, M. (2002). Computational methods for fluid dynamics. Berlin: Springer, 3, 196-200.

Huang, S. H., Li, Q. S., and Wu, J. R. (2010). A general inflow turbulence generator for large eddy simulation. *Journal of Wind Engineering and Industrial Aerodynamics*, *98*, 600–617.

Jarrin, N., Benhamadouche, S., Laurence, D. and Prosser, R. (2006). A synthetic-eddy method for generating inflow conditions for large-eddy simulations. *International Journal of Heat and Fluid Flow*, 27, 585-593.

Keating, A., Piomelli, U., Balaras, E., and Kaltenbach, H. J. (2004). A priori and a posteriori tests of inflow conditions for large-eddy simulation. *Physics of fluids*, 16, 4696-4712.

Kim, Y., Castro, I. P., and Xie, Z. T. (2013). Divergence-free turbulence inflow conditions for large-eddy simulations with incompressible flow solvers. *Computers & Fluids*, 84, 56-68.

Klotzbach, P. J., Bell, M. M., Bowen, S. G., Gibney, E. J., Knapp, K. R., and Schreck, C. J. (2020). Surface pressure a more skillful predictor of normalized hurricane damage than maximum sustained wind. *Bulletin of the American Meteorological Society*, 101, E830-E846.

Kornev, N., and Hassel, E. (2007). Method of random spots for generation of synthetic inhomogeneous turbulent fields with prescribed autocorrelation functions. *Communications in Numerical Methods in Engineering*, 23, 35-43.

Kornev, N., and Hassel, E. (2007). Synthesis of homogeneous anisotropic divergence free turbulent fields with prescribed second-order statistics by vortex dipoles. *Physics of Fluids*, 19, 068101.

Kraichnan, R.H. (1970). Diffusion by a random velocity field. *Physics of Fluids*, 13, 22-31.

Kröger, H., and Kornev, N. (2018). Generation of divergence free synthetic inflow turbulence with arbitrary anisotropy. *Computers & Fluids*, 165, 78-88.

Levitan, M. L., Mehta, K. C., Vann, W. P., and Holmes, J. D. (1991). Field measurements of pressures on the Texas Tech building. *Journal of Wind Engineering and Industrial Aerodynamics*, 38, 227-234.

Lund, T. S., Wu, X., and Squires, K. D. (1998). Generation of turbulent inflow data for spatially developing boundary layer simulations. *Journal of Computational Physics,* 140, 233–258.

Mansouri, Z., Selvam, R. P., and Chowdhury, A. G. (2022). Performance of different inflow turbulence methods for wind engineering applications. *Journal of Wind Engineering and Industrial Aerodynamics*, 229, 105141.

Marusic, I., and Perry, A. E. (1995). A wall-wake model for the turbulence structure of boundary layers. Part 2. Further experimental support. *Journal of Fluid Mechanics*, 298, 389–407.

Mooneghi, M. A., Irwin, P., and Chowdhury, A. G. (2016). Partial turbulence simulation method for predicting peak wind loads on small structures and building appurtenances. *Journal of Wind Engineering and Industrial Aerodynamics*, 157, 47–62.

Moravej, M. (2018). Investigating scale effects on analytical methods of predicting peak wind loads on buildings. Ph.D. thesis, Florida International University, Miami, Florida.

Nozawa, K., and Tamura, T. (2002). Large eddy simulation of the flow around a low-rise building immersed in a rough-wall turbulent boundary layer. *Journal of Wind Engineering and Industrial Aerodynamics*, 90, 1151–1162.

Orszag, S. A. (1979). Spectral methods for problems in complex geometrics. Numerical methods for partial differential equations, 273-305. Academic Press.

Patruno, L., and Ricci, M. (2017). On the generation of synthetic divergence-free homogeneous anisotropic turbulence. *Computer Methods in Applied Mechanics and Engineering*, 315, 396–417

Perry, A. E., and Chong, M. S. (1982). On the mechanism of wall turbulence. *Journal of Fluid Mechanics, 119,*173–217.

Poletto, R., Craft, T., and Revell, A. (2013). A new divergence free synthetic eddy method for the reproduction of inlet flow conditions for LES. *Flow, turbulence and combustion*, 91, 519-539.

Richards, P. J., Hoxey, R. P., Connell, B. D., and Lander, D. P. (2007). Wind-tunnel modelling of the Silsoe Cube. *Journal of Wind Engineering and Industrial Aerodynamics*, 95, 1384–1399.

Selvam, R. P. (1997). Computation of pressures on Texas Tech University building using large eddy simulation. *Journal of Wind Engineering and Industrial Aerodynamics*, 67, 647–657.

Smagorinsky, J. (1963). General circulation experiments with the primitive equations: I. The basic experiment. *Monthly Weather Review*.

Tabor, G.R. and Baba-Ahmadi, M.H. (2010). Inlet conditions for large eddy simulation: A review. *Computers and Fluids*, 39, 553-567.

Taylor, G. I. (1938). The spectrum of turbulence. *Proceedings of the Royal Society of London. Series A-Mathematical and Physical Sciences*, 164, 476-490.

Versteeg, H. K., and Malalasekera, W. (2007). An introduction to computational fluid dynamics: the finite volume method. Pearson Education.

Woods, J. (2019). Turbulent Effects on Building Pressure using a Two-Dimensional Finite Element Program. Master's thesis, Department of Civil Engineering, University of Arkansas.

Wu, X. (2017). Inflow turbulence generation methods. *Annual Review of Fluid Mechanics*, 49, 23-49.

Xie, Z. T., and Castro, I. P. (2008). Efficient generation of inflow conditions for large eddy simulation of street-scale flows. *Flow, Turbulence and Combustion*, 81, 449–70.

Yu, Y., Yang, Y., and Xie, Z. (2018). A new inflow turbulence generator for large eddy simulation evaluation of wind effects on a standard high-rise building. *Building and Environment*, 138, 300–313.

Chapter 3- Paper 3

Teaching Modeling Turbulent Flow Around Building Using LES Turbulence Method and Open-source Software OpenFOAM

Zahra Mansouri, Sumit Verma, and R. Panneer Selvam

Department of Civil Engineering, BELL 4190 University of Arkansas, Fayetteville, AR 72701, USA

Abstract:

In our earlier work (https://github.com/rpsuark/ASEE21-OpenFOAM-Introduction), it was reasoned that open-source software OpenFOAM would be a cost-effective and more accessible alternative for teaching Computational Fluid Dynamics (CFD) than commercial software. Commercial software like *Ansys Fluent* costs more than $10k per year for one user. The above-mentioned work models wind flow around a building for smooth flow, whereas extreme winds, which tend to be irregular, can cause various structural failures of buildings. These kinds of irregular wind flows are called turbulent flows. Thus, in this contribution, an additional three-week class module is provided for the 'CFD for Wind Engineering' class which includes hands-on material on modeling turbulent wind flow around a building using open-source software OpenFOAM and ParaView. To model the turbulence, Large Eddy Simulation (LES) is considered with a logarithmic inlet profile. To connect the log profile in a coarse grid, the law of the wall condition is also introduced in the OpenFOAM environment. To illustrate the application, the wind flow around a cubic building is considered. The current study's case files and the extended report are provided at https://github.com/rpsuark/ASEE21-OpenFOAM-LES.

Keywords

Computational Fluid Dynamics, OpenFOAM, Large Eddy Simulation, Wall Function, Logarithmic Velocity Profile.

3.1. Introduction

3.1.1. Suggested Course Module in CFD for Industrial Application Purposes

Computational Fluid Dynamics (CFD) and wind engineering are some of the most important courses taught in universities which provide exposure to the students about the potentially catastrophic damages that can be brought by severe winds. These courses are basically driven with the motive to train and educate students to compute the wind velocities and pressures on building so that with a better estimate of wind loads, the structures and buildings could be designed better. At the University of Arkansas, CFD and Computational Wind Engineering (i.e., CWE 563) are taught by introducing a lab session consisting of real-world problem solving using research codes adapted for teaching purposes. Such methods of course instruction and delivery were found to be greatly beneficial to students as they introduced the theoretical concepts and provided decent exposure to real-world problem-solving. However, due to complexity, developing new code is impossible for every engineer in the industry, hence using commercial and open-source software is more likely. Using full-fledged CFD commercial software like Ansys Fluent costs more than $10k per year for one user for teaching and research purposes. Hence, in the current work, open-source CFD software OpenFOAM as well as open-source visualization program ParaView will be illustrated to model realistic wind flow. This open-source CFD software is a cost-effective alternative tool for teaching and students can develop it further for their future research and industrial applications. This work is an extension of Verma et al. (2021), wherein OpenFOAM is

introduced. Verma et al. (2021) contribution was primarily meant for the introduction of OpenFOAM and ParaView for teaching CFD and Fluid courses, so, the problem considered in (Verma et. al., 2021) was relatively simple and lacked several important aspects required to model a realistic wind flow case around a building that adequately resembles a real-world wind flow scenario. For instance, the case file from Verma et. al. (2021) is limited to laminar flow; laminar flow is smooth and regular flow and occurs in a very slow-moving fluid. As the flow speed increases, the flow tends to be more unstable and irregular. Most flows in nature are categorized in this type of flow which is also called turbulent flow.

The disastrous failure of structures caused by strong winds is mainly due to the underestimation of peak wind pressures while designing the building components. Strong winds are highly turbulent and so if turbulence is not well accounted for in the numerical model then, the computed wind loads (in the form of pressure coefficients) would not be adequate for building design purposes and are more likely to fail during severe storms/winds events. For instance, the maximum peak pressure coefficient obtained from ASCE 7-16 is -3 for a low-rise building. However, field measurements (of turbulent winds in nature) have reported that the maximum peak pressure coefficients on a low-rise building can be even lower than -8. Thus, it is necessary to consider correct peak pressures in building design. As conducting field measurements for designing purposes is expensive and time-consuming, CFD can be an economical tool for engineers to estimate accurate wind pressures on buildings.

Thus, in this work, a three-week lab component of the course module using open-source software programs OpenFOAM and ParaView is proposed as an extension to 2 weeks module proposed by (Verma et. al., 2021) by incorporating the important aspects (i.e., Large Eddy Simulation (LES), wall function and log profile as explained in detail in following sections), which are important to

capture the real physics of wind flow around a building. In the proposed module, first, a brief introduction to LES, log profile, and wall function is included followed by the implementation of LES for wind flow around the building and then implementation of wall function at the wall boundaries. Finally, the procedure of implementing logarithmic velocity profile at the inlet is discussed after which some flow visualizations are included. The relevant OpenFOAM implementation case files including an extended report and description to obtain various visualizations included in this work are provided as hands-on material at Mansouri et. al. (2021).

3.1.2. Turbulence

The plot shown in Fig. 3.1 is for a turbulent flow in which the velocity is recorded in time at a particular point in space. In Fig. 3.1, the instantaneous velocity is given by $u = U + u'$, where U is the time-averaged velocity and u' is the velocity fluctuation over time. As the variation in time does not follow or repeat in a periodic manner, so, such flows are random and chaotic and are called turbulent flows.

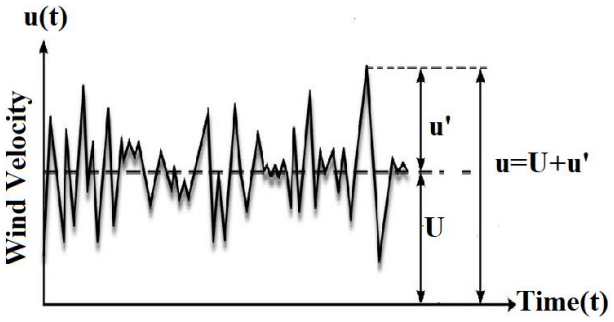

Fig. 3.1. Wind velocity in time at one point

The dimensionless parameter, Reynolds Number (*Re*) is defined by Eqn.3.1 and it helps to distinguish between the laminar and turbulent flow.

$$Re = \frac{UH}{\nu} \tag{3.1}$$

In Eqn. 3.1, U (m/s) is the free stream velocity, v is kinematic fluid viscosity (m^2/s), and H (m) is the building height. The flow with Re higher than $Re = 5 \times 10^5$ at boundary layer normally is turbulent.

3.1.3. Turbulence Modeling and Large Eddy Simulation Method

Turbulent flow is irregular and due to this irregularity, the turbulent flow appears difficult to be expressed as a function of space and time. To model turbulent flow, we should use turbulence modeling. Turbulence modeling is a mathematical approximation to model the physical behavior of turbulent flows. The Navier Stokes (NS) equations for incompressible flow are provided in Eqn. 3.2 and Eqn. 3.3 in tensorial notation (Versteeg and Malalasekera, 2007).

$$\frac{\partial u_i}{\partial t} + u_j \frac{\partial u_i}{\partial x_j} = -\frac{1}{\rho}\frac{\partial p}{\partial x_i} + \frac{\partial}{\partial x_j}\left(\nu \frac{\partial u_i}{\partial x_j}\right) \tag{3.2}$$

$$\frac{\partial u_i}{\partial x_i} = 0 \tag{3.3}$$

If we average the NS equation in time or space and consider $u_i = U_i + u'$ we have:

$$U_j \frac{\partial U_i}{\partial x_j} = -\frac{1}{\rho}\frac{\partial p}{\partial x_i} + \frac{\partial}{\partial x_j}\left((\nu + \nu_t)\frac{\partial U_i}{\partial x_j}\right) \tag{3.4}$$

$$\frac{\partial U_i}{\partial x_i} = 0 \tag{3.5}$$

The details of derivation can be found from (Versteeg and Malalasekera, 2007; Davidson, 2015). Turbulence modeling methods try to approximate the equivalent viscosity or solve directly NS

equations to consider turbulence (Pope, 2000; Wilcox, 1998). Turbulence modeling can be categorized into three methods (Smagorinsky, 1963; Wilcox, 1998):

4. Reynolds-averaged Navier–Stokes (RANS) based models: In this model, eddy viscosity similar to molecular viscosity is assumed to approximate turbulence quantities. An example of this method is two-equation models such as *k*-*ε*. In the *k*- *ε* model, in addition to the time-averaged NS equations, transport equations for *k* and *ε* must be solved. Since the time averaged equations are used, time-dependent effects cannot be captured.
5. Direct numerical simulation (DNS) solves the equations for all eddies. With the available computer resources, it is very difficult to apply for practical problems.
6. Large-eddy simulation (LES): With LES, larger eddies that can be captured by mesh are calculated directly, whereas the smaller eddies are modeled by Subgrid Scale Stress (SGS) model which is similar to RANS methods. Here, the Smagorinsky–Lilly SGS model developed by Smagorinsky (1963) is used for the SGS model and it estimates the equivalent viscosity for the turbulence of smaller eddies by Eqn. 3.6.

$$\nu_{SGS} = \sqrt{\frac{C_k^3}{C_e}}\Delta^2\sqrt{2\overline{S_{ij}}.\overline{S_{ij}}}\,, \quad \overline{S_{ij}} = \frac{1}{2}\left(\frac{\partial u_i}{\partial x_j} + \frac{\partial u_j}{\partial x_i}\right) \tag{3.6}$$

Where Δ is the grid size and *C* is constant. This method assumes that the energy production and dissipation are in equilibrium for small scales.

These three turbulence modeling methods are shown also in Fig. 3.2 with respect to eddy size variation in the wind spectrum. In Fig. 3.2, an eddy is shown as a circular vortex. As it can be seen, all eddy sizes are resolved in DNS whereas the effect of all the eddies of different length scales

are modeled in RANS. However, in LES, large eddies are resolved and the effects of smaller eddies are modeled.

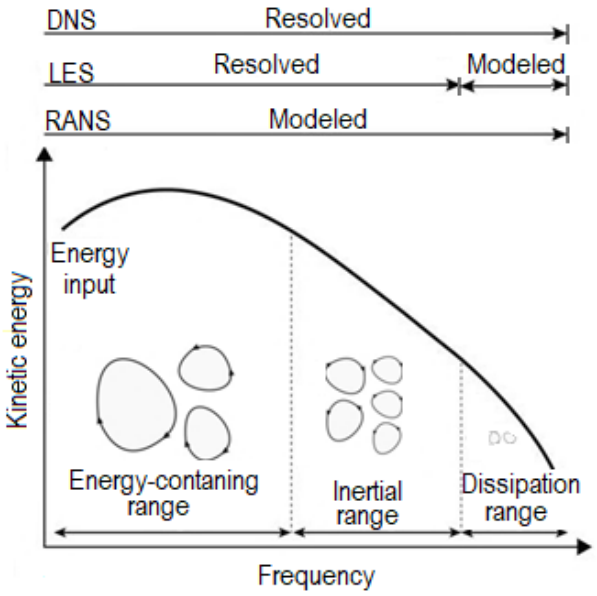

Fig. 3.2. Comparing different turbulence models with respect to eddy size variation in the wind spectrum.

3.1.4. Large Eddy Simulation Method Selection Reason

The complexity of turbulence makes it impossible to consider a single turbulence model as a universal model for modeling any turbulent flows. Thus, RANS turbulence models should be considered as engineering approximations rather than a scientific law. Turbulence is locally dynamic in some flows, and time averaging completely removes these turbulence features. LES approximates these local flow variables. Because of this, DNS and LES have got attention in recent decades. Whereas RANS models deal with time-averaged fields, transient eddies are not calculated even if they are larger than the mesh size. On the other hand, in LES, any eddies larger than mesh size are calculated. For instance, as an analogical example, RANS calculates approximately how

many people are passing the crosswalk. Whereas, in LES, we can capture each person's movement at each moment.

Although DNS and LES have enhanced capability in predicting the unsteadiness in the flow field, DNS can only be used for low Reynolds number flows and simple geometries. The flow details provided by DNS are not required for design purposes. Space-averaged quantities are appropriate for engineering applications. Highly resolved flow fields obtained from LES rather than modeled effect of RANS k-ε could be of greater interest in the industry in the future.

3.1.5. Boundary Layer Velocity Profile

Additionally, the wind flow near the ground due to friction is zero, and as the height increases, velocity increases till the height that these obstructions cannot affect wind flow anymore. There are two approximations for this velocity profile, one of them is named logarithmic velocity profile. Verma et al. (2021) stated that a region in space called computational domain has to be considered around a building for computing wind flow around a building. However, the shortcoming of the model (Verma et al., 2021) is that uniform inflow is introduced at the inlet. If the uniform flow is considered, a large region needs to be modeled on the upstream side of the building to develop the logarithmic velocity profile before the flow approaches the building. This would increase the computational time and subsequently the computational cost. Hence, to optimize, a logarithmic velocity profile can be selected for the inlet, which saves both computational time and cost and at the same time resembles a closer reflection to real-world atmospheric flows.

3.1.6. Standard Wall Function

Furthermore, the velocity gradient close to the wall is very high near the ground due to ground friction. Therefore, to solve flow correctly, we need to refine the mesh near the walls; however,

mesh refinement close to the walls increases the computational time and cost tremendously. An alternative round-about technique to obtain realistic flows without refining mesh close to the ground is to use the standard wall functions (Wilcox, 1998). However, Verma et. al. (2021) did not consider either the law of the wall or mesh refinement near the walls. Thus, in this work, wall functions are used in the wall boundary faces to capture steep velocity gradients near the walls.

3.1.7. Objectives

Following teaching module components will be provided as hands-on material for students:

1. OpenFOAM as part of the CFD course to consider turbulence in the flow.

2. Applying standard wall function to use coarser mesh and save computational time and cost.

3. Applying logarithmic velocity profile at the inlet to model boundary layer wind.

4. Plotting mean, maximum, and minimum peak pressure on a building by retrieving time-series data from OpenFOAM and performing statistical analysis.

3.2. Problem Statement (Turbulent Wind Flow Around the Building)

The wind loads required for the structural design of structures can be obtained using numerical (CFD) models. In the current study, the turbulent wind around a cubical building (i.e., Silsoe building) is modeled using OpenFOAM. To capture the turbulence effects in wind flow, LES with Smagorinsky–Lilly SGS model is used as a turbulence modeling method. A region around the building called the computational domain shown in Fig. 3.3 must be considered to compute wind flow around a building. The flow characteristics used as initial conditions are provided in Table 3.1.

To estimate wind load accurately, a numerical model should be able to capture the real flow physics. In the real boundary layer, the velocity is zero close to the ground due to the friction and increases with height, hence, the wind velocity near the ground is approximated by the logarithmic velocity profile. Similarly, the standard wall function is implemented at walls to capture high velocity gradient near the ground.

Table. 3.1. Field data for the Silsoe building [9].

Test Characteristics	Explanation	Full Scale
H	Building height	6 m
U_H	Flow velocity at building height	9.52 m/s
z_0	Roughness length	0.1 m

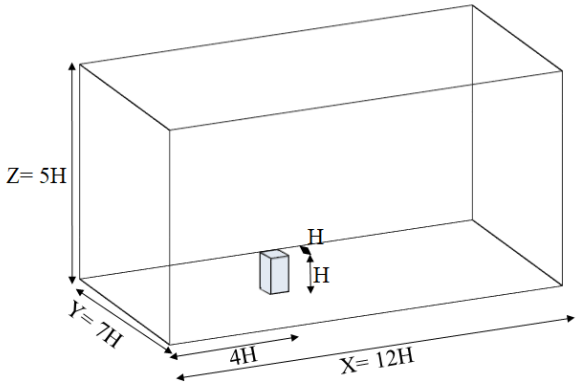

Fig. 3.3. 3D view of the computational domain

3.2.1. Numerical Setup

In this study, the turbulent wind flow around the Silsoe building with a dimension of 1H is modeled, where 'H' is the height of the building. For the computational domain, enough regions should be considered around the building. The size of the computational domain should be large enough so that the influence of the cube is not felt much by the outside boundary. The size of the

computational domain is 12*H* in X-direction, 7*H* in Y-direction, and 5*H* in Z-direction. In this region, governing equations (i.e., 3D incompressible Navier–Stokes (NS) equation) are solved to obtain flow field details around the building. Mesh and geometry generations are explained by Verma et al. (2021). The grid spacing size is 0.1H in each of X, Y, and Z-direction as shown in Fig 3.4. The total number of cells in the mesh of the computational domain is 419,000.

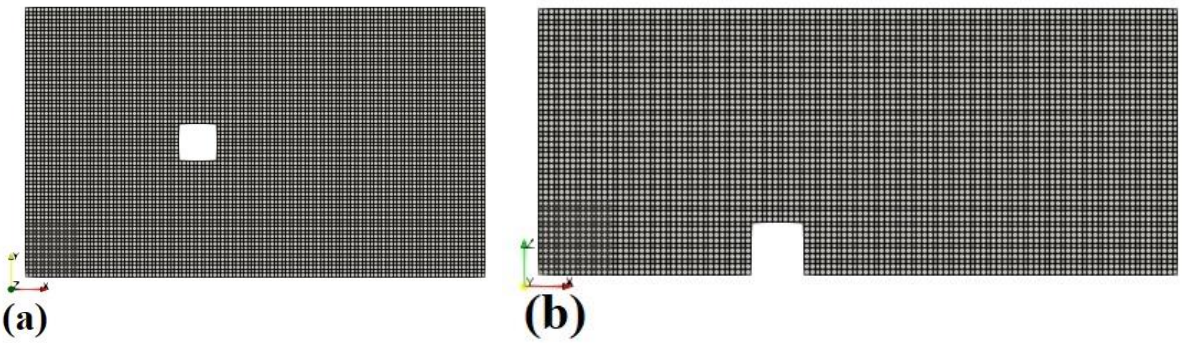

Fig. 3.4. Mesh of computational domain in (a) XZ-plane at y = 3.5 (b) XY-plane at z = 0.5.

3.2.1.1. Boundary Condition

Setting correct boundary conditions is important to obtain a real physical model. These initial and boundary conditions are used to solve governing equations numerically. The boundary conditions are indicated for all boundary faces in Fig. 3.5. The symmetric boundary conditions are implemented on the sidewalls, and the outflow boundary condition is specified at the outlet similar to what is used by Verma et. al. (2021). However, the inlet and wall boundary conditions are chosen differently for this study due to capture the wind flow physics around a building better in the CFD model.

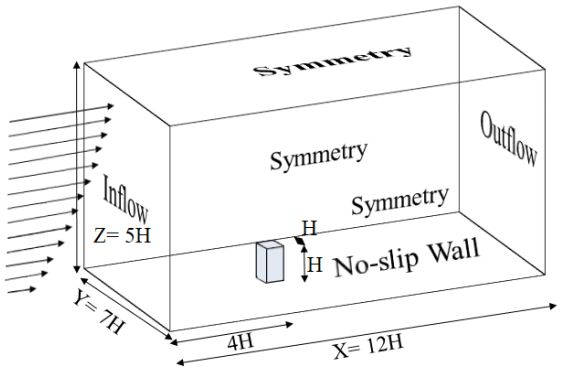

Fig. 3.5. Domain dimensions and domain boundary conditions.

3.2.1.1.1. Wind Profile Velocity at Inlet:

Ground obstructions close to the ground surface slows down the winds. Due to ground obstructions, wind velocity changes from zero at the ground surface to a maximum at a certain height from the ground where airflow is no longer affected by the obstructions. The height at which the airflow becomes unaffected by the ground obstructions is a function of ground roughness as can be seen in Fig. 3.6. The variation of velocity as a function of height taking ground roughness into account is given by a well-known and accepted velocity profile approximation called the logarithmic velocity profile defined by Eqn. 3.7.

$$U(z) = \frac{u^*}{\kappa}\ln\left(\frac{z}{z_0}\right) \ (m/s) \quad and \quad V = W = 0 \tag{3.7}$$

Where *U*, *V*, and *W* are streamwise, spanwise, and ground-normal flow speed (m/s) respectively. u^* is friction velocity (m/s) and $\kappa = 0.41$ is von *Kármán* constant. z and z_0 are height and roughness length (m) respectively (Dyrbye and Hansen, 1997). The roughness length, z_0, is the height above the ground where the flow velocity is zero. As in this work, the non-dimensional

form of NS equations is considered, the nondimensional roughness is considered as $z_0 = 0.1/6 = 0.016 \approx 0.01$ in the numerical model.

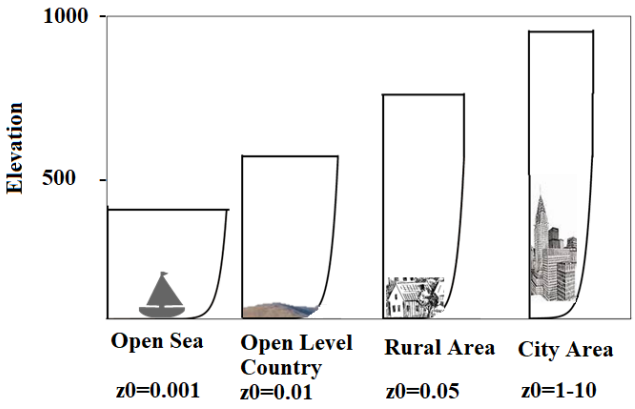

Fig. 3.6. Variation of velocity as a function of height for different roughness and terrain exposure condition.

2.1.1.2. Wall Functions for Near Wall Treatment

Wind velocity close to the ground due to friction is zero, and as the height increases, velocity increases. This velocity gradient close to the wall is very high and the flow near the wall can be categorized into three different sublayers (i.e., viscous sublayer, inner region, and buffer layer) as shown in Fig.3.7. In the viscous sublayer, flows are almost smooth and laminar close to the wall, and the viscosity determines the flow behavior. Whereas, far from the wall, flows are fully irregular and turbulent in the inner layer. In between, there is a layer is called the buffer layer in which the effects of viscosity and turbulence are both important. To capture this steep flow gradient close to the wall, a very fine mesh resolution is required. However, it needs considerable computational resources in complex geometries or three-dimensional flows. To decrease computational costs without compromising the accuracy of the solution, empirical equations are used to satisfy the physics in the near-wall region. These formulas are called wall functions (Wilcox, 1998). In

OpenFOAM, different wall functions are provided. In the current study, the nutkWallFunction is implemented at walls. The implementation of the wall function is explained in section 3.3.6.

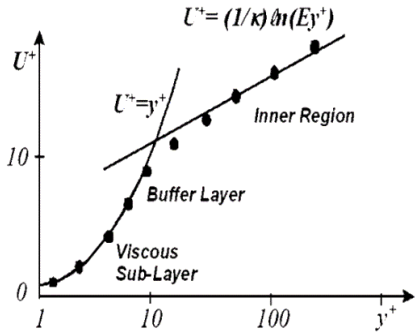

Fig. 3.7. Velocity in the near wall region.

3.3. OpenFOAM Implementation

As stated in the introduction, case files from Verma et al. (2021) provided in Selvam's github need to be modified for a realistic model. In this section step by step, each file that needs to be modified is explained in detail. The modified case file name is BuildingLES provided in (Mansouri et al., 2021). In this file, LES is used for turbulence modeling, the logarithmic velocity is used for boundary conditions at the inlet, and the wall function is implemented at walls.

3.3.1. System Folder

Four files are placed in this folder: blockMesh, ControlDict, fvSchemes and fvSolution. Running time parameters (i.e., start/end time and time step) are set in ControlDict. The numerical schemes for terms are set in the fvSchemes file. In the fvSolution file, equation solvers, convergence tolerances, relaxation factors and other algorithm controls are set. Using blockMesh file and blockMesh command the mesh files (i.e., polyMesh files located at *constant* folder) will be created.

Firstly, a proper solver for turbulent flow should be determined. pimpleFoam, pisoFoam, and simpleFoam are solvers for turbulent flow provided in OpenFOAM. SimpleFoam is steady, whereas pimpleFoam and pisoFoam are transient. For coupling velocity and pressure, pimpleFoam uses the merged Piso-Simple algorithm and pisoFoam uses the Piso algorithm. For this work, pisoFoam is chosen and is included in the ContolDict file.

In ContolDict file inside the system folder, time step (*dt*) is taken as 0.025, total time=50, and the output files for visualization are written every 1 time units.

3.3.2. Constant Folder

Two files (transportProperties, turbulenceProperties) and a folder (polyMesh) are placed in this folder. PolyMesh files are created when the 'blockMesh' command is used before running the case file. In transportProperties file, the properties of the fluid are included such as the viscosity of the fluid. In this work, air is considered.

In turbulenceProperties file, the turbulence model is specified, and its parameters are set. In polyMesh folder, all the data for the mesh (i.e., points, edges, faces, and so on) is located. This folder can be created in different ways such as manually, using and transforming the data from other software to OpenFOAM such as Salome, or using OpenFOAM native meshing tools such as blockMesh and snappyHexMesh. The boundary file also is located in this folder where boundary names are defined.

It should be noted that for applying LES we use turbulenceProperties file.

3.3.3. “0” Folder: Boundary Condition

The boundary conditions are included in this folder. Depending on the turbulence model we are working with, different boundary condition files are needed to be included in addition to typical boundary conditions such as velocity, pressure, and so on. The boundary conditions will be set for each boundary face and the structure will be the following:

```
Name_of_the boundary face
{
type Type of boundary face
value Value
}
```

The boundary condition type will be set depending on the wall definition. For each wall definition, there are some values available that can be found in OpenFOAM User Guide (2012).

3.3.4. Applying LES

To apply LES with Smagorinsky SGS model for turbulence modeling, the following lines are included in turbulenceProperties file.

```
simulationType LES;
LES
{
LESModel        Smagorinsky;
turbulence      on;
printCoeffs     on;
delta           cubeRootVol;
```

```
cubeRootVolCoeffs
{
deltaCoeff      1;
}
SmagorinskyCoeffs
{
Ck              0.094;
Ce              1.048;
}
}
```

3.3.5. Applying Nonuniform Velocity at Inlet

Using the codedFixedValue we can define logarithmic velocity profile as the inlet boundary condition which is a characteristic of the wind boundary layer. Hence, we should use the following code as the inlet boundary condition in *U* files.

```
inlet
{
type codedFixedValue;
redirectType velocity_inlet;
code
#{
scalar Ustar=0.089;
scalar k=0.41;
scalar z0=0.01;
```

```
fixedValueFvPatchVectorField myPatch(*this);
forAll(this->patch().Cf(),i)
{
myPatch[i]=vector(Ustar/k*(Foam::log((this->patch().Cf()[i].z())/z0)),0,0);
}
operator==(myPatch);
#};
value $internalField;
}
```

3.3.6. Applying Wall Function

To apply wall function, in the nut file under ‘0’ folder, the wall function should be specified for walls boundary condition as follows:

```
Wall
{
type            nutkWallFunction;
value           uniform 0;
}
```

3.4. Visualization of Results

The post-processing step of every numerical modeling is visualization plots in which we can find the detailed characteristics of flow field. Data files are stored each limited number of time steps setting the write interval inside ControlDict file. For current work, simulation was run for a total time of 50 units and the data files were written by solver every 40 time steps. We can use ParaView

in Windows or Linux systems. To open result files in ParaView, the ControlDict file should be chosen firstly, and then the OpenFOAMReader should be chosen and applied.

Pressure contour and velocity contour plots of wind flow around the building are plotted at the 50 time units in Fig 3.8(a) and (b). The way of plotting is explained by Selvam (2021). There is a red colored region upstream of the building that shows the stagnation region. The positive pressure due to wind force is applied on the windward side of the building.

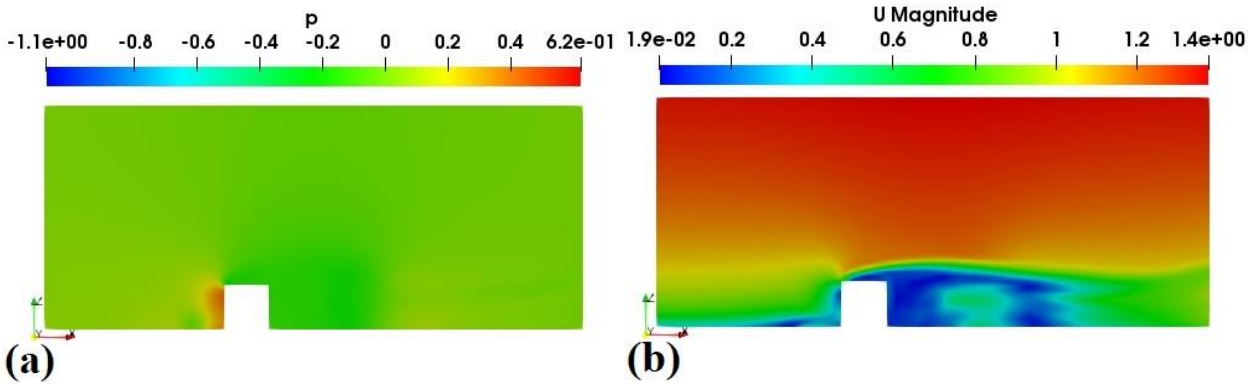

Fig. 3.8. Contour plots in the computational domain through XZ-plane at y = 3.5 (a) Pressure contour (b) Velocity contour at last time step.

The pressure contour and velocity contour plots in the XY-plane at roof height of the building (i.e. z = 1.0) are plotted respectively at 50 time units in Fig. 3.9(a) and (b). Here, we can also see the stagnation region on the windward side of the building which has high pressure values. On the leeward side of the building, the separation flow occurs because the velocity is near zero there.

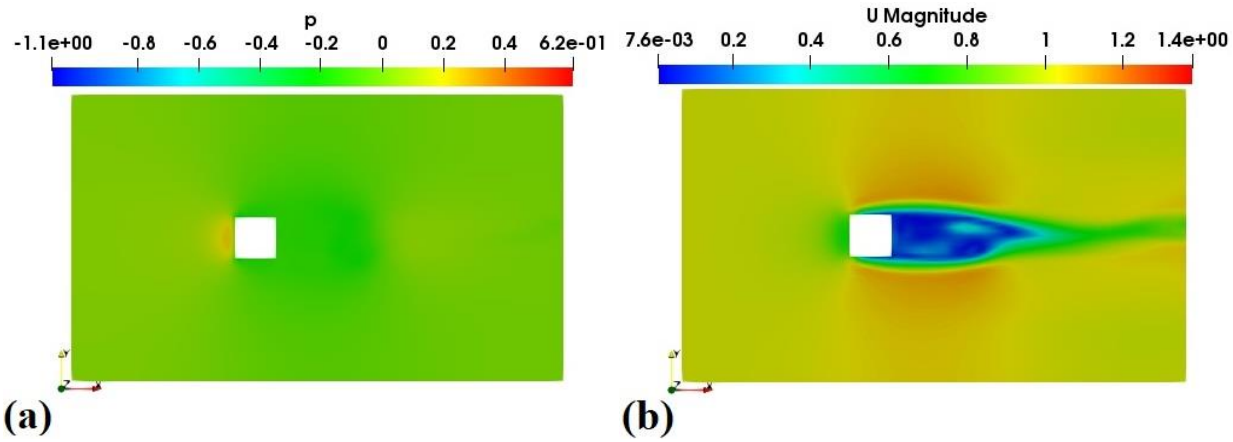

Fig. 3.9. Contour plots in computational domain through XY-plane at z = 1.0 (a) Pressure contour (b) Velocity contour at last time step.

The velocity profile at the inlet is plotted in Fig. 3.10 in the YZ-plane which clearly shows the logarithmic profile defined at the inlet. The way of plotting is explained in the report by Mansouri et al. (2021).

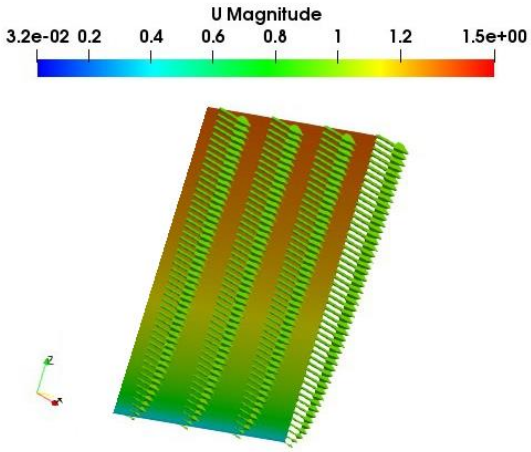

Fig. 3.10. Velocity profile at the part of the inlet.

3.5. Pressure Calculation:

To calculate pressure statistics the following steps can be followed:

1. Writing pressure at each point located along the building centerline by adding the following lines in the ControlDict file.

```
probes
{
type            probes;
libs            ("libsampling.so");
writeControl    timeStep;
writeInterval   1;
fields
(U p );
probeLocations
(
(4 3.5 0.1)
……
(5 3.5 0.1)
);
}
```

2. Removing the first 10 time units pressure coefficients.
3. Calculating the maximum, minimum, and average of pressure coefficients amount at each point based on every time steps from 10 to 50 time units by using excel functions.

Using the above-mentioned steps, 9 points at the windward and leeward of the building and 11 points at the roof are considered. The distance between every two consecutive points is *H/10*. The

final plot is shown in Fig. 3.11. As it can be seen, the maximum positive pressure coefficient occurs on the windward face of the building, whereas the minimum occurs at the roof edge.

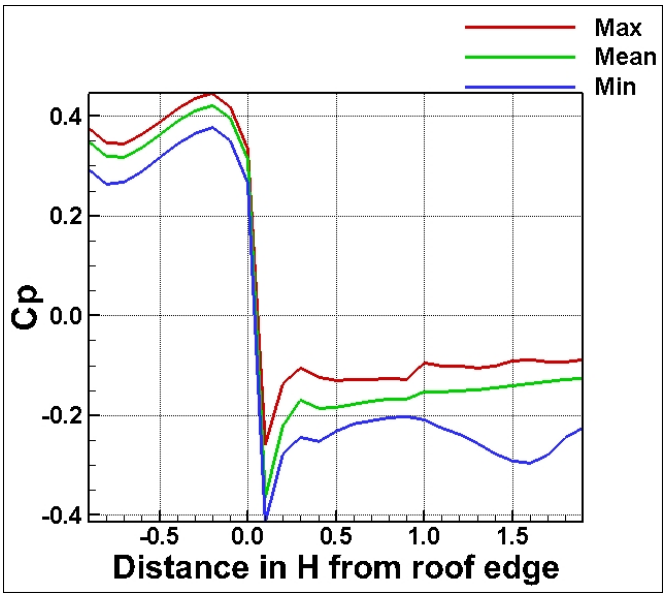

Fig. 3.11. Mean, maximum, and minimum Cp plot along the centerline of building the grid spacing size of H/10.

In Fig. 3.12, the pressure coefficient is plotted over time at the roof edge. According to Fig. 3.12, the minimum pressure coefficient could be around -0.4.

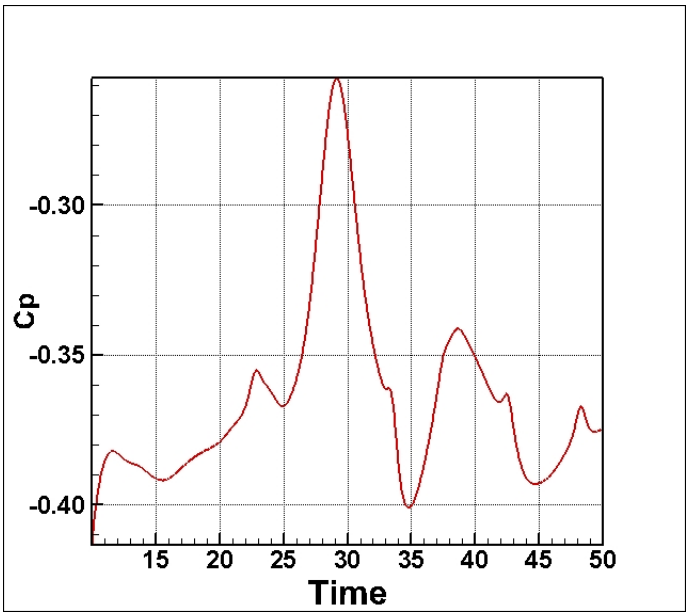

Fig. 3.12. Cp plot at a point near the roof edge at (4.1, 3.5, 1) over time.

3.5.Conclusion:

Solving realistic problems in CWE is necessary for engineers to be able to design real structures. Using theoretical and numerical methods to solve these problems saves a lot of costs compared to experimental studies. Furthermore, numerical results give more details of the flow field such as detailed velocity and pressure at every point in the computational domain. Engineers and researchers should know CFD and fluid mechanics to be able to analyze and solve complex real fluid-related problems, obtain wind loads, and have a successful structural design.

In this contribution, a teaching method including open-source software packages such as OpenFOAM for teaching CFD and CWE is suggested because open-source software OpenFOAM would be a cost-effective and more accessible alternative than commercial software for teaching learning purposes. In this method, it is tried to bring as an example of realistic wind related

problem, flow around the building with real physical condition. To model real turbulent wind flow, LES as a turbulence model is used for turbulence modeling. Furthermore, to save computation time and cost and make the numerical model closer to the physical boundary layer, the logarithmic velocity profile is used at the inlet, and the standard wall function is implemented at walls. Open-source software packages such as OpenFOAM and ParaView is the advantageous option compared to commercial software for teaching these courses. In addition, the ability to customize it makes the open-source software more flexible to teach a wide range of computational fluid dynamics problems. Therefore, using this work and the case file and extended report provided at https://github.com/rpsuark/ASEE21-OpenFOAM-LES by the authors, students can develop a good understanding of the case set up in OpenFOAM (Mansouri et al., 2021).

Acknowledgment

The authors acknowledge the support received from National Science Foundation (NSF) under award number CMMI-1762999. Ms. Zahra Mansouri acknowledges the financial support from the James T. Womble Professorship from the University of Arkansas.

References

Davidson, P. A. (2015). Turbulence: An Introduction for Scientists and Engineers. Oxford University Press.

Dyrbye, C., and Hansen, S. O. (1997). Wind loads on structures. Wiley, Chichester, UK.

Mansouri, Z., Verma, S., and Selvam, R.P. (2021). Teaching Modeling Turbulent Flow Around Building Using LES Turbulence Method and Open-source Software OpenFOAM- Extended Report. https://github.com/rpsuark/ASEE21-OpenFOAM-LES.

Mooneghi, M. A., Irwin, P., and Chowdhury, A. G. (2016). Partial turbulence simulation method for predicting peak wind loads on small structures and building appurtenances. *Journal of Wind Engineering and Industrial Aerodynamics*, 157, 47–62.

OpenFOAM: User Guide (2012). openfoam.com https://www.openfoam.com/documentation/guides/latest/doc/guide-bcs-derived-wall.html

Pope, S. B. (2000). Turbulent Flows. Cambridge University Press.

Sagaut, P. (2006). Large Eddy Simulation for Incompressible Flows (Third ed.). Springer.

Selvam, R. P. (2021). ASEE21-OpenFOAM-Introduction, github.com https://github.com/rpsuark/ASEE21-OpenFOAM-Introduction

Smagorinsky, J. (1963). General circulation experiments with the primitive equations: I. The basic experiment. *Monthly Weather Review*.

Verma, S., Mansouri, Z., and Selvam, R. P. (2021). Incorporating Two Weeks Open-Source Software Lab Module in CFD and Fluids Courses. In Proc. 2021 ASEE Midwest Section Virtual Conference, Sep. 13-15.

Versteeg, H. K., and Malalasekera, W. (2007). An introduction to computational fluid dynamics: the finite volume method. Pearson Education.

Wilcox, D. C. (1998). Turbulence Modeling for CFD. La Cãnada, Calif: DCW Industries.

Chapter 4- Paper 4

Maximum Grid Spacing Effect on Peak Pressure Computation Using Inflow Turbulence Generators

Zahra Mansouri[1], Rathinam Panneer Selvam[2*] Ph.D. , P. Eng., F. ASCE, and Arindam Gan Chowdhury[3] Ph.D. , A.M. ASCE

[1]Graduate Student, BELL 4190, University of Arkansas, Fayetteville, AR 72701, USA, zmansour@uark.edu

[2*]University Professor, BELL 4190, University of Arkansas, Fayetteville, AR 72701, USA, rps@uark.edu

[3] University Professor, Florida International University, Miami, FL, chowdhur@fiu.edu

Abstract: The peak pressures are computed using computational fluid dynamics (CFD) with the synthetic inflow turbulence generator and compared with 1:6 scale Texas Tech University (TTU) wind tunnel measurements. The inflow turbulence is calculated using the Consistent Discrete Random Flow Generation Method (CDRFG) method. The maximum and minimum frequencies from the field or experimental measurements as input to the inflow turbulence generator without considering the largest grid spacing used in the CFD model leads to high pressure error. For one case, more than 100% error in peak pressure results is observed. In addition, spurious pressures are observed at the building location without building. By varying maximum frequencies systematically for each computational mesh size and comparing the velocities and pressures at the inflow and the building location without building, possible causes of the error are explained. From

the investigation, it is suggested not to use the maximum frequency in the inflow turbulence generator beyond the frequency that can be transported by the largest grid spacing.

Keywords: Computational fluid dynamics, Synthetic inflow turbulence, Peak pressure, TTU building, Large eddy simulation.

4.1. Introduction

Significant infrastructure damage, economic loss, and even deaths are caused by severe windstorms such as hurricanes and tornadoes. The National Weather Service (NWS, 2019) reported 38 fatalities, 202 injured, and damages resulting in costs of 187.67 million dollars caused by severe thunderstorm wind in 2019. Based on this report, the number of fatalities and costs of structural failures increased by 14 people and 31.81 million dollars in 2019 compared to 2018. Because wind flows have higher intensity currently compared to the past, and it is expected to increase more in the future (Woods, 2019). Hence, a better estimation of wind peak pressures and loads on buildings is required to design structures. As an illustration, for component and cladding, the maximum peak pressure coefficient (*Cp*) obtained from ASCE 7-16 is -3.2 for a low-rise building. However, field measurements have reported that the maximum peak *Cp* on a low-rise building can be lower than -8 (Mooneghi et al., 2016). As conducting field measurement is time-consuming and costly to estimate wind loads on structures, computational fluid dynamic (CFD) can be used as an economical alternative tool. With the cutting-edge improvements in the CFD, the possibility of computing peak pressures is very near. A well-validated CFD with field measurements can fill this gap and help to reduce the loss of damage and loss of life.

As strong winds are highly turbulent, turbulence needs to be well accounted for in CFD. The turbulence's effects in wind can be incorporated in CFD by using various turbulence modeling

methods. Large Eddy Simulation (LES) is more reliable and applicable in the industry compared to all other turbulence modeling methods. However, a critical aspect of the numerical LES investigation is defining the right inflow turbulence condition to predict peak pressure correctly. Selvam (1997) reported at least 30% error in CFD peak *Cp* compared to field measurements is rooted in low grid resolution and inflow boundary conditions (BC). Primary methods to generate inflow turbulence fields are (a) precursor database, (b) recycling method, and (c) synthetic turbulence (Keating et al., 2004). The weakness of the first method is the need for the precursor database that makes this method computationally expensive. The second method is not practical because it is computationally costly and is sensitive to roughness.

4.1.1. Peak Pressure on Low-rise Buildings' Estimation Status Using Synthetic Inflow Methods

As synthetic inflow turbulence does not require prior flow simulations, recent studies used it as a preferable method (Patruno and Ricci , 2017; Aboshosha et al., 2015; Ding et al., 2019, Yu et al., 2018). In these studies, the time-varying pressures on buildings due to different synthetic turbulent inflows are reviewed and not mentioned here. Numerous synthetic inflow turbulence methods are in use and can be categorized into (1) Random Flow Generation method (RFG), (2) Digital Filtering Method (DFM), and (3) Synthetic Eddy Method (SEM). In all the mentioned references, improved RFG methods are used to compute flow around the Commonwealth Aeronautical Advisory Research Council (CAARC) standard tall building. For instance, Aboshosha et al. (2015) developed and used the 4th generation of RFG methods (i.e., Consistent Discrete Random Flow Generation (CDRFG)) to compute peak pressure on tall buildings. Whereas Aboshosha et al. (2015) used two terms in their Fourier series, Yu et al. (2018) used one term to reduce the computation time of inflow generation by at least 5 times. As examples for other synthetic

methods, Daniels et al. (2013) used the modified DFM by Kim et al. (2013) for the CAARC standard tall building, and Poletto et al. (2013) used SEM for channel flow.

However, in the works of Daniels et al. (2013), Aboshosha et al. (2015), and Yu et al. (2018), the root-mean-square (RMS) and the mean pressure coefficients for the CAARC tall building are compared with wind tunnel (WT) results, and results are very encouraging. Daniels et al. (2013) focused on the surface pressures correlation with WT results comparison. Hence, there is no comparison of CFD peak pressure with WT or field measurements for a low-rise building, and the current work focuses on that. In this work, to improve the predictive capability of low-rise building damages, the Texas Tech University (TTU) building is considered as a benchmark problem. Wind tunnel measurements of peak pressures on the TTU building are provided by Moravej (2018). Furthermore, the inflow turbulence field is calculated using CDRFG. In addition to the CDRFG method, the other RFG method used in our group is Narrowband Synthesis Random Flow Generator (NSRFG) method introduced by Yu et al. (2018). The NSRFG method's results are provided by Atencio (2021) and Selvam (2022), and in this study, only the results related to CDRFG are presented. The MATLAB code for the CDRFG method is provided in the appendix by Aboshosha et al. (2015). The verification and validation of the model are reported in detail by Aboshosha et al. (2015).

4.1.2. Relation Between Maximum Grid Spacing and the Maximum Possible Frequency

Turbulent flow includes some circular movement of fluid called eddies. In a typical turbulent flow, there exists a wide range of eddy sizes fluctuating at different frequencies (i.e., large eddies have large velocity fluctuations of low frequency and vice versa). To capture each addy in LES, minimum four CFD mesh is required as shown in Fig. 4.1(a). Mesh can resolve different sizes of eddies as shown in Fig. 4.1(b). As each eddy fluctuates at a specific frequency, hence, only a

certain range of frequency can be transported by a specific maximum grid spacing in LES (Selvam, 2017; Sagaut et al., 2003). The largest frequency that a grid can resolve is called f_{LES} as shown in Fig. 4.2. Additionally, to avoid LES filtering effects, the filter length (Δ) is considered equal to grid spacing size (h) (i.e., Δ/h=1) in the current LES modeling. Hence, eddies with the wavelength (L) smaller than filter length (Δ) which equals to mesh size here (i.e., Fig. 4.1 (c)) cannot be resolved and are modeled by a sub-grid scale model such as Smagorinsky model. In Fig. 4.2, the non-dimensional maximum and minimum frequency from field measurements or WT is referred *to* f_{maxe} and f_{mine}. Furthermore, the non-dimensional maximum frequency (f_{max}) used as input to the inflow turbulence models is referred to f_{max} and the minimum one is f_{min}.

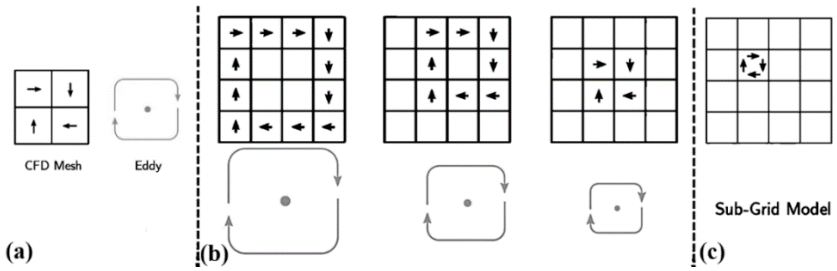

Fig. 4.1. Different eddy sizes compared to the mesh size.

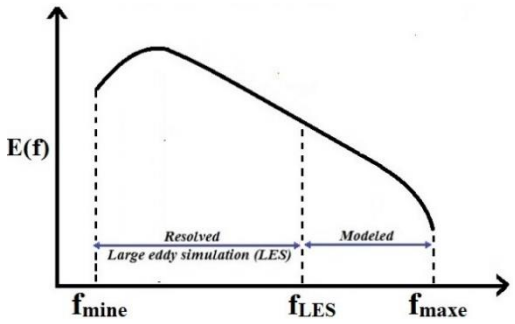

Fig. 4.2. Frequency region resolved and modeled by LES

For a specific grid spacing of h, the minimum wavelength L of a wave in the form of sine or cosine function transported by the Fourier spectral method is $2h$ (Orszag, 1979). The corresponding

frequency is called the Nyquist frequency in the spectral analysis. Even though transport of Nyquist frequency is possible with the spectral method, the amount of error using the finite difference method (FDM) is very high. Consequently, to have fewer errors, Ferziger and Peric (2002) and Kravchenko and Moni (1997) suggested *L=4h* for finite difference or control volume method, which its corresponding frequency is f_{grid}. Even to have more than 90% accuracy, Selvam (2017) recommended using *L=10h*, but this level of the refined grid is not practical. An example of transporting a sine wave with the wavelength of 2h and 4h is provided in appendix 4.B to understand it. In the appendix 4.B, the error of transporting of a sine wave with the wavelength of 2h is shown around 100%, which is not acceptable. For the wavelength of 4h, it is around 25%.

As discussed, the highest frequency that can be transported by the grid will be f_{grid} and it equals f_{LES} in the LES studies. As a result, with a reasonable error, *L=4h* can transport a wave with the frequency of n_{LES} and the corresponding non-dimensional frequency of f_{LES}. f_{LES} *in* terms of L is calculated by Eq. 1 as the relation between frequency and wavelength is $L = U_H/n$.

$$f = \frac{1}{\lambda} = \frac{H}{L} = \frac{nH}{U_H} \tag{4.1}$$

Where λ is the non-dimensional wavelength, H is the building height, and U_H is the mean velocity at the building height. Hence, the suggested highest non-dimensional frequency transported in the flow using the FDM and LES is calculated as $f_{LES}=f_{grid}=H/4h$ using Eqn. 4.1. As an example, for *L=4h* and *h=H*/16 grid, f_{LES} is calculated as $f_{LES} = H/(4H/16) = 4$. Rana et al. (2011) reported that the inflow turbulence using Digital Filter Method (DFM) dissipate immediately in the computational domain because the energy is not distributed over the required range of frequencies. Similarly, Kokkinos's et al. (2020) tried to budget energy to low-frequency to reduce the numerical dissipation of the scheme and thus improve the accuracy of the results, particularly for under-

resolved grids. Hence, this study tries to present the effect of choosing frequency beyond f_{LES} on peak pressure results.

4.1.3. Definition of Spurious Pressure

Rigall et al. (2021), Haywood (2019) and Lebovitz (2017) reported that spurious pressure occurs due to using many of inflow turbulence generator methods. Rigall et al. (2021) used the adapted RFG method and Lebovitz [16] used DFM. In all these works, the mentioned spurious pressure happens when the pressure frequncy is higher than the velocity frequncy. As an example, when the inflow turbulence field is calculated using CDRFG for the $f_{max}=10$ and the grid spacing of $h=H/16$, the Nyquist frequency is $H/2h=H/2(H/16)=8$ for this grid. In Fig. 4.3, the pressure is plotted at the inlet and building location for this case. If frequencies are taken as the number of peaks or cycles per unit time, the pressure frequency is about 9 to 10. As velocity frequency cannot be higher than Nyquist frequencuy, spurious pressures are pressures that have freqencies higher than the Nyquist frequency in this study. Hence, the above-mentioned case has spurious pressures.

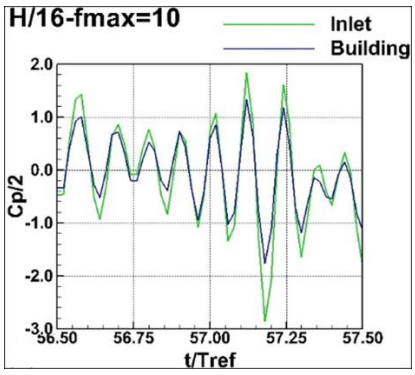

Fig. 4.3. Non-dimensional velocity at the inlet and the building location and pressures coefficient at the building location without building for $h=H/16$, $f_{max}=10$, and for 1 time unit.

It should be noted that previous researchers identified pressure fluctuation and stated some reasons for these unwanted pressures. As an example, if an inflow does not preserve momentum for each

spatial direction (i.e., does not respect the Taylor hypothesis) or does not respect mass conservation (i.e, being divergence-free), produces unwanted pressure fluctuations as explained by Patruno and Ricci (2017). In addition, boundary condition mismatches lead to unwanted pressure productions near boundaries as explained in detail by Patruno and Ricci (2018). Patruno and Miranda (2020) developed a method to mitigate unwanted pressures created due to violation of divergence free condition and Taylor hypothesis. However, they used only a sine wave that respects LES frequency and wavenumber and they stated pressure fluctuation decreases after a distance from the inlet (Fig. 4.4). Whereas, what is declined is the amplitude of pressure fluctuation and not its frequency (Fig. 4.3). In Fig. 4.3, pressure is plotted at the building height at the inlet and the building location. As it can be seen in this figure, the amplitude of pressure decreases at the building location compared to the inlet location. However, the frequency of pressure remains unchanged. Mansouri et al. (2022) showed similar issues using other methods such as the digital filter method.

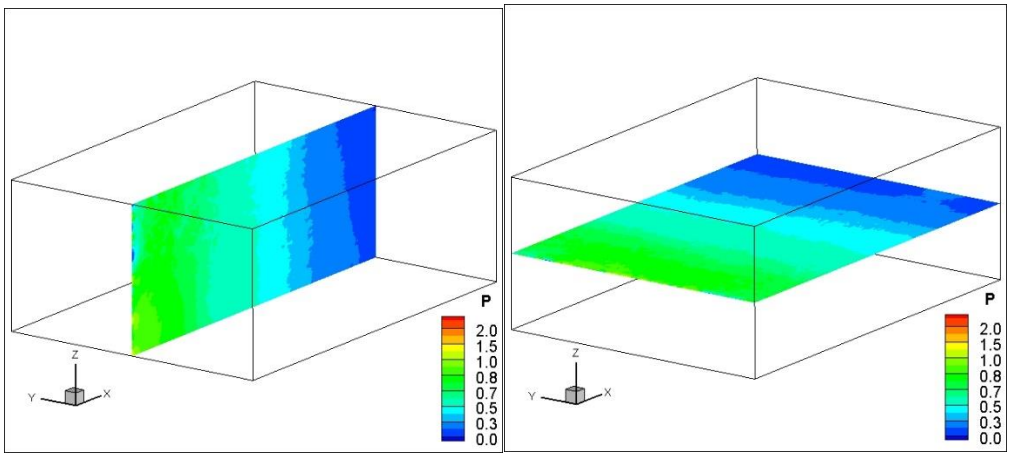

Fig. 4.4. Pressures coefficient contour without building for $h=H/16$, $f_{max}=10$

4.1.4. Objectives

Generally, $f_{max}=f_{maxe}$ and $f_{min}=f_{mine}$ are used as input to inflow turbulence generators regardless of the CFD grid size.

1. To understand the effect of various f_{max} on spurious pressures, CFD model without building is considered for f_{max} of f_{maxe} and f_{LES} for the grid spacing of $H/16$, and then the pressure coefficient over time is plotted at the building location.

2. To show the effects of spurious pressure on peak pressures, CFD model with building is considered. First, the peak pressures on the 1:6 scale TTU building are calculated for f_{max} equal to f_{maxe} and f_{LES} for various grid spacing (i.e., $H/8$, $H/16$, and $H/24$). These results are compared with the WT and field measurements results reported by Moravej (2018). Since the finest grid leads to 8.62 million grid points, we did not go for further refinements, and *H/16* are chosen to use for investigating the effect of f_{max} used in the inflow turbulence model on peak pressures. The f_{max} in the CDRFG is varied from less than f_{LES} to f_{maxe}.

3. Finally, based on the analysis of the above work, a proper procedure to use the synthetic turbulence method to calculate peak pressures with less error is proposed.

4.2. Numerical Setup

4.2.1. Computer Modeling and Boundary Conditions.

The 3D incompressible Navier–Stokes (NS) equations are used for flow computations, and Large Eddy Simulation (LES) with Smagorinsky one equation model is used for turbulence modeling. The three-dimensional equations for an incompressible fluid using LES model in general tensor notation are as follows:

Continuity equation: $U_{i,i} = 0.$ (4.2)

Momentum equation: $U_{i,t} + U_j U_{i,j} = -(p/\rho + 2k/3)_{,i} + \left[(\nu + \nu_t)\left(U_{i,j} + U_{j,i}\right)\right]_{,j,}$ (4.3)

Where, $\nu_t = (C_s h)^2 \left(S_{ij}^2/2\right)^{0.5}, S_{ij} = U_{i,j} + U_{j,i}, h = (h_1 h_2 h_3)^{0.333}$ for $3D$, and $k = (\nu_t/(C_k h))^2$; empirical constants are $C_s = 0.1$, and $C_k = 0.094$

The details of the equations and the solution procedure for the NS equation based on the fractional step are reported by Selvam (1997). The variables in the NS equations are approximated by the central difference method. A non-staggered grid system is used. The variables in time are approximated by the Crank-Nicolson method. The momentum equations are solved by line iteration, and pressure equations are solved by preconditioned conjugate gradient (PCG) method. The PCG algorithmic details are provided in Selvam (1996). A maximum sub-iteration of 10 is used in addition to reducing the error for required convergence in momentum and continuity equations at each time step. Hence, the errors in all the equations are eliminated. The NS equations are non-dimensionalized using the building height (H) and the average velocity at the building height (U_H) as the reference values. The corresponding reference time (T_{ref}) is calculated as H/U_H. The roughness length (z_0) is 0.05 m.

The uniform grid spacing of $H/8$, $H/16$, and $H/24$ (where H is the building height of the TTU building) in all directions are considered in the current study. The domain size used for computation is $13.3H \times 9.375H \times 5H$, and the location of the building within the computational domain is shown in Fig. 4.5. The grid size equals $213 \times 151 \times 81$ with 2,605,203 nodes for $H/16$ grid spacing and $319 \times 226 \times 121$ with 8,723,374 nodes for H/24 grid spacing. The building is located at $4H$ from the inflow. The dimension of the TTU building is $2.25\text{H} \times 3.375\text{H} \times \text{H}$, where H is 3.96m. The flow is considered to be along with the shorter length ($2.25H$) of the TTU building. Although CFL (Courant–Friedrichs–Lewy) can be greater than 1.0 because of using implicit solvers, the *CFL* criterion is kept less than 1.0 to capture all the time-variant issues. The maximum velocity around the building is approximately $2U_H$ based on the computation; thus, the $dt =$

$dX/U_{max} = (H/16)/2U_H = 0.03125(H/U_H)$ or the non-dimensional time step dt should be less than 0.03125 to preserve $CFL < 1.0$. In this study, a non-dimensional time step of $\mathrm{dt} = 0.02$ is used, and the corresponding *CFL is equal to 0.64.* The computation is conducted for 100 non-dimensional time units (5000 time steps for *H*/16 grid). The Reynolds number ($\mathrm{Re}=HU_H/\nu$) used in the CFD model is $2.5\text{x}10^6$. The Re is calculated based on the full-scale dimensions reported in Table 4.1.

Table 4.1. Turbulent Characteristics for the TTU Building (Mooneghi et al., 2016; Aboshosha et al., 2015).

Parameters	**Full-Scale Model**
Reference height	$H = 3.96\ m$
Reference wind velocity	$U_H = 7.66\ m/s$
Mean velocity	$U_{ave} = U_H\left(\frac{z}{H}\right)^{\alpha}\ m/s, \alpha = 0.326$
Turbulence Length scale	$L_j = L_{jH}\left(\frac{z}{H}\right)^{dLj}, m\ j = u, v, w$ $L_{uH} = 0.302\ m, L_{vH} = 0.0815\ m, L_{wH} = 0.0326\ m$ $dL_u = 0.473, dL_v = 0.881, dL_w = 1.539$
Turbulent intensity I	$I_j = I_{jH}\left(\frac{z}{H}\right)^{-dj}, j = u, v, w$ $I_{uH} = 0.216, I_{vH} = 0.207, I_{wH} = 0.120$ $d_u = 0.191, d_v = 0.123, d_w = 0.005$
Minimum frequency	$n_{min} = 0.19\ (Hz)$ $f_{min} = 0.1$
Maximum frequency	$n_{max} = 1.93, 3.9, 5.8, 7.74, 15.44, and\ 19.23\ (Hz)$

	$f_{max} = 1, 2, 3, 4, 8, and\ 10$
number of time step	5000 for *H*/8 & *H*/16 grid and 10,000 for *H*/24
Time step	$dT = 0.0103$ s for *H*/8 & *H*/16 and 0.005s for *H*/24 $dt = 0.02$ units for *H*/8 & *H*/16 and 0.00965 units for *H*/24
M, Number of frequency segments	100
N, Number of random frequencies in one segment	100
Frequency steps	$\Delta n = \left(\frac{n_{max} - n_{min}}{M - 1}\right) = 0.02, 0.04, 0.06, 0.08, 0.15, \& 0.19$ (Hz) $\Delta f = \left(\frac{f_{max} - f_{min}}{M - 1}\right) = 0.01, 0.02, 0.03, 0.04, 0.08, \& 0.1$

The boundary conditions are indicated for all surfaces in Fig. 4.5. The symmetric boundary conditions are implemented on the sidewalls, and the outflow boundary condition is specified at the outlet. On the wall, no slip with the law of the wall condition is implemented. At the inflow, the calculated velocities using the CDRFG method are applied at each time step. The details of the inflow velocity computation are described in section 4.2.2. The CDRFG method calculates velocity field as follows:

$$u_i(x_j, t) = \sum_{m=1}^{M} \sum_{n=1}^{N} p_i^{m,n} cos\left(k_j'^{m,n} x_j^m + 2\pi f_{m,n} t\right) + q_i^{m,n} sin\left(k_j^{m,n} x_j^m + 2\pi f_{m,n} t\right) \quad (4.4)$$

In this equation, x_j^m are non-dimensionalized coordinates by dividing real coordinates x_j to $L_j^m = U_{ave}/\gamma C_j f_m$, , and $k_j'^{m,n}$ are coordinates of uniformly distributed points on a unit radius sphere that satisfy the divergence-free condition in the CDRFG method. Details for calculation constants

(i.e., C_j and γ) and amplitudes (i.e., $p_i^{m,n}$and $q_i^{m,n}$) based on the wind spectrum are described by Aboshosha et al. (2015).

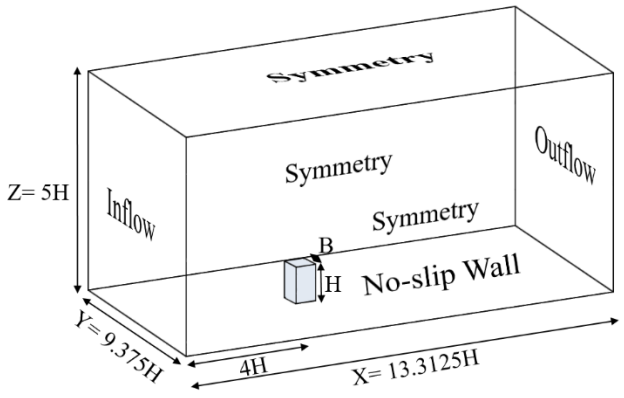

Fig. 4.5. Boundary conditions for the numerical modeling.

4.2.2. The Inflow Turbulence Computation Details

The input data details for the CDRFG MATLAB program are provided by Aboshosha et al. (2015). The velocity at the inflow is computed for the actual TTU building and then the velocity is scaled to non-dimensional value via dividing by U_H. The considered turbulent characteristics in the field indicated in Table 4.1 are derived from Mooneghi et al. (2016). The turbulent spectra equations used for the three velocities and the coherence functions used are reported in detail by Aboshosha et al. (2015) and they are not repeated here. An analytical equation for the WT spectra is not available for the 1:6 scale study and so we used the von Karman spectra until the peak values of the WT spectra match with the von Karman spectra. Since the verification and validation were conducted in the above reference using the MATLAB code, this work focuses mainly on the effects of spurious pressure error and high-frequency wind at the inflow on peak pressures on the building.

The f_{min} is kept at a constant value of f_{mine}=0.1. The f_{max} varies for different grids. If f_{max}=f_{LES} is kept as per section 4.1.2, then for *H*/8, *H*/16, and *H*/24 grid the f_{max} comes to be 2, 4, and 6

respectively. The different f_{max} used in the CFD calculations are between $f_{max}<f_{LES}$ and $f_{max}=f_{maxe}$ frequencies are 1,2,3, 4, 8, and 10. The dimensional frequency n_{max} can be calculated knowing f_{max} using Eq. 4.1. As an example, for f_{max}=10, $n_{max}=f_{max}U_H/H$=10x7.66/3.96=19.34 Hz. Similarly, other ones can be converted to dimensional ones and are reported in Table 4.1. Aboshosha et al. (2015) calculated the number of frequency segments (i.e., *M*) of 50 using the formula $M=f_{max}/2f_{min}$ for f_{max}=10 and f_{min}=0.1. They used random frequencies number *N* in one segment (i.e., *N*) as 100. In the current study, *N* has kept the same value of 100, and *M* is kept 100 for all cases. The dimensional time step (dT) used in the CDRFG is calculated knowing the non-dimensional time step of dt=0.02 for *H*/16 and *H*/8 grid as follows:

$$dt = \frac{dT}{T_{ref}} \Rightarrow dT = dt \times T_{ref} = dt \times \frac{H}{U_H} = 0.02 \times \frac{3.96}{7.66} = 0.0103 \quad (4.5)$$

The CDRFG program is run using the above-mentioned initial data, and the velocities at the inlet are stored for 5000 time steps or 100 non-dimensional time units for *H*/8 and *H*/16 grid and 10,000 time steps for *H*/24 grid. The produced dimensional velocities from CDRFG are converted to the non-dimensional ones via dividing the velocities by U_H. Then, these inlet velocities are read from the input file at each time step. The initial conditions in the computational domain for velocities are provided as mean velocities.

4.3.Wind Tunnel Test Detail

In the 1:6 scale WT study conducted by Mooneghi et al. (2016) and Moravej (2018), the TTU building model height was 0.66 m and the mean wind speed at the building height was 19.48 m/s. For this large-scale testing, the Re was $8.6x10^5$, which is much closer to the field Re of $2.5x10^6$, compared to that in any other WT study in the literature. The wind spectrum from the WT study

was compared with the Von Karman spectrum in Moravej (2018). The discrepancy of the 1:6 WT spectrum with respect to the Von Karman spectrum in the low-frequency range (f<0.1) is explained in detail. The local pressures on the building were measured using 204 pressure taps. The pressure taps were located exactly at the same location as in the field measurements for allowing meaningful comparison. The pressure coefficients were measured and reported for various wind directions with respect to the building (0° to 360°, at an increment of 3°). In this study, only the 90° wind direction range is considered for comparison with CFD computation. Further details on the WT study can be found in Moravej (2018).

4.4.Results and Discussions

The CDRFG method is chosen to investigate the effects of maximum frequency on the mentioned spurious pressure. Afterward, the effects of maximum frequency regarding different grid spacing sizes on the peak and mean pressure coefficients are investigated.

To validate the CDRFG method, the time-averaged velocity is calculated and compared with the targeted mean velocity profile for the grid spacing size of $H/16$ and f_{max}=10 (Fig. 4.6(a)). According to this figure, there is not any difference between the targeted and the calculated mean velocity profile. Furthermore, the velocity spectrum is plotted at the inlet and compared with the Von Karman spectrum (Fig. 4.6(b)). Likewise, a reasonable correlation exists between the CDRFG velocity spectrum and the Von Karman spectrum.

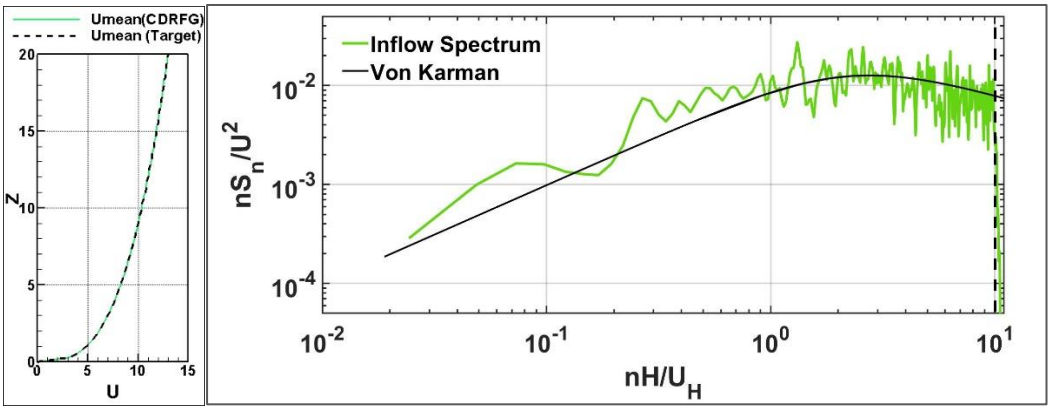

Fig. 4.6. Comparing a) the CDRFG mean velocity profile to the targeted one and b) the inlet velocity spectrum to the Von Karman spectrum.

6.1. Effects of $f > f_{LES}$ on Spurious Pressure at the Building Location

According to Fig. 4.7, pressure over time is plotted for f_{max}=10 and $f_{max} = f_{LES} = 4$ for the grid spacing size of H/16, on way to investigate the effects of maximum frequency on spurious pressures. In Fig. 4.7 (c) and (d), the pressure variation has the frequency of 10 and 7 respectively for f_{max}=10 and $f_{max} = f_{LES} = 4$ at the building location. Hence, as f_{max} decreases from 10 to f_{LES}, the frequency of pressure variation at the building location decreases to less than Nyquist frequency. Consequently, it seems the error of grid resolution considerably influences the spurious pressure fluctuations.

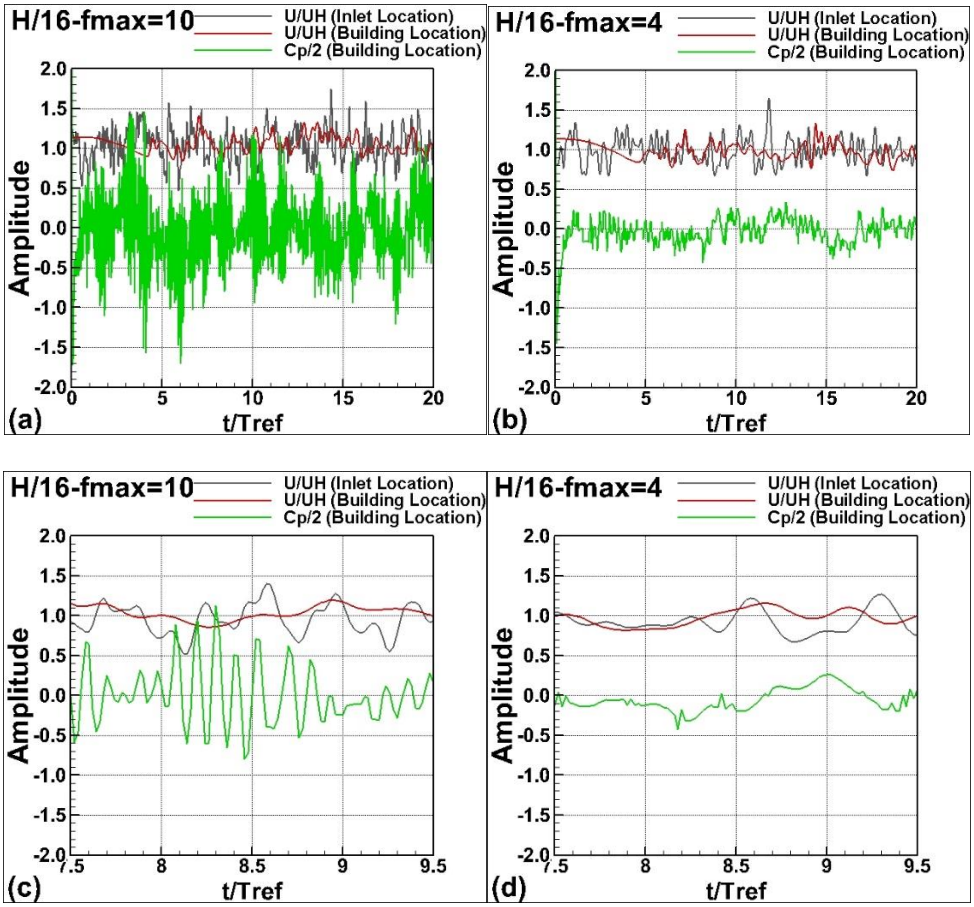

Fig. 4.7. Non-dimensional velocity at the inlet and at the building location and pressures coefficient at the building location without building for $h=H/16$ (a) f_{max}=10 (b) f_{max}=4 (c) f_{max}=10 close up to 2 time units (d) f_{max}=4 close up to 2 time units.

4.4.1. Effect of Spurious Pressure on the Peak Pressure Results

To investigate the effects of spurious pressure existence on the pressure results, the peak pressure is firstly compared with WT and field pressure measurements for different grid sizes at f_{max}= 10 and $f_{max}=f_{LES}$. To calculate the peak pressure, the following procedure is used. Generally, about 10 time units are needed for the turbulent flow to be fully developed and hence it is ignored. The remaining data from 10 time units to 100 time units are considered to capture the peak pressures at each point in time. Then, the peak pressure results will be compared with WT pressure

measurements for different f_{max} for the grid size of H/16. Finally, it will be shown that the mean pressure result as an evaluation option is not reliable.

4.4.2. Comparison of Minimum and Maximum Peak Pressures for Various Grid Size Spacing for fmax =10 and Grid's fLES with WT and Field Measurements

In the LES computation, the grid spacing h determines the f_{max} used as we discussed in detail before. Hence, for different grid spacing, different $f_{max}=f_{LES}$ are used in Fig. 4.8(d) to (f). To compare the current procedure of using f_{max}=10 and $f_{max}=f_{LES}$, the minimum pressure coefficient C_{pmin} is reported in Fig. 4.8 for 3 different grid sizes (H/8, H/16 and H/24). The top figures are for f_{max}=10 and the bottom figures are $f_{max}=f_{LES}$. From left to right the grid is refined. One can see the high error for f_{max}=10 in Fig. 4.8(a) to (c). The pressure coefficients are approaching the WT values from higher absolute value for f_{max}=10 case as in Fig. 4.8(a) to (c) and from lower absolute value for $f_{max}=f_{LES}$ case as in Fig. 4.8(d) to (f). The $f_{max}=f_{LES}$ case is similar to solid mechanics grid convergence studies. The high error in H/8 grid in Fig. 4.8(d) may be due to not having the necessary grid resolution as well as violating the isotropic assumption of the LES. So, systematic convergence due to grid refinements are observed in Fig. 4.8(e) to (f) using $f_{max}=f_{LES}$ more clearly than in Fig. 4.8(a) to (c) using f_{max}=10. In Fig. 4.8(a), for not having proper grid refinement C_{pmin} should be less than the WT and field measurement but shows the other way because of numerical error, spurious pressure error, and other errors before. The roof error is reduced and the C_{pmin} is much close to WT and field measurements when $f_{max}=f_{LES}$ but the windward and leeward errors are high even for the case of $f_{max}=f_{LES}$. From Fig. 4.8(d) to (f) one can also see that H/16 grid C_{pmin} values are close to H/24 grid and this is the reason H/16 grid is considered for many comparisons in the next sections. If $f_{max}=f_{grid}=f_{LES}$>10, then some of the numerical errors mentioned in Fig.

4.8(a) to (c) could be avoided automatically but with extensive computer storage and computer time. The *H*/24 grid took close to 8 days whereas *H*/16 grid took about a day for each computation.

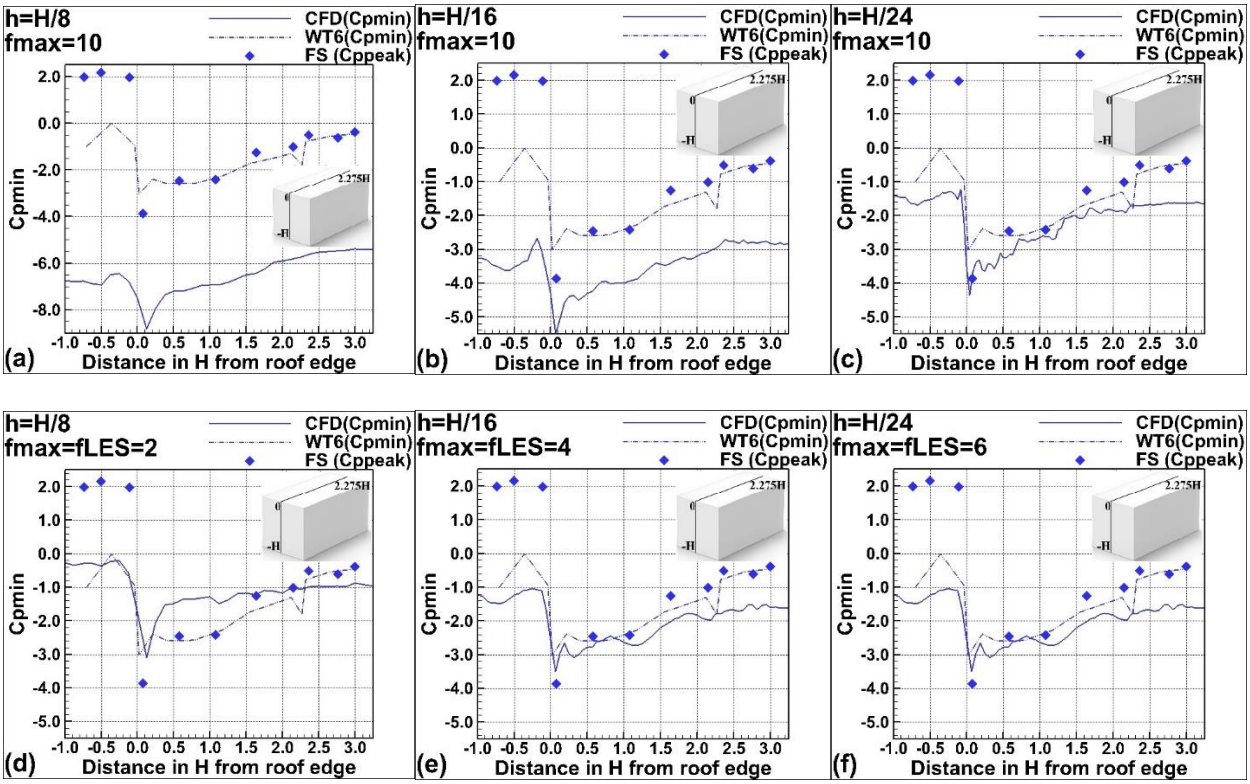

Fig. 4.8. Grid convergence study for minimum pressure coefficients for (a) $h=H/8$ and $f_{max}=10$, (b) $h=H/16$ and $f_{max}=10$, (c) $h=H/24$ and $f_{max}=10$, (d) $h=H/8$ and $f_{max}= f_{LES} =2$, (e) $h=H/16$ and $f_{max}= f_{LES} =4$, and (f) $h=H/24$ and $f_{max}= f_{LES} =6$.

Similarly, to compare the current procedure of using $f_{max}=10$ with $f_{max}=f_{LES}$, the maximum pressure coefficients C_{pmax} are plotted in Fig. 4.9 for 3 different grid sizes (H/8, H/16 and H/24). The top figures are for $f_{max}=10$ and the bottom figures are $f_{max}=f_{LES}$. From left to right the grid is refined. One can see the high error for $f_{max}=10$ in Fig. 4.9(a) to (c). In Fig. 4.9(f) for *H*/24 grid, the maximum peak pressure coefficient is in much better agreement with field data than *H*/16 and H/8 grids. In Fig. 4.9(d) to (f) also one can see that on the windward wall the error is less for *H*/8 grid than *H*/16. For computing negative pressure *H*/8 grid is not sufficient.

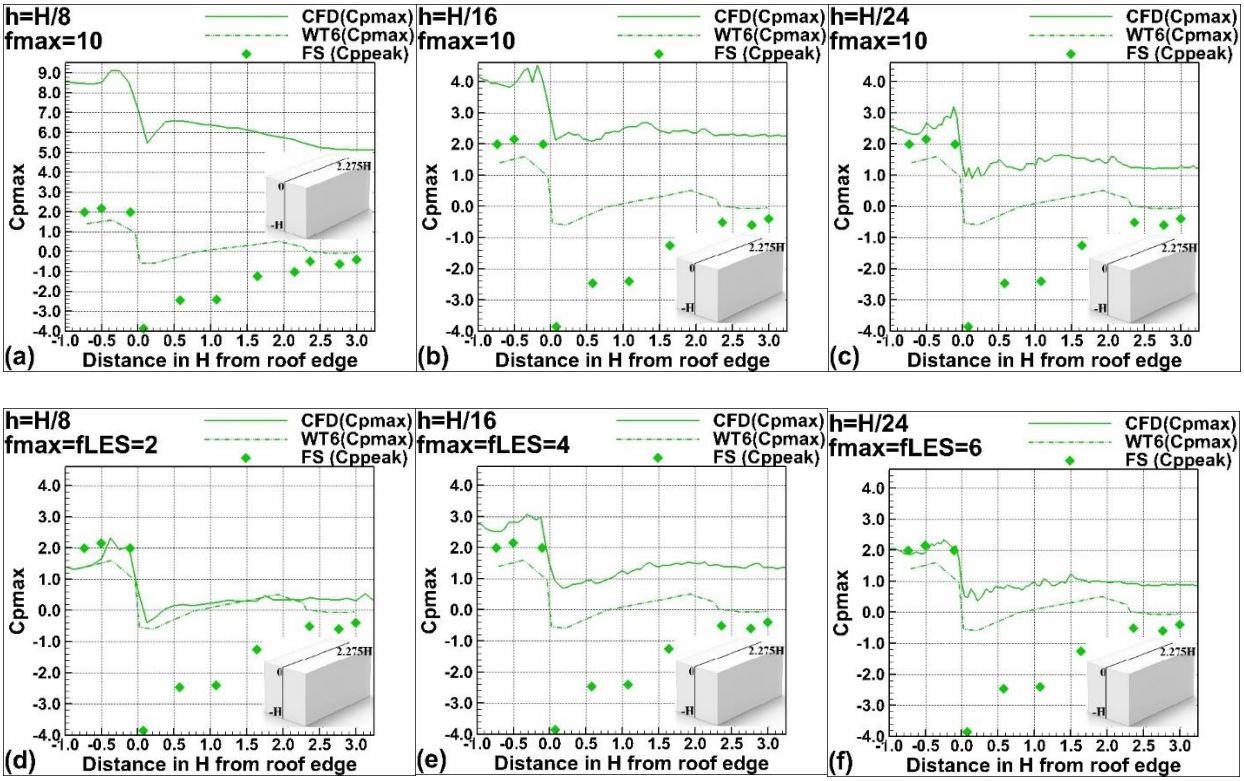

Fig. 4.9. Grid convergence study for maximum pressure coefficients for (a) $h=H/8$ and f_{max}=10, (b) $h=H/16$ and f_{max}=10, (c) $h=H/24$ and f_{max}=10, (d) $h=H/8$ and $f_{max}= f_{LES}$ =2, (e) $h=H/16$ *and* $f_{max}= f_{LES}$ =4, and (f) $h=H/24$ and $f_{max}= f_{LES}$ =6.

4.4.3. Comparison of Minimum and Maximum Peak Pressures for Various fmax with WT

To evaluate that f_{LES} is chosen correctly, the minimum peak pressure coefficients C_{pmin} for the six f_{max} cases are plotted in Fig. 4.10 for $H/16$ grid. The minimum values are calculated using the same 10 time units to 100 time units data. The CFD peak pressures are compared with WT6 and field data. The error on the roof is very high for f_{max}=10 (Fig. 4.10(a)), and as f_{max} decreases, the error decreases systematically (Fig. 4.10(b) to (f)). The maximum errors on the roof are around 100%, 92%, 33%, 33%, 31% and 33% for f_{max} values of 10, 8, 4, 3, 2, and 1 respectively. Whereas the errors are far higher in all the six cases on the windward and leeward sides, the errors are reduced somewhat for lower f_{max}.

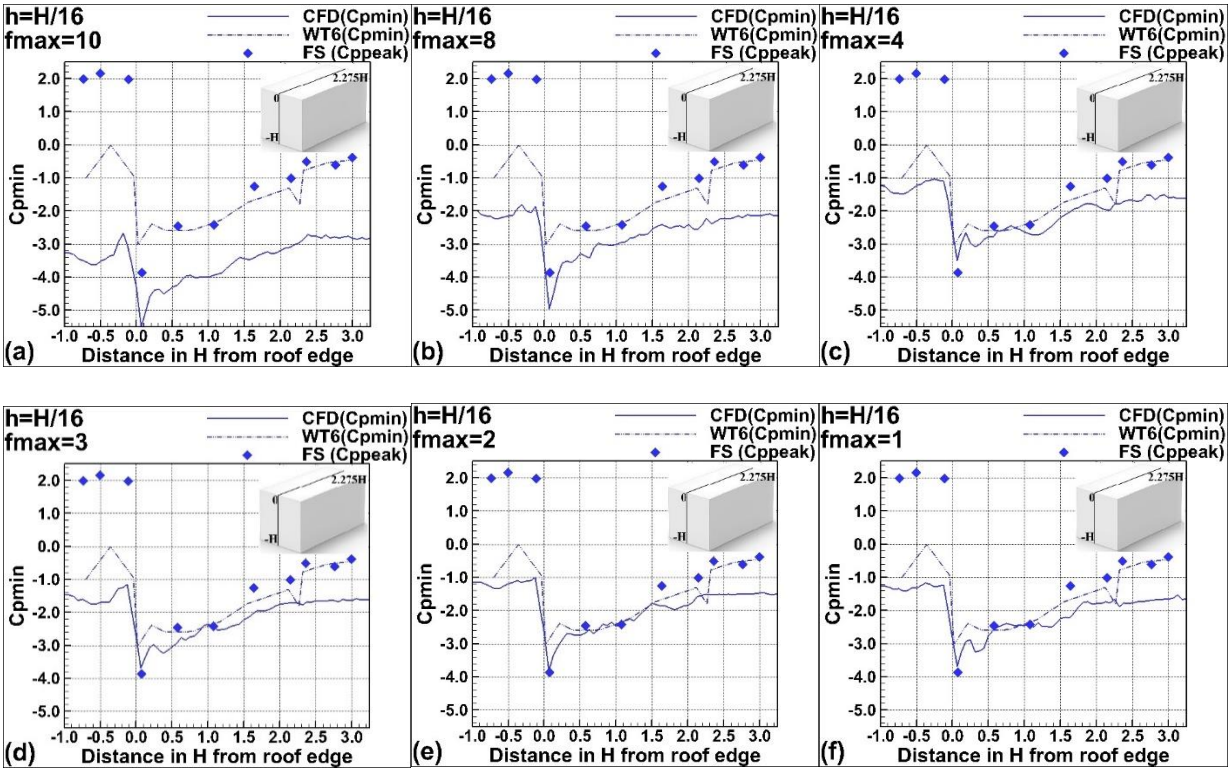

Fig. 4.10. Minimum pressure coefficients for various f_{max} using $H/16$ grid spacing (a) f_{max}=10, (b) f_{max}=8, (c) f_{max}=4, (d) f_{max}=3, (e) f_{max}=2, and (f) f_{max}=1.

The maximum errors on the windward and leeward side for the six cases in the order of decreasing f_{max} are 600% to 200%. Therefore, the f_{LES} cutoff issues on the C_{pmin} can be seen. According to Fig. 4.10(a) to Fig. 4.10(c), a dramatic reduction in error on the roof and side walls is observed due to f_{LES} issue or the error in transporting high-frequency velocities that cannot be transported by the given grid spacing of h. The changes are not noticed from Fig. 4.10(c) to (f). The suggestion of 4 points to represent the shortest wave or for f_{LES} by Ferziger and Peric (2002) is reasonable in this case.

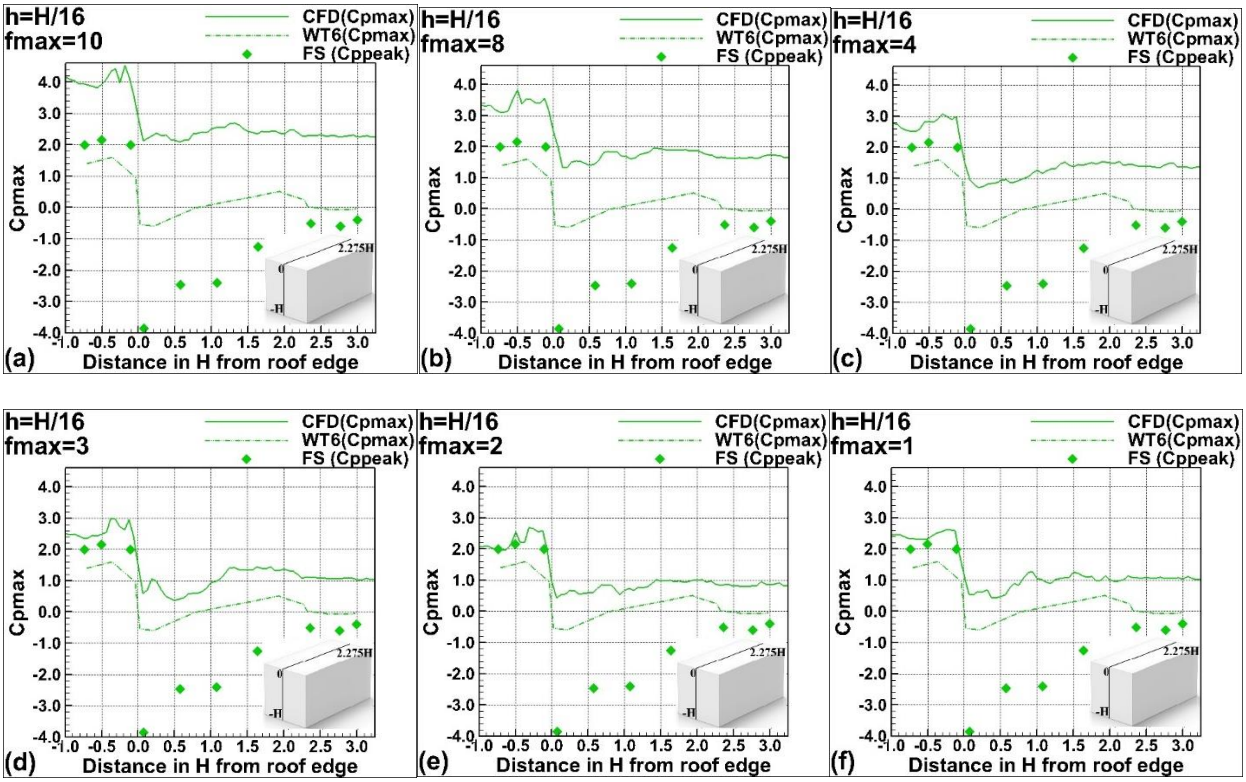

Fig. 4.11. Maximum pressure coefficients for various f_{max} using H/16 (a) f_{max}=10, (b) f_{max}=8, (c) f_{max}=4, (d) f_{max}=3, (e) f_{max}=2, and (f) f_{max}=1.

The maximum pressure coefficients C_{pmax} are also compared in Fig. 4.11(a) to (f) with WT and field measurements using H/16 grid for the same f_{max}. The effect of $f_{max}>f_{LES}$ has the same trend as before. The CFD C_{pmax} were approaching the WT and field measurements on all sides as the f_{max} decreases up to four. For f_{max}=4 or less, the CFD C_{pmax} has high errors (more than 200%) on the roof with respect to WT measurements. Whereas in Fig. 4.10, the roof pressures are much closer (around 20% error) compared to WT measurements.

As it can be seen, peak pressure on the building gets high errors due to spurious pressure. In CDRFG methods, there is not any control on initializing the maximum wavenumber and it is chosen randomly and then corrected with forcing continuity equations. To illustrate this, the

maximum wavenumber can be carried by the grid, the CDRFG wavenumber, and general methods wavenumber are provided below:

These wavenumbers are calculated for the grid spacing size of $H/16$ and $f_{max}=f_{LES}$ = 4, in the building height of H=3.96 m, and U_H =7.66 m/s.

1. For the CDRFG method, the equivalent wavenumber is $k_j^{m,n} = k'^{m,n}_j f_m \gamma C_j / U_{ave}$ from Eqn. 4.4 (i.e., the CDRFG method's velocity equation). Hence, the maximum dimensional wavenumber can be calculated as $k_{d_{CDRFG}} = 65.6$ (1/m) in the direction X (driven from CDFRG output). Subsequently, the maximum nondimensional wavenumber is $k_{n_{CDRFG}} = 260$.

2. In general, for other methods, the relation between wavenumber and frequency in the many RFG methods is $k_{d_G} = 2\pi n / U_{ave}$. Hence, the maximum dimensional wavenumber is $k_{d_G} = 2\pi n_{max} / U_H = 6.55$ (1/m) in the direction X. Subsequently, the maximum nondimensional wavenumber is $k_{n_G} = 25.97$.
3. The dimensional LES wavenumber is $k_{d_{LES}} = 2\pi/(4h)$ (1/m) in the direction X as the maximum wavelength is $L=4h$ for LES. Subsequently, the nondimensional LES wavenumber is $k_{n_{LES}} = 2\pi H/(4h) = 25.12$.

As it can be seen, using $f_{max}=f_{LES}$ leads to having a wavenumber less than k_{LES} in methods that considered the general relation between frequency and wavenumber. Whereas, in the CDRFG, using $f_{max}=f_{LES}$ does not lead to wavenumber being less than k_{LES} and it led to existing peak pressure errors even for $f_{max}=f_{LES}$.

4.4.4. Comparison of Mean Pressure Coefficients for Various fmax with WT

The mean pressure coefficients C_p are calculated from 10 time units to 100 time units at each point along the centerline of the TTU building. The mean C_p values are comparable with WT6 as shown in Fig. 4.12(a) to (f) for the six f_{max} considered. Only minimal differences from one plot to another are noticed. The maximum error of 20% between WT and CFD is noticed at the windward roof edge, and in other places, the errors are less than this value. This discrepancy could be due to the particular inflow turbulence method used. This also can be easily seen that the mean pressure coefficient does not show the differences which exist and have been shown with peak pressure results.

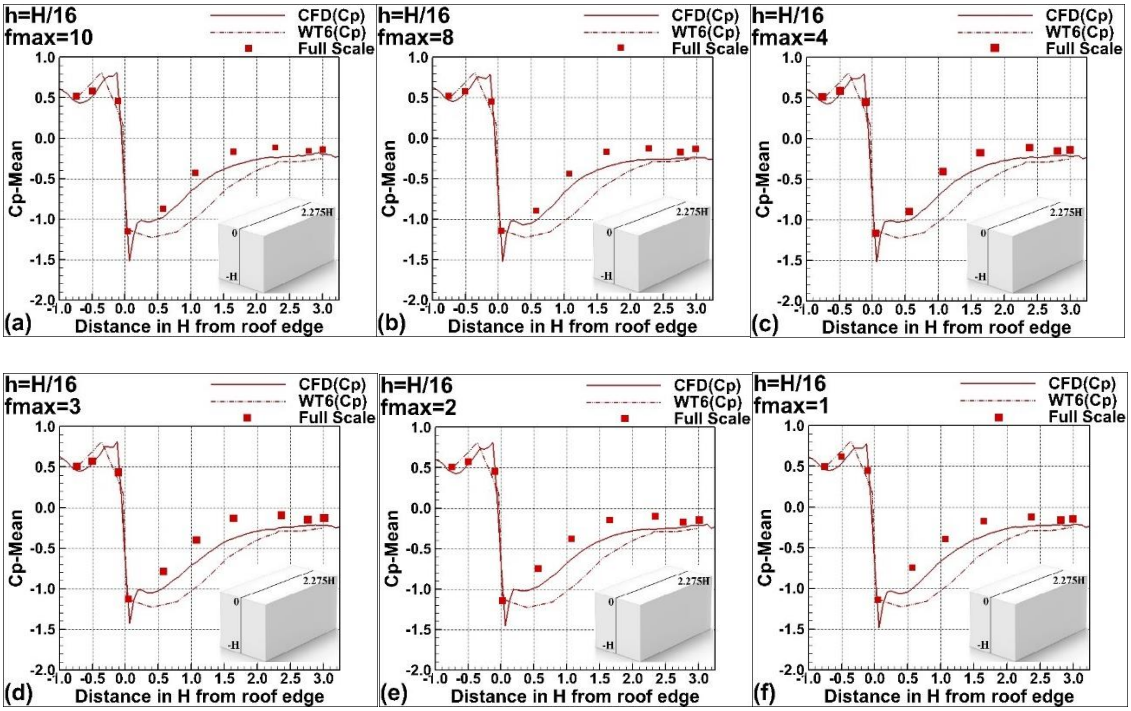

Fig. 4.12. Mean pressure coefficients for various f_{max} using H/16 grid spacing (a) f_{max}=10, (b) f_{max}=8, (c) f_{max}=4, (d) f_{max}=3, (e) f_{max}=2, and (f) f_{max}=1.

4.4.5. Suggestion to Use f_{max}= f_{LES} In Synthetic Inflow Methods

The inlet velocity spectrums, as well as the corresponding velocity spectrums at the windward edge of the building without the building, are shown in Fig. 4.12 at the building height of f_{max}=2, 4, and 10 as a sample. The targeted f_{max} is realized at the inflow as shown in Fig. 4.13(a) to (c). A dashed vertical line is placed in each figure to show the f_{max} point. According to Fig. 4.12(a) for f_{max} of 10, the high-frequency amplitude or energy is cut off beyond f_{max}= f_{LES} =4 at the building location due to the grid resolution effect. Whereas there is a reasonable correlation between the inlet and building location spectrum in Fig. 4.13(b) and (c) when the f_{LES} is less than or equal to f_{LES} =4. However, for all cases oversampled more than the targeted f_{max}. This f_{max}=2 is for the smallest wavelength of $8h$. Generally, it is proposed to use more than 10 points for a wave using FDM to have less error but this can take more computer time. However, as peak pressure results error for smaller f_{max} than 4 roughly equal to the peak pressure results for f_{max} of 4, hence, choosing f_{max} of 4 (i.e., L of $4h$) is reasonable to avoid computational costs.

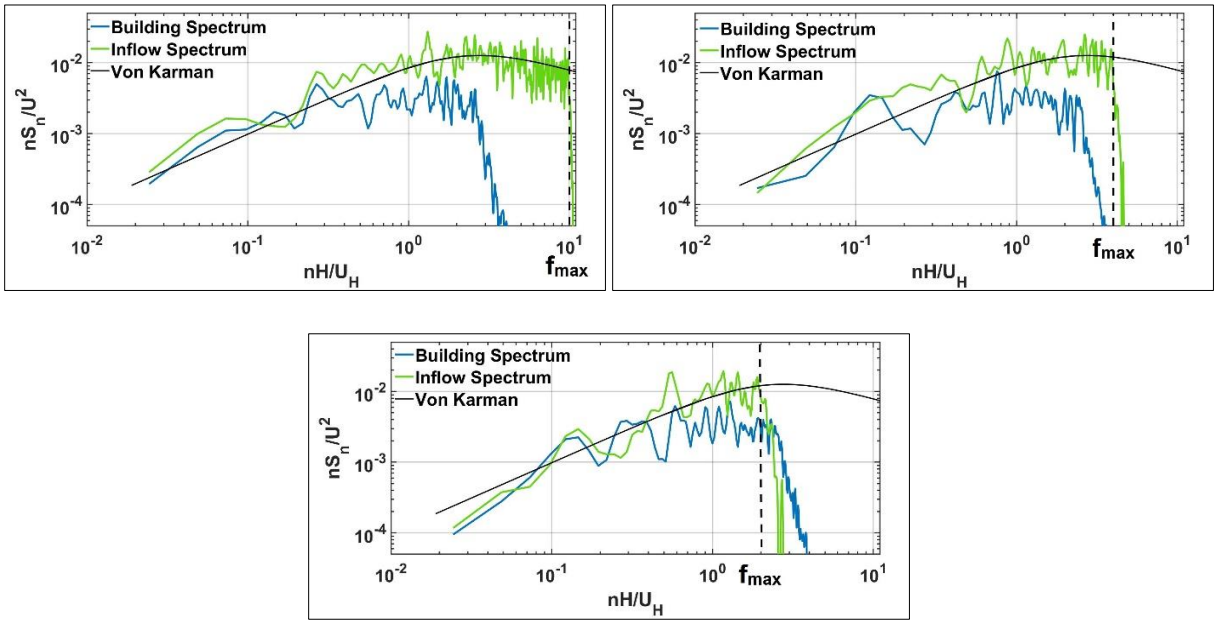

Fig. 4.13. Velocity spectrum at the inlet and building location without building for various f_{max} using H/16 grid (a) f_{max}=10 (b) f_{max}=4 and (c) f_{max}=2.

Overall observations from this analysis are as follows:

1. As per the LES theory, for a given grid spacing *h*, the f_{max} to be used in the inflow spectrum is f_{grid} (4 when $L=4h$ for $h=H/16$) and this is called f_{LES}. The high frequencies beyond this value are modeled by subgrid-scale modeling like the Smograinsky model. If this is violated there are spurious pressures. This is illustrated using velocity and pressure plots at the building location without building computations.
2. Due to spurious pressure, the peak pressure on the building gets high errors and this is not illustrated in the past.
3. Thus the $f_{max}>f_{LES}$ effect on peak pressure is not been properly understood from the CFD point of view in the past. This is illustrated systematically by considering different f_{max}.
4. From our calculations, it is found that even for $f_{max}=4$, the peak pressure has some error for $H/16$ grid. This is because frequency cutoff does not lead to wavenumber cutoff in the CDRFG method.
5. The final conclusion is, the peak pressures are affected by f_{max} and one has to be careful in making the proper choice of f_{max} for a given grid size.

Procedure for computation of inflow turbulence using synthetic inflow turbulence method:

1. Get the f_{maxe} and f_{mine} from the field or wind tunnel experiment.
2. Decide on the largest grid spacing h to be used for the CFD modeling. This depends upon the computer storage and time available. Using this *h* calculate $f_{grid} = H/L_{min}$ where $L_{min}=4h$. Then keep $f_{max}=f_{LES}=f_{grid}=H/L_{min}$ in the inflow turbulence generator
3. The smallest frequency f_{min} is kept as f_{mine}.

4. Using these parameters calculate the inflow turbulence.

4.5. Conclusions

The following conclusions are made by comparing the CFD peak pressures with 1:6 scale TTU wind tunnel peak pressures for different grid spacing.

1. The largest grid spacing h in the computational domain determines the highest frequency of the velocity fluctuations transported by the grid (f_{grid}) from the inflow turbulence. In the LES computation, the suggested highest frequency transported in the flow using the finite difference method (FDM) is $f_{LES}=f_{grid}=H/4h$ where $4h$ is the smallest wavelength resolved by the grid.
2. If $f_{max}>f_{LES}$ velocity spectrum is considered at the inlet, these velocities introduce spurious pressures at the building locations.
3. *S*purious pressures lead to having high errors in peak pressure results (more than 600% error on the sidewall and 100% on the roof for H/16 grid) on the building. This is illustrated by comparing the CFD pressure with WT measurement for the TTU building.The computed inflow turbulence using the CDRFG method for $f_{max}=f_{LES}$ input cases also has some level of spurious pressures due to k_{LES} violation in the CDRFG method. However, using $f_{max}=f_{LES}$ for all the grid spacing size of H/8, H/16, and H/24 leads to reductions of spurious pressure and improvement of peak pressure results.

Data Availability Statement

Some or all data, models, or code generated or used during the study are available from the corresponding author by request.

All plotted data.

Acknowledgments

Ms. Zahra Mansouri acknowledges the financial support from the James T. Womble Professorship from the University of Arkansas. For this research, wind tunnel data from the NHERI WOW EF were used. The authors acknowledge the help provided by Dr. M. Moravej from Walker Consultants in delivering the wind tunnel data in a way we could use it in this work. The authors also acknowledge Dr. G. Bitsuamlak and his research group for providing the CDRFG MATLAB code to generate the inflow turbulence.

Notation

The following symbols are used in this paper:

A = Amplitude of the wave equation

C_p = Mean pressure coefficient

C_{pmin} = Minimum pressure coefficient

C_{pmax} = Maximum pressure coefficient

dt = Non-dimensional time step

dT = Dimensional time step

f = Non-dimensional frequency= $nH/U_H = H/L$

f_{LES} = Maximum frequency cutoff for LES

f_{grid} = Maximum frequency transported by the grid spacing h using FDM

f_{max} = Maximum frequency provided for MATLAB code for inflow computation

f_{min} = Minimum frequency provided for MATLAB code for inflow computation

f_{maxe} = Maximum frequency from the field or WT velocity spectrum

f_{mine} = Minimum frequency from the field or WT velocity spectrum

$H =$ Building height

$h =$ Maximum grid spacing

$I_u =$ Turbulence intensity in x direction

$I_v =$ Turbulence intensity in y direction

$I_w =$ Turbulence intensity in z direction

$k_m =$ Wavenumber in the many RFG methods.

$k_j^{m,n} =$ Wavenumber in the CDRFG method.

$k_{H_{max}}^{m,n} =$ Maximum wavenumbers at the building height.

$k_j'^{m,n} =$ coordinates of uniformly distributed points on a unit radius sphere that satisfy the divergence-free condition in the CDRFG method.

$L =$ Wavelength for a given frequency n

$L_{min} =$ Smallest wavelength transported by LES

$L_u =$ Turbulence length scale in *x* direction

$L_v =$ Turbulence length scale in *y* direction

$L_w =$ Turbulence length scale in *z* direction

$M =$ Number of random frequencies in one segment for CDRFG

$N =$ The number of frequency segments for CDRFG

$n =$ Dimensional frequency

$n_{max} =$ Maximum dimensional frequency

$n_{min} =$ Minimum dimensional frequency

$Re =$ Reynolds number $= U_H H/\nu$

$T_{ref} =$ Reference time

$U_{ave} =$ Average velocity

U_H = Average velocity at building height

x_j = Real coordinates

x_j^m = Non-dimensionalized coordinates

z_0 = Roughness length

Δ = Filter length in LES

λ = Non-dimensional wavelength = $L/H = U_H/nH$

References

Aboshosha, H., Elshaer, A., Bitsuamlak, G. T., and El Damatty, A. (2015). Consistent inflow turbulence generator for LES evaluation of wind-induced responses for tall buildings. *Journal of Wind Engineering and Industrial Aerodynamics*, 142, 198-216

Atencio Mojica, Z. D. (2021). Frequency Effect on Peak Pressure Coefficients Using the Narrowband Synthesis Random Flow Generator (NSRFG) Method, Graduate Theses and Dissertations Retrieved from https://scholarworks.uark.edu/etd/4204.

Chow, F. K., and Moin, P. (2003). A further study of numerical errors in large-eddy simulations. *Journal of Computational Physics*, 184, 366-380.

Daniels, S. J., Castro, I. P., & Xie, Z. T. (2013). Peak loading and surface pressure fluctuations of a tall model building. *Journal of wind engineering and industrial aerodynamics*, 120, 19-28.

Davidson, L. (2018). Fluid mechanics, turbulent flow and turbulence modeling. Chalmers University of Technology, Goteborg, Sweden, Available from: http://www.tfd.chalmers.se/˜lada/MoF/text book.html

Ding, F., Kareem, A., and Wan, J. (2019). Aerodynamic tailoring of structures using computational fluid dynamics. *Structural Engineering International*, 29, 26-39.

Ferziger, J. H., and Perić, M. (2002). Computational methods for fluid dynamics. Berlin: Springer, 3, 196-200.

Haywood, J. S. (2019). Turbulent inflow generation methods for Large Eddy Simulations, Mississippi State University.

Keating, A., Piomelli, U., Balaras, E., and Kaltenbach, H. J. (2004). A priori and a posteriori tests of inflow conditions for large-eddy simulation. *Physics of fluids*, 16, 4696-4712.

Kim, Y., Castro, I. P., and Xie, Z. T. (2013). Divergence-free turbulence inflow conditions for large-eddy simulations with incompressible flow solvers. *Computers & Fluids*, 84, 56-68.

Kokkinakis, I. W., Drikakis, D., Ritos, K., and Spottswood, S. M. (2020). Direct numerical simulation of supersonic flow and acoustics over a compression ramp. *Physics of Fluids*, 32, 066107.

Kravchenko, A. G., and Moin, P., (1997). On the effect of numerical errors in large eddy simulations of turbulent flows, *Journal of Computational Physics*, 131, 310-322.

Lebovitz L. (2017) Modelling and time-resolved numerical simulations of urban turbulent wind flows around buildings, Master's thesis, ETH Zurich.

Mansouri, Z., Selvam, R. P., and Chowdhury, A. G. (2022). Performance of different inflow turbulence methods for wind engineering applications. *Journal of Wind Engineering and Industrial Aerodynamics*, 229, 105141.

Mooneghi, M. A., Irwin, P., and Chowdhury, A. G. (2016). Partial turbulence simulation method for predicting peak wind loads on small structures and building appurtenances. *Journal of Wind Engineering and Industrial Aerodynamics*, 157, 47–62.

Moravej, M. (2018) Investigating scale effects on analytical methods of predicting peak wind loads on buildings, Ph.D. thesis, FIU. Miami, Florida.

National Weather Service (NWS), (2019). National Oceanic and Atmospheric Administration. https://www.weather.gov.

Orszag, S. A. (1979). Spectral methods for problems in complex geometrics. Numerical methods for partial differential equations, 273-305. Academic Press.

Patruno, L., and Ricci, M. (2017). On the generation of synthetic divergence-free homogeneous anisotropic turbulence. *Computer Methods in Applied Mechanics and Engineering*, 315, 396–417

Patruno, L., and Ricci, M. (2018). A systematic approach to the generation of synthetic turbulence using spectral methods. *Computer Methods in Applied Mechanics and Engineering*, 340, 881-904.

Patruno, L., and de Miranda, S. (2020). Unsteady inflow conditions: A variationally based solution to the insurgence of pressure fluctuations. *Computer Methods in Applied Mechanics and Engineering*, 363, 112894.

Poletto, R., Craft, T., and Revell, A. (2013). A new divergence free synthetic eddy method for the reproduction of inlet flow conditions for LES. *Flow, turbulence and combustion*, 91, 519-539.

Rana, Z. A., Thornber, B., and Drikakis, D. (2011). On the importance of generating accurate turbulent boundary condition for unsteady simulations, *Journal of Turbulence***,** 12, N35.

Rigall, T., Cotté, B., and Lafon, P. (2021). Low-noise synthetic turbulence tailored to lateral periodic boundary conditions, *Fluids*, 6, 193.

Sagaut, P., Garnier, E., Tromeur, E., Larchevêque, L., and Labourasse, E. (2003). Turbulent inflow conditions for LES of supersonic and subsonic wall bounded flows. In *41st Aerospace Sciences Meeting and Exhibit*, 68.

Selvam, R. P. (1996). Computation of flow around Texas Tech building using k-ϵ and Kato-Launder k-ϵ turbulence model. *Engineering structures*, 18, 856-860.

Selvam, R. P. (1997). Computation of pressures on Texas Tech University building using large eddy simulation. *Journal of Wind Engineering and Industrial Aerodynamics*, 67, 647–657.

Selvam, R. P. (2017). CFD as a tool for assessing wind loading. Bridge Structural Engineer, 47, 1-8.

Selvam, R. P. (2022). Computational Fluid Dynamics for Wind Engineering: Chichester, Wiley-Blackwell.

Woods, J. (2019). Turbulent effects on building pressure using a two-dimensional finite element program. Master's thesis, Department of Civil Engineering, University of Arkansas.

Yu, Y., Yang, Y., and Xie, Z. (2018). A new inflow turbulence generator for large eddy simulation evaluation of wind effects on a standard high-rise building. *Building and Environment*, 138, 300–313.

Appendix 4.A - Details of the Pressure Coefficient Graphs

The pressure results were reported in different plot types explaining in the following to understand the effects of different inflow turbulence conditions on the building peak pressure. The average, maximum, and minimum C_p versus x-distance along the building centerline with the origin on the roof edge (Fig. 4.A.1).

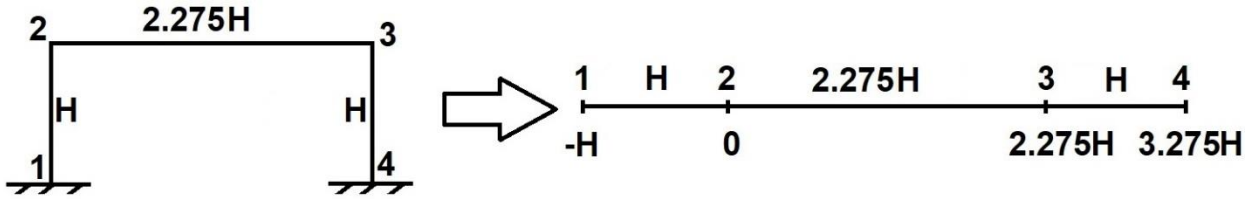

Fig. 4.A.1. The centerline of the building with the origin on the roof edge considering in peak pressure result presentations.

Appendix 4.B. - Grid Spacing *h* and the Wave Frequency (f_{grid}) Transported Using FDM with Less Error Example:

To understand the amount of error involved in transporting a sine wave with wavelength *L=2h* and *4h*, let us transport a sine wave of amplitude A with constant velocity for a computational domain length of 2L. Thus the number of grid points (*IM*) in the computational domain will be *IM=5* for *L=2h* and *IM=9* for *L=4h*. The governing equation and boundary conditions are:

$$\frac{\partial A}{\partial t}+\frac{\partial A}{\partial x}=0.0 \text{ with } 0<x<2L, \begin{cases} at\ x=0 \Rightarrow\ A=sin\left(-\frac{2\pi t}{L}\right) \\ at\ t=0\ \Rightarrow\ A=sin\left(\frac{2\pi x}{L}\right) \end{cases} \qquad (B.1)$$

The exact value of *A* for any x and t is: $A=sin[(2\pi/L)(x-t)]$

Here L is considered to be 1 unit and the computational domain length is considered to be 2. The propagation speed is unit value. The wave equation is approximated by the central difference (CD) method in space and Crank-Nicolson method in time. On the left end at *x*=0, the sine function is specified in time. By keeping the CFL number to be 0.1, computation is done for 2.25 units of time. In the LES computation, central difference method is used for space approximation because of no numerical dissipation as discussed by Davidson [29].The upwind schemes have some level of numerical dissipation and that affect the accuracy of the LES computation with inflow turbulence generation. To illustrate this issue, upwind (UW) method with *h=L/4* case is also considered for comparison. Even though practical applications of CFD are three-dimensional and in the turbulent flow, computations get more complicated, the one-dimensional problem gives some idea on the issue we are talking about.

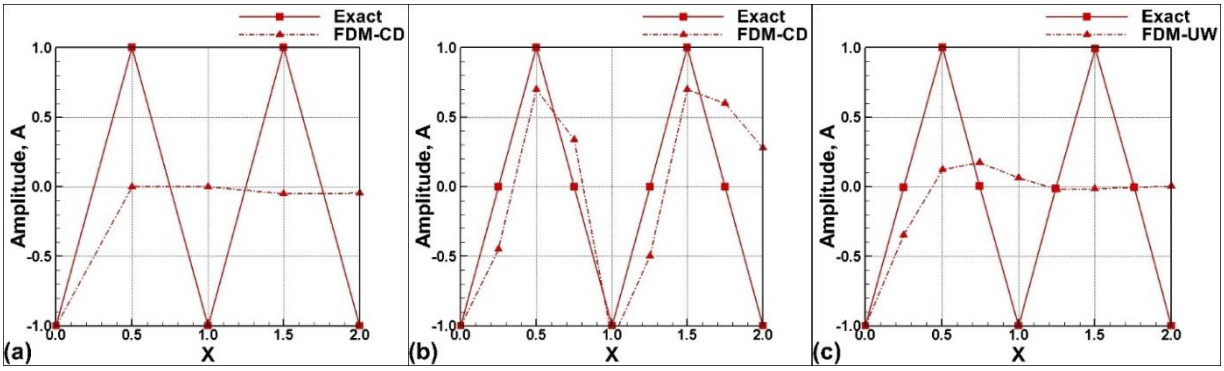

Fig. 4.B.1. Comparison of an exact sine wave transport with the FDM method after 2.25 time units. (a) $h=L/2=0.5$ units using CD method , (b) $h=L/4=0.25$ units using CD method and (c) $h=L/4=0.25$ units using UW method.

From Fig. 4. B.1(a) and (b), one can see that pretty much for $h=0.5$ ($L=2h$), the amplitude of the sine wave is close to zero and for $h=0.25$ ($L=4h$), one can see the sine wave with some error for CD method. To have a better visualization the exact solution is also plotted for comparison. The performance of UW method for $L=4h$ is shown in Fig. 4.B.1(c). Because of the diffusive nature of the UW scheme, the amplitude is lost within $2L$ distance of transport. From this illustration, we can conclude that for a given grid spacing h, a wave-length $L=4h$ or more can be transported, and the corresponding frequency f_{grid} can be calculated using Eq. 4.1. In calculating f_{grid} one should use the largest grid spacing at the inflow when variable grid spacings are used because any frequency greater than this will be filtered by the grid as shown in Fig. 4.12 (a) and it is illustrated in section 4.4.4.

Chapter 5- Paper 5

Performance of Different Inflow Turbulence Methods for Wind Engineering Applications

Zahra Mansouri[1], Rathinam Panneer Selvam[2] Ph.D., P. Eng., F. ASCE, and Arindam Gan Chowdhury[3] Ph.D., A.M. ASCE

[1]Graduate Student, BELL 4190, University of Arkansas, Fayetteville, AR 72701, USA, zmansour@uark.edu

[2*]University Professor, BELL 4190, University of Arkansas, Fayetteville, AR 72701, USA, rps@uark.edu

[3] University Professor, Florida International University, Miami, FL, chowdhur@fiu.edu

Abstract:

Defining the correct inlet boundary conditions for large eddy simulations is a critical issue in computational wind engineering. Since synthetic inflow turbulence does not require costly prior flow simulations like recycling or precursor methods, it is a preferable approach. In this study, different synthetic turbulence generator methods are considered to investigate their performance in wind engineering applications. The considered methods are a) Digital Filter Methods (DFM), b) Synthetic eddy methods (SEM) with different shape functions, c) Divergence Free Synthetic Eddy Method (DFSEM), and d) two types of Anisotropy Turbulent Spot Method (ATSM). These methods are provided in Turbulence Inflow Tool (TInF) from the SimCenter (https://simcenter.designsafe-ci.org/backend-components/tinf/). Additionally, velocity spectrum at the inlet and building location is compared to the Von Karman spectrum for different inflow

methods to determine how well the energy is carried from the inlet to the building location. Furthermore, different methods are evaluated to see whether they produce spurious pressure in the domain. It is concluded that spurious pressure exists in all the considered methods except SEM method with the Gaussian shape function (SEM-G). In addition, SEM-G is found to be a suitable method for peak pressure prediction on buildings with upmost 30% error.

Keywords: Synthetic inflow turbulence, Turbulence Inflow Tool, Large eddy simulation, Digital filter method, Synthetic eddy methods, Divergence free synthetic eddy method, Anisotropy turbulent spot method.

5.1.Introduction

Winds are the most damaging compared to all other environmental loads on buildings and structures. Almost 75 percent of all disaster claims paid by insurance providers have resulted from tornado and hurricane damage in the last 20 years (Exponent, n.d.). Wind engineering helps to mitigate the risk of future damage by understanding the wind's mechanism. When the wind is obstructed by a structure, it applies forces to the structure. The disastrous failure of structures caused by strong winds is mainly due to the underestimation of peak wind pressures while designing the building components. Building codes provide approximate wind pressure on buildings. More precise wind pressure estimation requires field measurements, wind-tunnel testing, or computational fluid dynamics (CFD) models of wind flow. As an illustration, for component and cladding, the maximum peak pressure coefficient (Cp), obtained from ASCE 7-16, is -3.2 for a low-rise building. However, field measurements have reported that the maximum peak Cp on a low-rise building can be even lower than -8 for the Silsoe building (Richards et al., 2007).

Conducting field measurements for design purposes is expensive and time-consuming, CFD can be an economical tool for engineers to estimate wind pressures on buildings. Furthermore, as the flow speed increases, the flow tends to be more unstable and irregular. Most flows in nature are categorized in this type of flow which is called turbulent flow. Strong winds are highly turbulent and if wind turbulence is not reasonably accounted for, the computed wind loads would not be accurate for building design purposes. Wind turbulence impacts can be incorporated using various turbulence modeling methods in CFD. Among all turbulence modeling methods, Large Eddy Simulation (LES) is economically feasible and provides an acceptable level of accuracy for peak pressure estimation.

5.1.1. Inflow Turbulence Generation Methods

LES simulations without an inflow turbulence field results in underestimation of peak pressure coefficients. As a result, a proper turbulent flow field at the inlet as an inflow boundary condition (BC) is required to predict peak Cp correctly. The turbulent flow field's behavior in the interior domain is extremely dependent on the inflow field's physical quality. Thus, a critical aspect of the numerical LES is defining the right inflow turbulence BC as mentioned by Selvam (1997). Selvam (1997) reported at least 30% error in CFD peak Cp compared to field measurements which was due to low grid resolution and inflow BCs. Thornber et al. (2010) reported that although very fine grid is needed to capture an appropriately broad range of initial scales, mixing layer growth is strongly dependent on initial boundary conditions. Enormous inflow turbulence generation methods are developed which are primarily categorized to (a) precursor database, (b) recycling method, and (c) synthetic turbulence (Keating et al, 2004). The weakness of the first and second methods is the need for a database that makes these methods computationally expensive. As synthetic inflow turbulence does not require costly prior flow simulations, it is a more

economically practical approach (Aboshosha et al., 2015; Ding et al., 2019). Synthetic turbulence methods include a wide range of methods that can be classified into a) Random Flow Generation Methods (RFG), b) Digital filter methods (DFM), and c) Synthetic Eddy Method (SEM). In following, a summary of the basics of each method is provided.

DFM filters a random velocity field to produce spatial and temporal coherent structures. This method does not satisfy the divergence-free condition and produces unphysically large pressure fluctuations in LES. Hence, Kim et al. (2013) first used a simple correction to maintain the constant mass flux in the inflow field, and then, inserted the generated turbulence inflow to the plane near the inlet during the procedure which led to velocities being adjusted by the velocity-pressure coupling procedure.

The idea of SEM, initiated by Jarrin et al. (2006), is rooted in the reproducing boundary layer using direct superposition of the representative coherent eddy structures. SEM assumes the flow contains randomly distributed turbulent spots. Every turbulent spot is modeled by a three-dimensional suitably normalized shape function with a compact support. Shape function depends on the two-point autocorrelation function and the power spectrum of the synthetic turbulence. In this study, for SEM, three different shape functions, i.e., Gaussian (SEM-G), Tent (SEM-T), and Step (SEM-S), are considered. For $0 \leq |x| < 1$, the equation of Tent shape function (Jarrin et al., 2009) is $f = \sqrt{3/2}\,(1 - |x|)$, for Step Shape function (Jarrin, 2008), it is $f = \sqrt{1/2}$, and for Gaussian Shape function (Jarrin, 2008), it is $f = Ce^{-9x^2/2}$, where C is a constant that satisfies $\int_{-1}^{1} f^2(x)dx = 1$. For $|x| \geq 1$, the amount of f is zero for all shape functions. In the Fig. 5.1, you can see the diagram for each shape function.

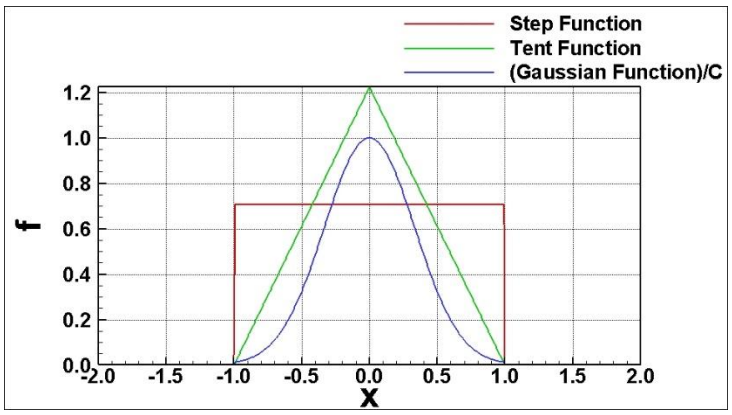

Fig. 5.1. Different SEM method shape functions

However, SEM like DFM is not divergence-free. Hence, Poletto et al. (2013) obtained a divergence-free method by applying SEM to the vorticity field and taking the curl of it to change back to the velocity field, i.e., Divergence Free Synthetic Eddy Method (DFSEM). Later, Kroger and Kornev (2018) proposed the Anisotropy Turbulent Spot Method (ATSM) method based on the superposition of vortical structures. This led to having explicit control on the three turbulence intensities and three integral length scales. The TInF tool refers Klein et al. (2003) and Xie and Castro (2008) for DFM, Jarrin et al. (2006) for SEM, Poletto (2013) for DFSEM, and Kröger and Kornev (2018) for ATSM as the source of the program they used in the OpenFOAM. The performance of these inflow turbulence methods is evaluated in this paper.

Nowadays, cutting-edge improvements in computational resources led to using higher grid resolution and the development of computational simulations with a promise of becoming adaptable, accessible, and reliable means for wind load estimations (Ding et al., 2019). However, there is not a proper evaluation of the characteristics and applicability of different synthetic inflow methods from the perspective of wind engineering. Hence, in this study, to evaluate different methods' performances for the wind engineering application, DFM, SEM with three different shape functions, DFSEM, and two types of ATSM are considered.

In the ATSM-R method Reynolds stresses are provided as input and only the two length scales (L_{11} and L_{22}) are taken from the input and the third one (L_{33}) is calculated internally from a constraint equation reported in Kroger and Kornev (2018). Similarly, in the ATSM-L method all the three length scales are given as input and the modified Reynolds stresses are calculated from minimization principle. The details of the derivations and the final equations are detailed in Kroger and Kornev (2018).

5.1.2. Velocity Spectrum at the Inlet and Building Location

Turbulent flow includes some circular movement of fluid called eddies. As turbulence is three-dimensional (3D) and unsteady with a large range of eddies that need to be resolved, it is necessary to develop the inflow velocity fields suitable for different scale features. In a typical turbulent flow, there exists a wide range of eddy sizes fluctuating at different frequencies (i.e., large eddies have large velocity fluctuations of low frequency and vice versa). The wind velocity spectrum describes the frequency distribution of turbulent wind flow and shows which range of eddies are produced by the inflow method. Hence, firstly, the velocity spectrum produced by the inflow method should be comparable to the Von Karman spectrum which describes the frequency distribution of the real turbulent wind flow. Furthermore, to have more accurate numerical results, the energy should not be dissipated in the building location compared to the inlet location. Rana et al. (2011) reported that DFM turbulent inflow data dissipates immediately in the computational domain because the energy is not distributed over the required range of frequencies. To reduce the numerical dissipation of the scheme and thus improve the accuracy of the results, Kokkinos's et al. (2020) tried to budget energy to low-frequency, particularly for under-resolved grids. Mansouri et al. (2022) stated that the maximum frequency as an input for the inflow methods should be determined using the largest grid spacing size in the computational domain to have a similar velocity spectrum

at the inlet and building location. In this study, DFM, SEM with three shape functions, DFSEM, and two types of ATSM are considered. The inputs to these methods are Reynolds stresses and length scales, therefore, maximum and minimum frequency cannot be predetermined as inputs. Hence, the maximum frequency of inlet velocity spectrum produced by these methods is regardless of the grid spacing size. Consequently, it is not clear how well the inlet and building location velocity spectrums are similar.

5.1.3. Spurious Pressure Due to High Frequency

As mentioned above, Mansouri et al. (2022) reported the largest grid spacing (h) in the computational domain determines the highest frequency of the velocity fluctuations that can be transported by the grid. For a specific grid spacing of h, the theoretical wavelength (L) of a wave in the form of sine or cosine function transported by a spectral method is $2h$ (Orszag, 1979). The corresponding frequency is called Nyquist frequency in the spectral analysis. Even though transport of Nyquist frequency is possible with the spectral method, the amount of error using the finite difference method (FDM) is significant. Hence, the smallest wavelength resolved by a grid is $\lambda_{grid} = 4h$ (Mansouri et al., 2022). Hence, the maximum non-dimensional frequency transported in the flow using the finite difference method (FDM) is calculated as $f_{grid} = H/4h$ using Eqn. 5.1. The high frequencies beyond this value are modeled by subgrid-scale modeling like the Smograinsky model (Mansouri et al., 2022).

$$f = \frac{H}{\lambda} = \frac{nH}{U_H} \tag{5.1}$$

Where n is dimensional frequency, λ is the wavelength, H is the height of the building, and U_H is the mean velocity at the building height. Mansouri et al. (2022) reported that if $f_{max} > f_{grid}$, then there are spurious pressures (f_{max} is the maximum frequency as the input to the inflow method).

Spurious pressures happen when the frequency of pressure goes beyond Nyquist frequency (Mansouri et al., 2022). They showed that the building peak pressure had high errors due to spurious pressure. It should be noted that previous researchers identified pressure fluctuation and stated some reasons for these unwanted pressures. For instance, if an inflow does not respect the Taylor hypothesis or not being divergence-free, produces unwanted pressure fluctuations (Patruno and Ricci, 2017). In addition to mentinoed reasons, boundary condition mismatches leads to unwanted pressure productions near boundaries as explained in detail by Patruno and Ricci (2018). Patruno and Miranda (2020) developed a method to mitigate unwanted pressures created due to violation of divergence free condition and Taylor hypothesis. However, they used only a sinewave that respects maximum grid frequency and they stated pressure fluctuation decreases after a distance from the inlet. Whereas, Mansouri et al. (2022) indicated that pressure amplitude declined and the pressure frequency remained unchanged over the space. As here, spurious pressure was introduced based on the pressure frequency but not its amplitude, no one has evaluated inflow methods to see whether they produce spurious pressure. This study investigates spurious pressure production.

5.1.4. Objectives to Investigate Different Inflow Generation Method Performance

In this study, DFM, SEM with three shape functions, DFSEM, and two types of ATSM method are considered. Reynolds stresses and length scales inputs are prepared based on the information provided by Mooneghi et al. (2016) for the WT data of Texas Tech University (TTU) building. The major objective of this work is to evaluate the performance of different inflow turbulence generators for wind engineering applications. The criteria used to evaluate the inflow methods' performance are:

a) Comparing the velocity spectrum at the inlet location and building location with the Von Karman spectrum for two different grid spacing sizes. This determines how well the energy is carried from the inlet location to the building location.
b) Plotting the pressure overtime at the inlet and building location to see how much spurious pressure is produced by various inflow methods.
c) Finally, the flow with the building is modeled for the proper inflow methods and the resulted peak pressure is compared to WT measurements reported by Moravej (2018a) to compare the most proper inflow methods' performance in predicting peak pressures.

5.2.Numerical Setup

5.2.1. Computer Modeling and Boundary Conditions.

In this study, the CFD program OpenFOAM is used to model flow in the domain. The 3D incompressible Navier–Stokes (NS) equations are used for flow computations, and Large Eddy Simulation (LES) with the sub-grid scale of wall-adapting local eddy viscosity model (WALE) explained by Nicoud and Ducros (1999) is used for turbulence modeling. The generalized geometric-algebraic multi-grid (GAMG) solver with a tolerance of 1e-5 is used for the pressure, and the symmetric Gauss-Seidel solver with a tolerance of 1e-6 is used for the rest of the variables. For coupling velocity and pressure, the PISO method is used, and the algorithm solves two times the pressure equation and momentum corrector in each step.

In this study, two uniform grid spacing sizes of $H/8$ and $H/16$ (where H is the building height of the Texas Tech University (TTU) building) in all directions are considered. The grid is made using "BlockMesh" generator in the OpenFOAM. More details for grid generation using "BlockMesh" are provided in Mansouri et. al (2021), Verma et. al. (2021), and Selvam (2022). The dimension of the TTU building is $2.25H \times 3.375H \times H$, where H is 0.66 m. The flow is

considered to be along with the shorter length ($2.25H$) of the TTU building. The domain size used for computation is $13.3H \times 9.375H \times 5H$, and the building is located $4H$ from inflow in the computational domain as shown in Fig. 5.2. The grid size equals $107 \times 76 \times 41$ with 333,412 nodes for the grid spacing size of *H*/8 and the grid size equals $213 \times 151 \times 81$ with 2,605,203 nodes for *H*/16. First, the flow is modeled in the domain without building in this study, and then the flow is modeled in the domain with building for the most proper inflow method for wind engineering application. Results are provided at the inlet and building location.

The *CFL* (Courant–Friedrichs–Lewy) criterion is kept at less than 1.0 to capture all the time-variant issues. The maximum velocity around the building is approximately $2U_H$ based on the computation; hence, the dimensional time step (dt) should be less than $dt = dX/U_{max} = (H/8)/2U_H = 0.0021$ to preserve $CFL < 1.0$ ($U_H = 19.48\, m/s$). In this study, a dimensional time step of $dt = 0.002$ is used for the grid spacing size of *H*/8. Similarly, to preserve $CFL < 1.0$, a dimensional time step of $dt = 0.001$ is used for the grid spacing size of *H*/16. The computation is conducted for 20 seconds or 590 non-dimensional time units. The computer time for the grid space of *H*/8 is about 4 hours and for *H*/16 is near 3 days.

The boundary conditions are indicated for all surfaces in Fig. 5.2. The zero-gradient boundary conditions are implemented on the sidewalls, and the outflow boundary condition is specified at the outlet. The no-slip wall is implemented on the ground. At the inlet, the inflow turbulence is introduced. The inflow turbulence is calculated using the Turbulence Inflow (TInF) tool, which is explained in the next section.

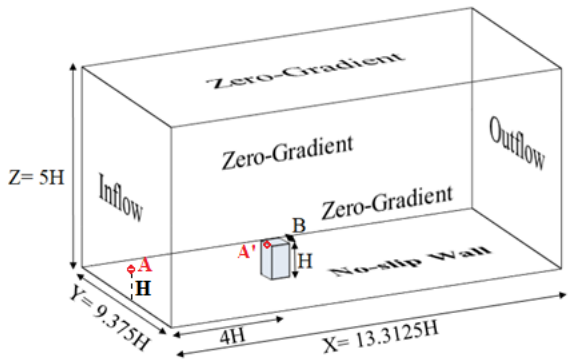

Fig. 5.2. Boundary conditions for the numerical modeling.

5.2.2. Initial Condition in TInF

After mesh generation, defining boundary conditions, and modifying all OpenFOAM case files (i.e., '0', 'constant', and 'system'), TInF is used to remodify files to apply a specific inflow turbulence generation method. The information provided in Table 5.1 is required to use TInF tool. For using TInF tool, after choosing the inflow method, the parameters related to inlet velocity profile, length scales, and Reynolds stresses should be inserted for the inlet boundary condition as explained in Appendix 5.A.

It should be noted that the length scales should be checked in the 'inflowProperties' file created by TInF tool in the 'constant' folder before running the case file. The length scale, L, should be defined in 'inflowProperties' file with a nine-component ($L_{11}, L_{12}, L_{13}, L_{21}, L_{22}, L_{23}, L_{31}, L_{32}, L_{33}$) for DFM and SEM, a three-component vector of the form (L_{11}, L_{22}, L_{33}) for the ATSM boundary condition, and one component scalar (L_{11}) for the DFSEM.

Table 5.1. Turbulent Characteristics for the TTU Building (Aboshosha et al., 2015; Mooneghi et al., 2016)

Test Characteristics	**WT 1:6 Model**

	$L_{11} = 0.43m, L_{12} = 0.2m \; and \; L_{13} = 0.13\,m$
Integral length scale	$L_{21} = 0.2L_{11} = L_{22} = L_{23}$
	$L_{31} = 0.3L_{11} = L_{32} = L_{33}$
Reference height	$H = 0.66\,m$
Reference wind velocity	$U_H = 19.48\,m/s$
Mean velocity	$\boldsymbol{U_{ave} = U_H \left(\frac{z}{H}\right)^{\alpha} m/s, \alpha = 0.326}$
Turbulent lengh scale *L*	$L_j = L_{1j} \left(\frac{z}{H}\right)^{dj} m$
	$L_{11} = 0.43, L_{12} = 0.2 \; and \; L_{13} = 0.13\,m$
	$dj = 0.473, 0.881, 1.539$ in the u, v and w directions
Reynolds stresses	R_{11}=4.3 R_{12}=1.8
	R_{22}=3.6 R_{23}=1.8
	R_{33}=3.5 R_{13}=1.8
Eddy density	1 only for SEM and DFSEM
Grid factor	1 only for DFM
Filter factor	4 only for DFM

The eddy density is a parameter to be given as input for SEM and DFSEM as reported in Table 5.1. Jarrin et al. (2009) and Poletto et al. (2013) defines eddy density 'd' as the volume of eddies in a box divided by the volume of the box. The volume of eddies is calculated as the number of eddies multiplied by the volume of an eddy. They recommend d=1 as the reasonable value and the TInF tool considers d=1 as the default value also. In the paper, we investigated further with d=1000 in section 5.3.2.

In case file preparation for the DFM method, the one correlation function (i.e., Gaussian, exponential or bessel) should be chosen. The details are provided in TInF tool report, section 10.2.1 (Wan and Mackenzie-Helnwein, 2020). In this study, the recommended function, i.e., exponential, is used. For exponential correlation function, it needs to provide values for grid factor and filter factor variables. In this study, the default value of 1 and 4 are used for grid factor and filter factor respectively.

5.3.Results and Discussion

Flow is modeled numerically for 590 nondimensional time units using different inflow turbulence generators as inflow for two grid spacing sizes of *H*/16 and *H*/8. The velocity spectrum at the inlet and building location (at the building height, which these points are shown in Fig. 5.2 as A(0,4.6875H,H) and A'(4H,4.6875H,H)) are plotted for 10000 time steps (i.e., about 300 nondimensional time units) using the modified MATLAB code provided by Moravej (2018b). To show the capability of each method in real wind turbulence field production and to determine how well the energy is carried from the inlet location to the building location, the velocity spectrum at the inlet and building location is compared to the Von Karman spectrum for different inflow turbulence fields. The velocity and pressure coefficients are plotted over time for different cases to investigate spurious pressure production and subsequently evaluate the performance of each inflow turbulence generation method. Finally, the flow with the building is modeled for the proper inflow methods and the resulted peak pressure is compared to WT measurements reported by Moravej (2018a) to compare the most proper inflow methods' performance in predicting peak pressures on buildings.

5.3.1. Velocity Spectrum at the Inlet and Building Location for Different Inflow Methods

The velocity spectrum is plotted for different inflow methods in Fig. 5.3 for the grid spacing size of $H/8$. According to Fig. 5.3(a), the DFM method wind spectrum is comparable to the Von Karman spectrum at the inlet location for the frequency range of (0.004-9) and has a sharp decline in energy beyond f=0.2 at the building location. The SEM-G method wind spectrum is comparable to the Von Karman spectrum at the inlet location for the frequency range of (0.004-0.4) and has a sharp decline in energy beyond f=0.2 at the building location from Fig. 5.3(b). This method has the most similar spectrum at the inlet and building locations.

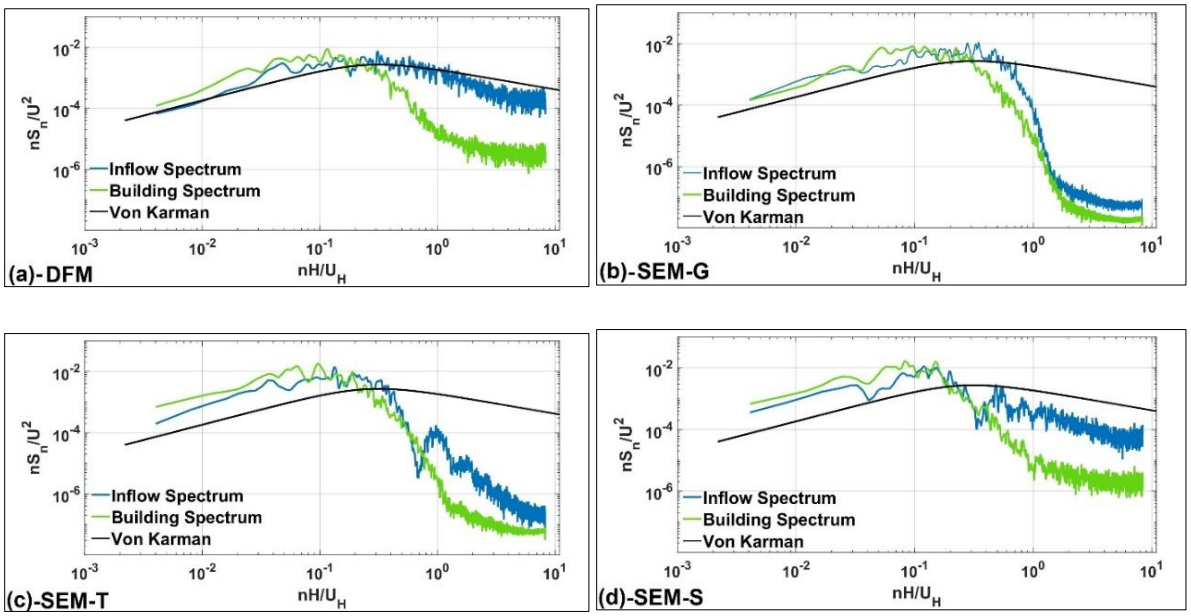

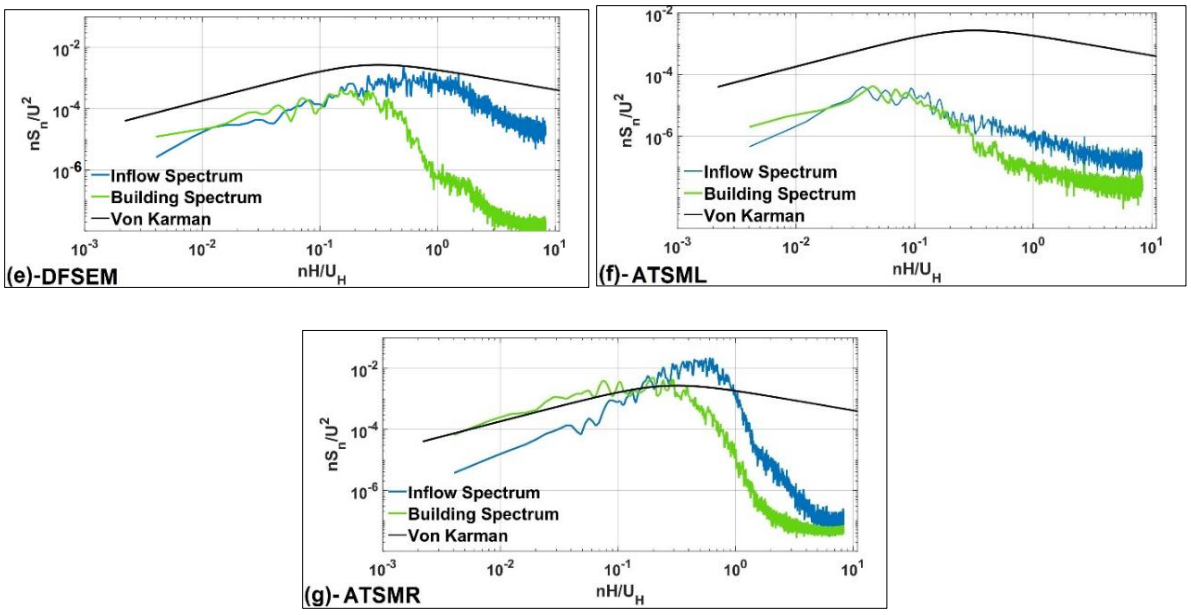

Fig. 5.3. Spectrum plot at the inlet and building location for (a) DFM, (b) SEM-G (i.e with guassian shape function), (c) SEM-T (i.e with tent shape function), (d) SEM-S (i.e with step shape function), (e) DFSEM with eddy density=1, (f) ATSML, and (g)ATSMR model for $dx=H/8$ and dt=0.002s (i.e. 0.03 units.

From Fig. 5.3(c) and (d), The SEM-T and SEM-S methods produced the amplitude slightly more than the Von Karman spectrum for the frequency range of (0.004-0.2). In the frequency range of (0.004-0.2), The SEM-T and SEM-S methods have approximately similar velocity spectrums at the inlet and building locations. The DFSEM and ATSML methods produce lower amplitudes of velocity spectrum compared to the Von Karman spectrum from Fig. 5.3(e) and (f). According to Fig. 5.3(g), the ATSMR method velocity spectrum has a higher amplitude in the low frequencies part compared to the Von Karman spectrum and vice versa.

According to Fig. 5.3, the SEM-G method produced the most comparable velocity spectrum at the inlet and building location. All of the considered methods produced frequency lower than the f_{grid}. The maximum frequency carried by the grid of $H/8$ is 2, whereas, all methods have a sharp decline

in energy around *f*=0.2 from Fig. 5.3. In fact, most methods do not have much energy in the frequency range of (0.2-2).

Similarly, the velocity spectrum is plotted for different inflow methods for the grid spacing size of *H*/16 in Fig. 5.4. According to Fig. 5.4(a), the DFM method inlet velocity spectrum is comparable to the Von Karman spectrum in the range of frequency of (0.008 to 11). Furthermore, the DFM velocity spectrum at the building location has a sharp decline in energy at about *f*=0.3. The DFM method produces a greater range of high frequencies turbulences for the grid spacing of *H*/16 compared to the grid spacing of *H*/8. The SEM-G method's wind spectrum is comparable to the Von Karman spectrum at the inlet location for the frequency range of (0.008-0.7) approximately and has a sharp decline in energy beyond *f*=0.35 at the building location from Fig. 5.4(b).

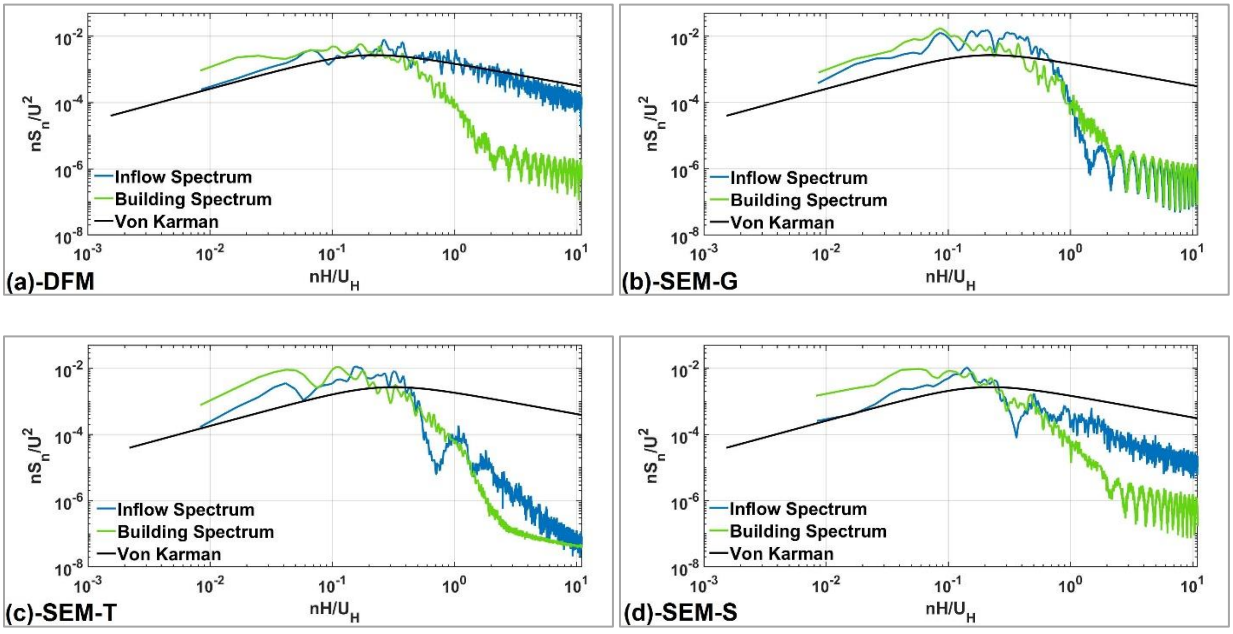

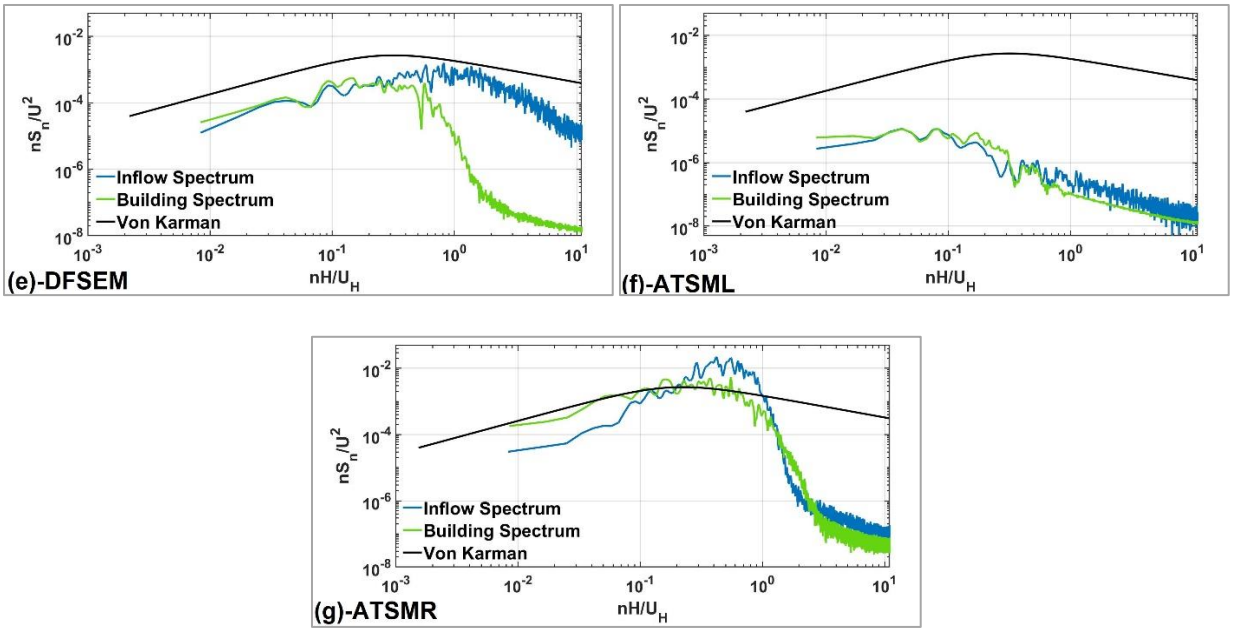

Fig. 5.4. Spectrum plot at the inlet and building location for (a) DFM, (b) SEM-G (i. e with guassian shape function), (c) SEM-T (i.e with tent shape function), (d) SEM-S (i.e with step shape function), (e) DFSEM, (f) ATSML, and (g)ATSMR model for $dx=H/16$ and dt=0.001s (i.e. 0.01 units)

From Fig. 5.4(c) and (d), the SEM-T and SEM-S methods produced the amplitude slightly more than the Von Karman spectrum for the frequency range of (0.008-0.2). Similarly, the DFSEM and ATSML methods produce lower amplitudes of velocity spectrum compared to the Von Karman spectrum for the grid spacing size of $H/16$ according to Fig. 5.4(e) and (f). From Fig. 5.4(g), the ATSMR method velocity spectrum has higher amplitude in low frequencies compared to the Von Karman spectrum and vice versa. However, the ATSMR velocity spectrum at the building location is comparable to the Von Karman spectrum in the frequency range of (0.008-0.7) and approximately has a sharp decline in energy beyond f=0.7 at the building location

According to Fig. 5.4, the SEM-G method produced the most comparable velocity spectrum at the inlet and building location. The maximum frequency carried by the grid of $H/16$ is 4. However, all

the considered methods produced frequency lower than the f_{grid}. The energy loss may be due to having high frequncy componenets greater than f_{grid} at the inlet, violation of divergence free condition, numerical error in using FDM, and energy cascade. During the pressure correction step, the high frequncy components are elimnated to get a continuous velocity and pressure at each time step and this changes the energy spectrum. Also, the energy cascade happens because none of the inflow methods satisfy the NS equation or memometum equation and this is an important factor as illustrated by Sescu and Hixon (2013). Since, several factors are involved in this issue and it is beyond the current objective, it will be investigated in the future.

5.3.2. The Effect of Eddy Density on Velocity Spectrum

To see the effect of eddy density as input for inflow methods like SEM and DFSEM on the velocity spectrum, the velocity spectrum at the inlet and building location is plotted for two different eddy densities using DFSEM as shown in Fig. 5.5. In one case the amount of eddy density is considered 1 and in the other one, it is considered 1000. According to Fig. 5.5, eddy density does not have any considerable effect on the velocity spectrum at the inlet and building location.

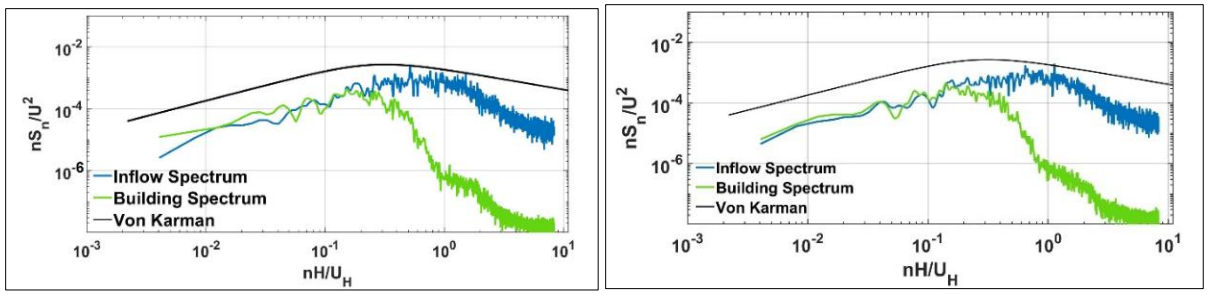

Fig. 5.5. Spectrum plot at the inlet and building location for DFSEM model with the eddy density of a) eddy density=1, b) eddy density=1000 for $dx=H/8$ and dt=0.002s (i.e. 0.03 units).

5.3.3. Spurious Pressure

To evaluate the inflow methods for spurious pressure production, the pressure coefficient is plotted at the building location. Spurious pressures happen when the frequency of pressure goes beyond Nyquist frequency. In Fig. 5.6, nondimensional velocity is plotted at the inlet and building location, and pressure also is plotted at the building location for different inflow turbulence fields. The grid spacing size is $dx=H/8$, and the time step is dt=0.002s (i.e. 0.03 units). According to this figure, all methods have damping in the velocity amplitude at the building location compared to the amount at the inlet location. However, the amount of this deduction is significant in the DFSEM model compared to others when one looks at it closer at several places. In Fig. 5.7 only a particular close up for 5-time units is shown. In this figure, pressure coefficients are computed using the relation of $C_p = P/(1/2\,\rho U^2)$.

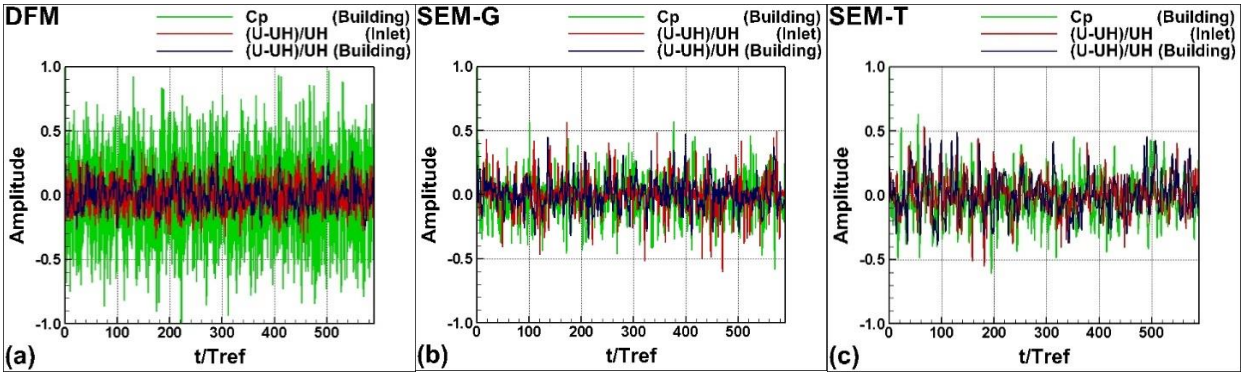

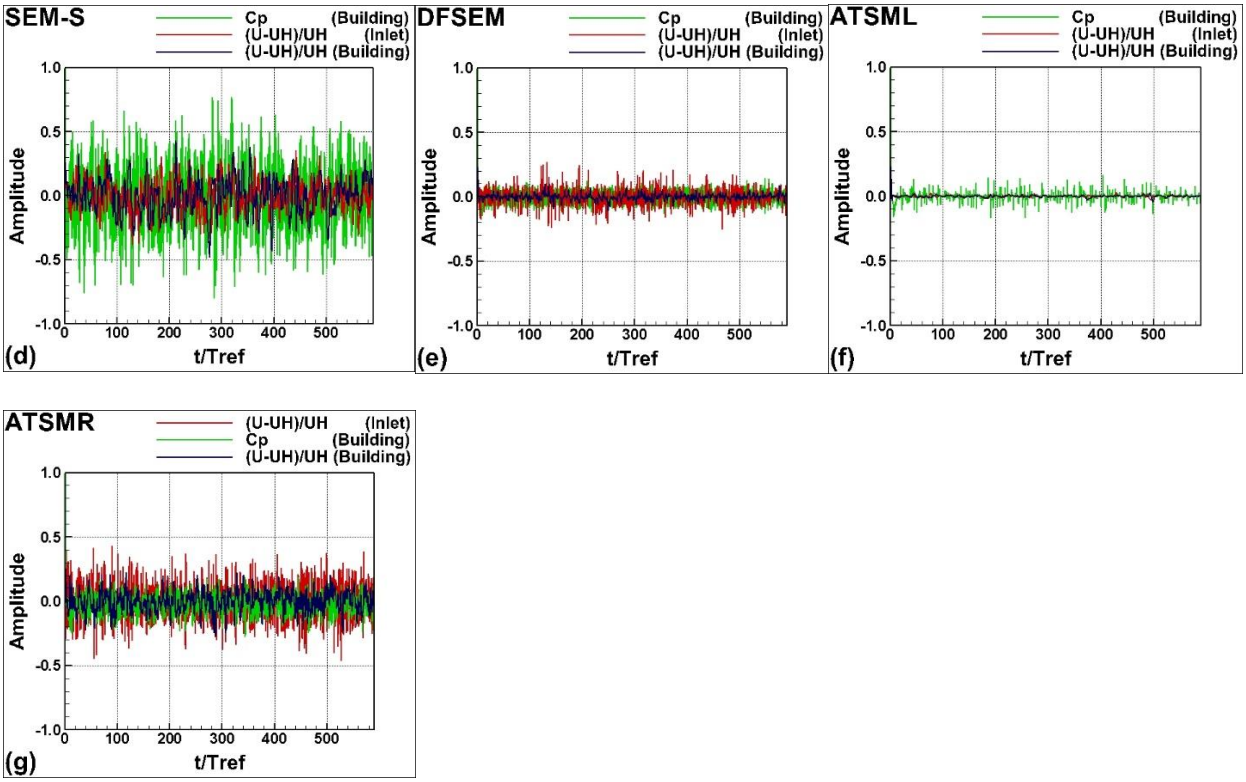

Fig. 5.6. Nondimensional velocity at the inlet and building location and Cp at the building location for (a) DFM, (b) SEM-G (i.e with guassian shape function), (c) SEM-T (i.e with tent shape function), (d) SEM-S (i.e with step shape function), (e) DFSEM, (f) ATSML, and (g)ATSMR model for $dx=H/8$ and dt=0.002s (i.e. 0.03 units).

In Fig. 5.7, the close-up of velocity and pressure coefficients are plotted over 5 time units. Spurious pressure occurs when pressure frequency is higher than Nyquist frequency. For the grid spacing size of $H/8$, the nondimensional Nyquist frequency is $H/(2h) = 8h/(2h) = 4$. If frequencies are taken as the number of peaks or cycles per unit time, pressure frequencies from Fig. 5.5 are 8, 1, 5, 5, 6,1, and 5 for DFM, SEM-G, SEM-T, SEM-S, DFSEM, ATSML, ATSMR respectively. Hence, spurious pressures are observed in DFM, SEM-T, SEM-S, DFSEM, and ATSMR. The spurious pressure is not observed in SEM-G and ATSML. According to Fig. 5.3 and Fig. 5.7, for

the SEM-G case as an example, when the wind velocity spectrum at the inlet is comparable to the building location one, then spurious pressure is not observed.

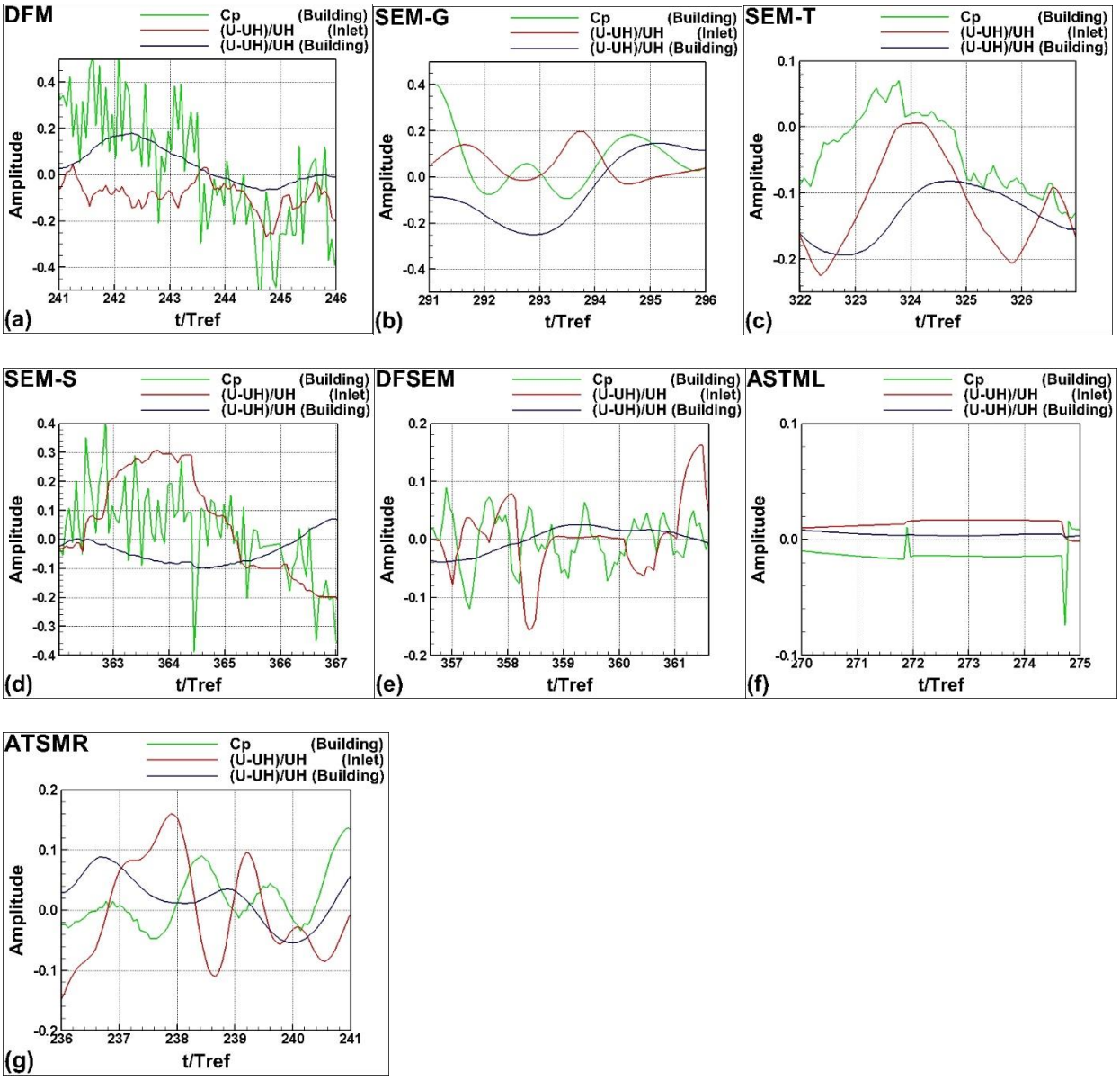

Fig. 5.7. Close up of nondimensional velocity at the inlet and building location and Cp at the building location for 5 time units for (a) DFM, (b) SEM-G (i.e with gaussian shape function), (c)

SEM-T (i.e with tent shape function), (d) SEM-S (i.e with step shape function), (e) DFSEM, (f) ATSML, and (g)ATSMR model for $dx=H/8$ and $dt=0.002$s (i.e. 0.03 units).

Similarly, in Fig. 5.8, nondimensional velocity is plotted at the inlet and building location, and pressure also is plotted at the building location for different inflow turbulence fields. The grid spacing size is $dx=H/16$, and the time step is $dt=0.001$s. Nyquist frequency for the grid spacing size of $H/16$ is 8.

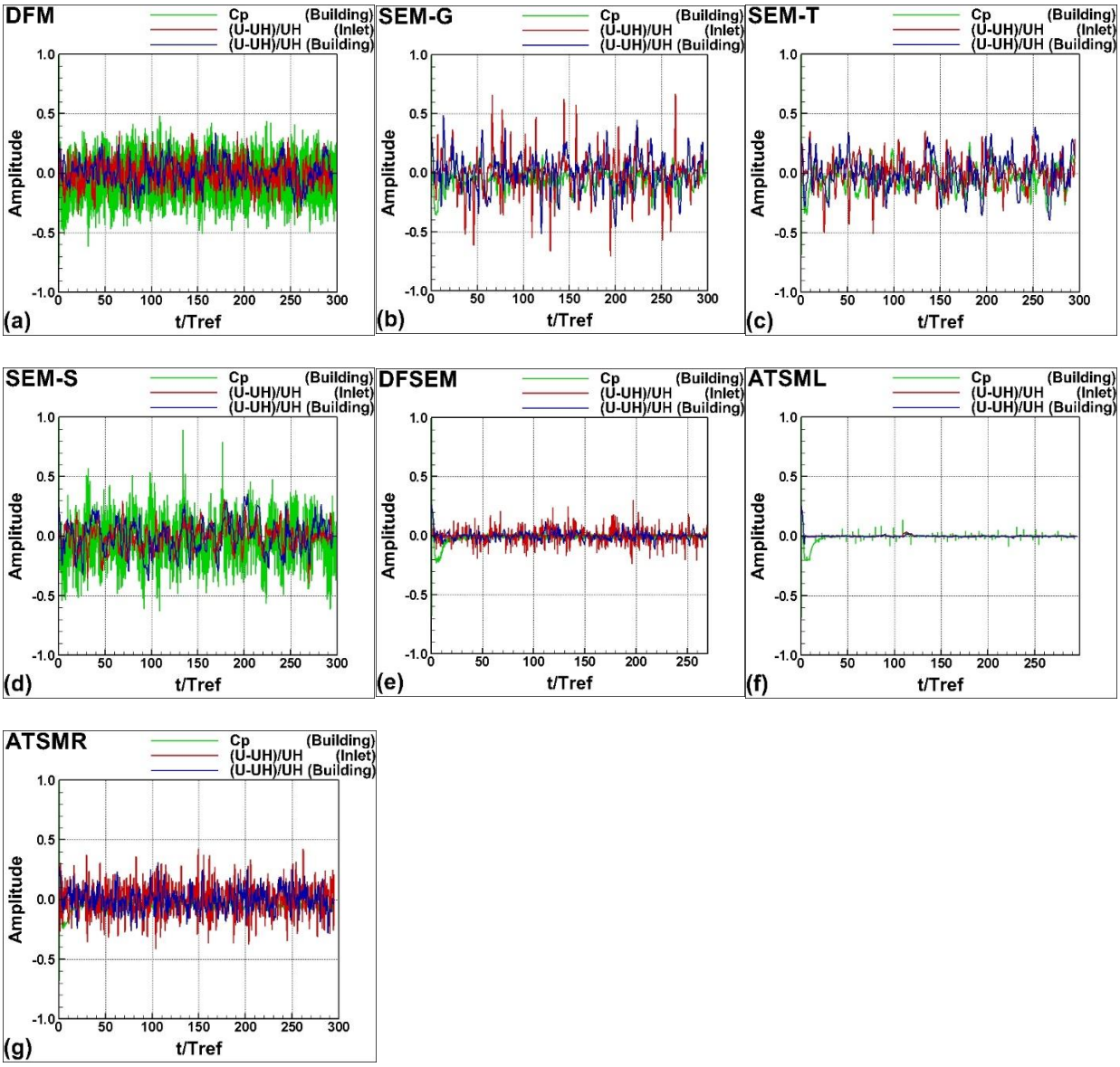

Fig. 5.8. Nondimensional velocity at the inlet and building location and Cp at the building location for (a) DFM, (b) SEM-G (i.e with guassian shape function), (c) SEM-T (i.e with tent shape function), (d) SEM-S (i.e with step shape function), (e) DFSEM, (f) ATSML, and (g)ATSMR model for $dx=H/16$ and dt=0.001s (i.e. 0.01 units).

In Fig. 5.9, the close-up of velocity and pressure coefficients are plotted over 5 time units. As mentioned previously, spurious pressure happens when pressure frequency is higher than Nyquist frequency. For the grid spacing size of $H/16$, the nondimensional Nyquist frequency is $H/(2h) = 16h/(2h) = 8$. According to Fig. 5.9, when pressure frequencies are taken as the number of peaks per unit time, pressure frequencies are 10, 1, 9, 9, 11,1, and 10 for DFM, SEM-G, SEM-T, SEM-S, DFSEM, ATSML, ATSMR respectively. Hence, spurious pressures are observed in DFM, SEM-T, SEM-S, DFSEM, and ATSMR. Similarly, the spurious pressure is not observed in SEM-G and ATSML.

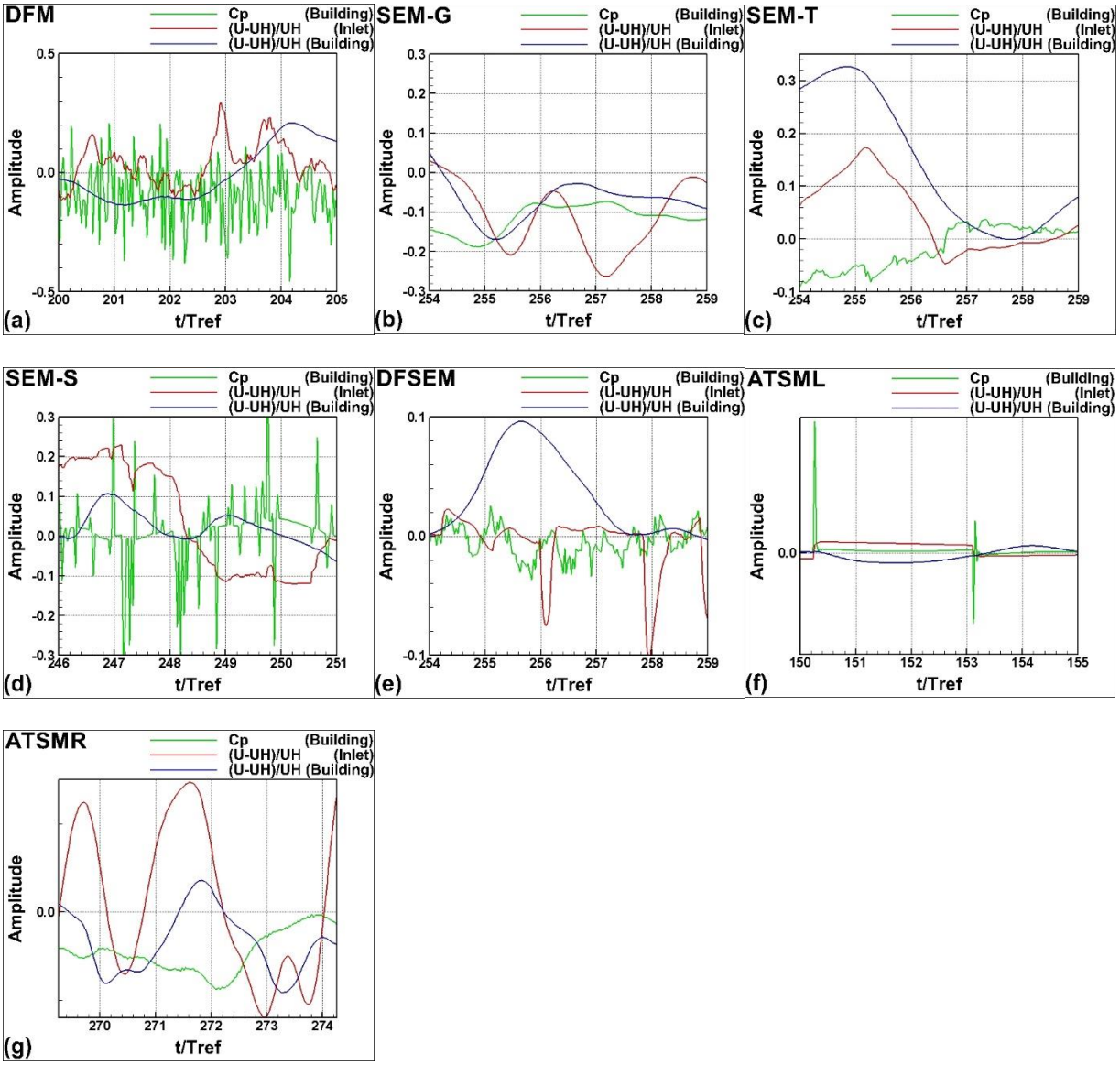

Fig. 5.9. Close up of nondimensional velocity at the inlet and building location and Cp at the building location for 5 time units for (a) DFM, (b) SEM-G (i.e with gaussian shape function), (c) SEM-T (i.e with tent shape function), (d) SEM-S (i.e with step shape function), (e) DFSEM, (f) ATSML, and (g)ATSMR model for for $dx=H/16$ and dt=0.001s (i.e. 0.01 units).

5.3.4. SEM-G For Wind Engineering Application

As, ATSML is not able to produce a comparable inlet velocity spectrum to the Von Karman spectrum, ATSML cannot be employed for the Wind Engineering Application. Among considered

methods, SEM-G does not produce spurious pressure. Furthermore, the SEM-G method produced a similar velocity spectrum at the inlet and building location, which is comparable to the Von Karman spectrum. To evaluate whether SEM-G is proper for wind engineering applications, the flow around the TTU building is modeled. The CFD peak and mean pressure coefficient (*Cp*) along the centerline of the TTU building are calculated and compared to the WT measurements reported by Moravej (2018a). To calculate the peak pressure, the following procedure is used. Generally, about 10 time units are needed for the turbulent flow to be fully developed, and hence it is ignored. The remaining data from 10 time units to 100 time units are considered to capture the peak pressures at each point in time. In Fig. 5.10 and Fig. 5.11, the CFD mean *Cp*, maximum *Cp* (*Cpmax*), and minimum *Cp* (*Cpmin*) are compared to WT scale 1:6 (WT6).

According to Fig. 5.10(a), the mean *Cp* error compared to WT6 is 30% at windward, 18% at the roof, and 24% at leeward. Corresponding to Fig. 5.10(b), the minimum CFD Cp error compared to WT6 is 30% at windward, 16% at the roof, and 20% at leeward. From Fig. 5.10(c), the maximum CFD *Cp* error compared to WT6 is 100% at windward, 40% at the roof. On the leeward side, the WT6 and CFD are approximately close together. Hence, considering at least 30% error in peak pressure estimation, SEM-G can be used in wind engineering applications.

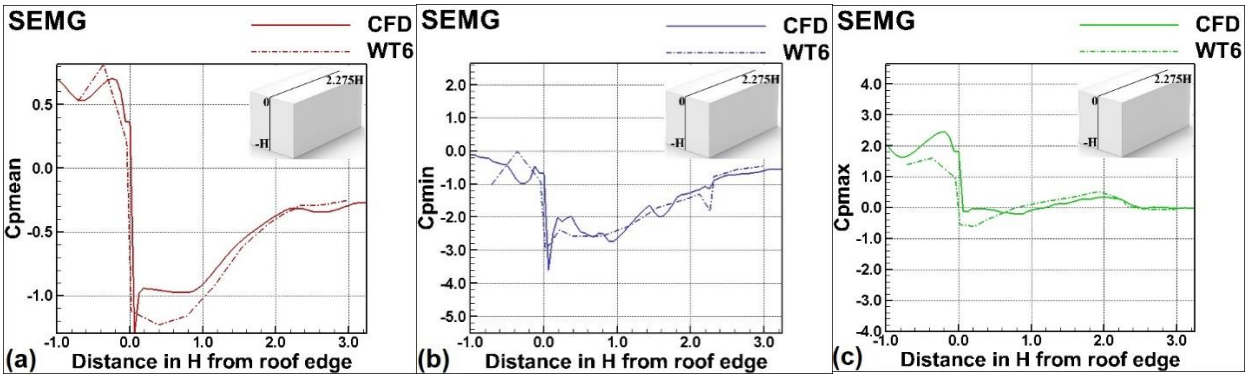

Fig. 5.10. CFD (a) mean, (b) minimum, and (c) maximum pressure coefficient (*Cp*) along the centerline of the TTU building in comparison to WT measurements for the grid spacing of H/16.

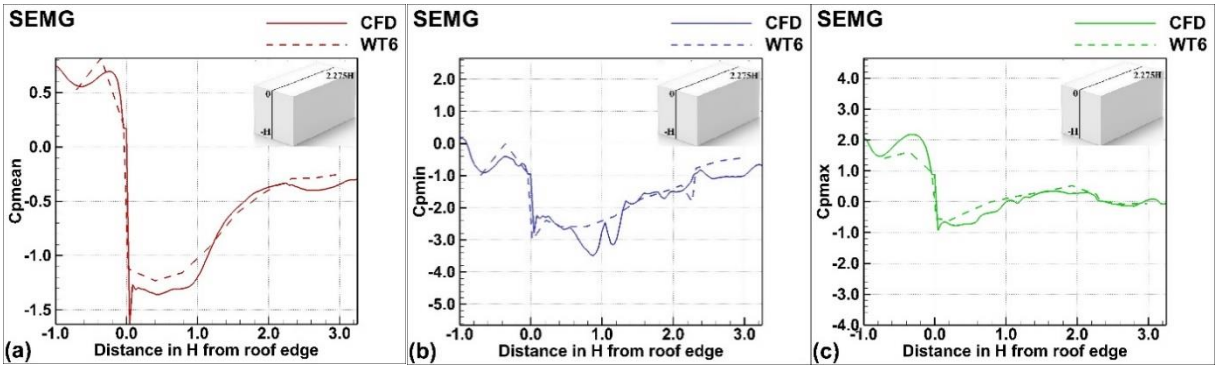

Fig. 5.11. CFD (a) mean, (b) minimum, and (c) maximum pressure coefficient (*Cp*) along the centerline of the TTU building in comparison to WT measurements for the grid spacing of H/24.

5.4.Conclusion

Flow is modeled numerically for 590 nondimensional time units using different synthetic turbulence generator methods, which are provided in the Turbulence Inflow (TInF) Tool. The considered methods are a) Digital Filter Methods (DFM), b) Synthetic eddy methods (SEM), c) Divergence Free Synthetic Eddy Method (DFSEM), and d) Anisotropy Turbulent Spot Method (ATSM). The resulted velocity, pressure coefficients, and velocity spectrum overtime at the inlet and building location (at the building height) are plotted for different cases and observed:

1. In FDM, the maximum frequency carried by the grid is 2 and 4 for grid spacing sizes of *H*/8 and *H*/16 respectively, whereas, all methods have a sharp decline in energy as observed in Fig. 2 and Fig. 3 when the frequency is less than f_{grid}.
2. When the pressure frequency is higher than the Nyquist frequency of the grid, then we say there is spurious pressure. In most methods, spurious pressures are observed except in SEM-G and ATSML as shown in Fig. 5.6 and Fig. 5.8. So other methods are eliminated for wind engineering application.

3. Out of SEM-G and ATSML methods that have less spurious pressure at the building location, the SEM-G wind spectrum at the inlet and at the building location is much closer to the Von Karman spectrum than ATSML wind spectrum. Hence SEM-G is preferred for wind engineering applications. Using SEM-G method, the building pressure coefficients are calculated and compared with WT measurements. The computed minimum and mean pressures have a maximum 30% error at windward side of the building compared to WT6 measurements.

Acknowledgments

Ms. Zahra Mansouri acknowledges the financial support from the James T. Womble Professorship from the University of Arkansas. For this research, wind tunnel data from the NHERI WOW EF were used. The authors acknowledge the help provided by Dr. M. Moravej from Walker Consultants in delivering the wind tunnel data in a way we could use in this study. The authors acknowledge the support from Dr. P. Mackenzie-Helnwein from NEHRI SimCenter to use the TInF tool in case file preparations for OpenFOAM.

Notation

The following symbols are used in this paper:

$C_p =$ Mean pressure coefficient

$C_{pmin} =$ Minimum pressure coefficient

$C_{pmax} =$ Maximum pressure coefficient

$dt =$ Non-dimensional time step

$dT =$ Dimensional time step

$f =$ Non-dimensional frequency$= nH/U_H = H/L$

f_{grid} = Maximum frequency carried by the grid

H = Building height

h = Maximum grid spacing

λ_{grid} = Smallest wavelength transported by grid

L_1 = Turbulence length scale in x direction

L_2 = Turbulence length scale in y direction

L_3 = Turbulence length scale in z direction

n = Dimensional frequency

T_{ref} = Reference time

U_{ave} = Average velocity

U_H = Average velocity at building height

References

Aboshosha, H., Elshaer, A., Bitsuamlak, G. T., and El Damatty, A. (2015). Consistent inflow turbulence generator for LES evaluation of wind-induced responses for tall buildings. *Journal of Wind Engineering and Industrial Aerodynamics*, 142, 198-216

Ding, F., Kareem, A., and Wan, J. (2019). Aerodynamic tailoring of structures using computational fluid dynamics. *Structural Engineering International*, 29, 26-39.

Exponent, Engineering and scientific consulting, wind engineering, https://www.exponent.com/services/practices/engineering/buildings--structures/capabilities/wind-engineering/?serviceId=c16fc389-0037-4f90-a173-4171d47c37ad&loadAllByPageSize=true&knowledgePageSize=7&knowledgePageNum=0&newseventPageSize=7&newseventPageNum=0&professionalsPageNum=1

Jarrin, N., Benhamadouche, S., Laurence, D. and Prosser, R. (2006). A synthetic-eddy method for generating inflow conditions for large-eddy simulations. *International Journal of Heat and Fluid Flow*, 27, 585-593.

Jarrin, N. (2008), Synthetic inflow boundary conditions for the numerical simulation of turbulence, Ph.D. thesis, University of Manchester.

Jarrin, N., Prosser, R., Uribe, J. C., Benhamadouche, S., and Laurence, D. (2009). Reconstruction of turbulent fluctuations for hybrid RANS/LES simulations using a synthetic-eddy method. *International Journal of Heat and Fluid Flow*, 30, 435-442.

Keating, A., Piomelli, U., Balaras, E., and Kaltenbach, H. J. (2004). A priori and a posteriori tests of inflow conditions for large-eddy simulation. *Physics of fluids*, *16*, 4696-4712.

Klein, M., Sadiki, A., and Janicka, J. (2003). A digital filter based generation of inflow data for spatially developing direct numerical or large eddy simulations. *Journal of computational Physics*, 186, 652-665.

Kim, Y., Castro, I. P., and Xie, Z. T. (2013). Divergence-free turbulence inflow conditions for large-eddy simulations with incompressible flow solvers. *Computers & Fluids*, 84, 56-68.

Kröger, H., and Kornev, N. (2018). Generation of divergence free synthetic inflow turbulence with arbitrary anisotropy. *Computers & Fluids*, 165, 78-88.

Kokkinakis, I. W., Drikakis, D., Ritos, K., & Spottswood, S. M. (2020). Direct numerical simulation of supersonic flow and acoustics over a compression ramp. *Physics of Fluids*, 32, 066107.

Mackenzie-Helnwein, P., Wan, J. J., and McKenna, F. (2020). NHERI-SimCenter /TurbulenceInflowTool: version 1.1.0 (v1.1.0). Zenodo. https://doi.org/10.5281/zenodo.3988635

Mansouri, Z., Selvam, R. P., and Chowdhury, A. G. (2022). Maximum grid spacing effect on peak pressure computation using inflow turbulence generators. *Results in Engineering*, 15, 100491.

Mansouri, Z., Verma, S., & Selvam, R. P. (2021). Teaching modeling turbulent flow around building using LES turbulence method and open-source software OpenFOAM. In *2021 ASEE Midwest Section Conference*.

Mooneghi, M. A., Irwin, P., and Chowdhury, A. G. (2016). Partial turbulence simulation method for predicting peak wind loads on small structures and building appurtenances. *Journal of Wind Engineering and Industrial Aerodynamics*, *157*, 47–62.

Moravej, M. (2018a). Investigating scale effects on analytical methods of predicting peak wind loads on buildings. Ph.D. thesis, Florida International University, Miami, Florida.

Moravej M., Chowdhury A. G., (2018b), Wind analysis tools: power spectra, DesignSafe-CI.

Nicoud, F., and Ducros, F. (1999). Subgrid-scale stress modelling based on the square of the velocity gradient tensor. *Flow, turbulence and Combustion*, 62, 183-200.

Orszag, S. A. (1979). Spectral methods for problems in complex geometrics. Numerical methods for partial differential equations, 273-305. Academic Press.

Patruno, L., and Ricci, M. (2017). On the generation of synthetic divergence-free homogeneous anisotropic turbulence. *Computer Methods in Applied Mechanics and Engineering*, 315, 396–417

Patruno, L., and Ricci, M. (2018). A systematic approach to the generation of synthetic turbulence using spectral methods. *Computer Methods in Applied Mechanics and Engineering*, 340, 881-904.

Patruno, L., and de Miranda, S. (2020). Unsteady inflow conditions: A variationally based solution to the insurgence of pressure fluctuations. *Computer Methods in Applied Mechanics and Engineering*, 363, 112894.

Poletto, R., Craft, T., and Revell, A. (2013). A new divergence free synthetic eddy method for the reproduction of inlet flow conditions for LES. *Flow, turbulence and combustion*, 91, 519-539.

Rana, Z. A., Thornber, B., and Drikakis, D. (2011). On the importance of generating accurate turbulent boundary condition for unsteady simulations, *Journal of Turbulence*, 12, N35.

Richards, P. J., Hoxey, R. P., Connell, B. D., and Lander, D. P. (2007). Wind-tunnel modelling of the Silsoe Cube. *Journal of Wind Engineering and Industrial Aerodynamics*, *95*, 1384–1399.

Selvam, R. P. (1997). Computation of pressures on Texas Tech University building using large eddy simulation. *Journal of Wind Engineering and Industrial Aerodynamics*, 67, 647–657.

Selvam R., (2022), Computational fluid dynamics for wind engineering: Chichester, Wiley-Blackwell.

Sescu, A., and Hixon, R. (2013). Toward low-noise synthetic turbulent inflow conditions for aeroacoustic calculations. *International Journal for Numerical Methods in Fluids*, 73, 1001-1010.

Thornber, B., Drikakis, D., Youngs, D. L., and Williams, R. J. R. (2010). The influence of initial conditions on turbulent mixing due to Richtmyer–Meshkov instability. *Journal of Fluid Mechanics*, 654, 99-139.

Wan, J. and Mackenzie-Helnwein, P. (2020), TInF tool release 1.1.0, Report.

Verma, S., Mansouri, Z., & Selvam, R. P. (2021). Incorporating two weeks open-source software lab module in CFD and fluids courses. In *2021 ASEE Midwest Section Conference*.

Appendix 5.A-Using TInF

a. To use TInF, by pressing ‘Locate’, the source file including ‘0’, ‘constant’, and ‘system’ files should be chosen. Afterward, the ‘inlet’ face should be chosen in the ‘select what boundary to modify’ which is shown in Fig. 5.A.1.

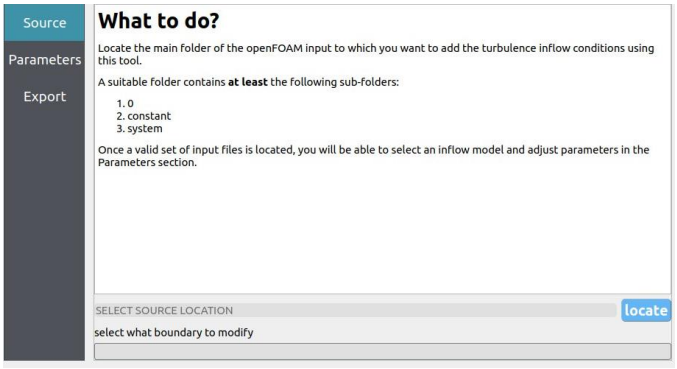

Fig. 5.A.1. The source section of TInF tools.

b. Based on Table 5.1, parameters should be inserted in the parameter section, which is indicated in Fig. 5.A.2.

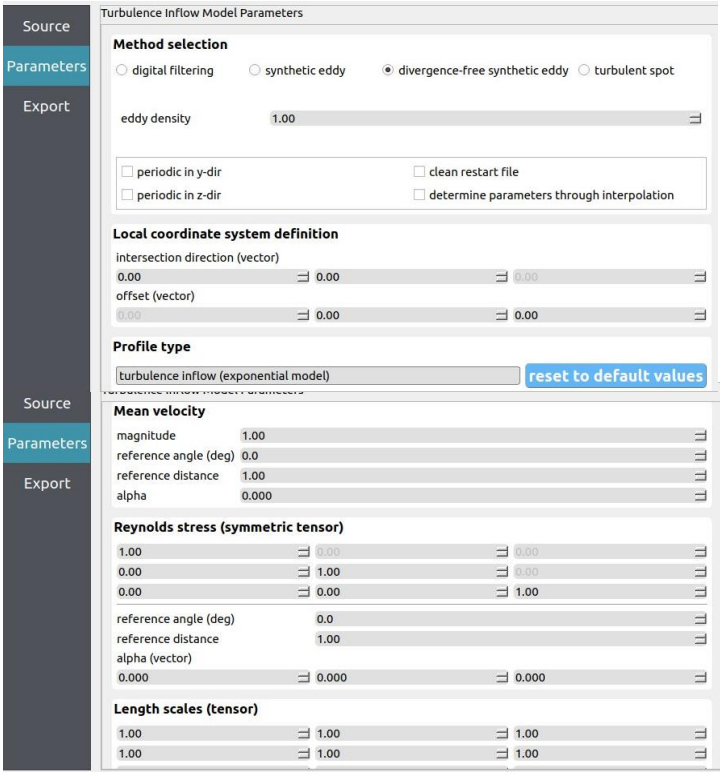

Fig. 5.A.2. The parameters section of TInF tools.

c. Finally, the ‘inlet’ face should be chosen in the ‘select what boundary to modify’ in the ‘Export’ section. Then the ‘Export’ key should be pressed to modify files (Fig. 5.A.3.).

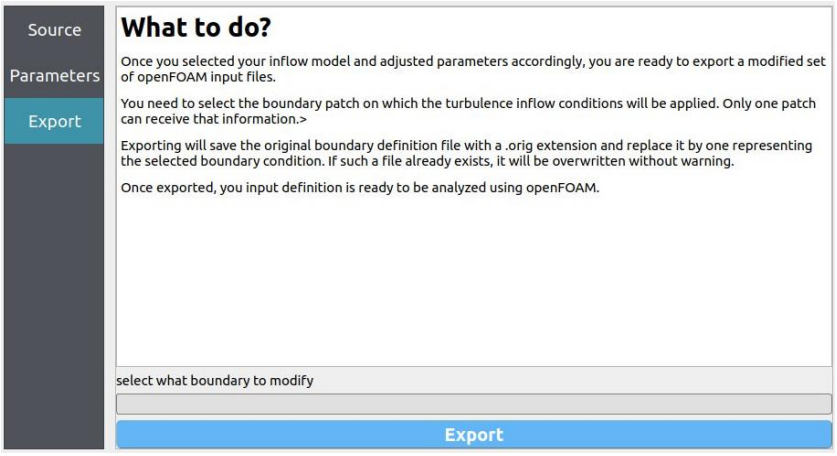

Fig. 5.A.3. The source section of TInF tools.

Chapter 6- Conclusions

5.5.Summary

Extreme winds, which tend to be irregular, can cause various structural failures of buildings. These kinds of irregular wind flows are called turbulent flows. To avoid these devastating structural damages, it is necessary to consider correct peak pressures in building design. As conducting field measurements for estimation of peak pressures and design purposes is not applicable and expensive, Computational Fluid Dynamics (CFD) can be an economical tool for engineers to estimate accurate wind pressures on buildings. In CFD, the effects of turbulence in wind can be incorporated by using various turbulence modeling methods such as Large Eddy Simulation (LES), which is more reliable and applicable in the industry compared to other methods. However, CFD modeling of wind flow around the building is challenging. In LES, a turbulent flow field at the inlet is required to apply to estimate wind load accurately, as LES without inflow turbulence field underestimates peak pressure on buildings. Furthermore, the turbulent flow behavior in the domain interior is extremely dependent on this inflow physical quality. Thus, a critical aspect of the numerical LES investigation is defining the right inflow turbulence. This study tries to obtain a proper evaluation of the characteristics and applicability of different synthetic inflow methods from the perspective of wind engineering. The inflow methods' performances are evaluated for producing a real turbulent wind flow at the inlet and spurious pressure in the domain.

This study firstly explained that Nyquist frequency produces significant error in FDM, and the maximum frequency that can be carried by the gird in FDM is f_{grid}= (Nyquist frequency/2). Furthermore, this study clarified that spurious pressures happen when the pressures in the domain have frequency greater than Nyquist frequency. As spurious pressures are observed when some synthetic inflow methods are used as inflow boundary condition, the CDRFG method is chosen to

understand more about the possible reasons for spurious pressures. It is indicated that some portion of spurious pressure is rooted in choosing maximum (f_{mas}) and minimum (f_{mis}) non-dimensional frequencies based on the field or wind tunnel (WT) spectrum and regardless of their maximum grid size. Whereas the largest grid spacing h in the computational domain determines the highest frequency of the velocity fluctuations transported by the grid (f_{grid}) from the inflow turbulence. In the LES computation, the suggested highest frequency transported in the flow using the finite difference method (FDM) is $f_{LES}=f_{grid}=H/4h$ where $4h$ is the smallest wavelength resolved by the grid. According to velocity spectrum at the inlet and building location comparison, if maximum frequency equals or is smaller than f_{grid}, we have similar velocity spectrum at the inlet and building location. However, if $f_{max}>f_{grid}$, the velocities with frequency greater than f_{grid} are filtered and it introduces spurious pressures at the domain. Spurious pressures lead to high errors (around 600%) in peak pressure results on the building. However, using $f_{max}=f_{grid}$ for all the grid spacing size led to reductions of spurious pressure and improvement of peak pressure results. However, there is still some error in peak pressure results at windward and leeward sides of building. It is due to when the maximum frequency is initially limited to the specific number at CDRFG, but the maximum frequency is oversampled and limited roughly to that number. Furthermore, in the CDRFG method, the wavenumber (i.e., spatial frequency) are changed in the enforcing the divergence-free condition step. For the CDRFG method, more than half of resulted inflow velocities have the wavenumber greater than the maximum wavenumber determined based on the grid spacing size. This leads to spurious pressures production in the domain.

Afterward, different synthetic inflow turbulence generator methods (i.e., a) Digital Filter Methods (DFM), b) Synthetic eddy methods (SEM), c) Divergence Free Synthetic Eddy Method (DFSEM), and d) Anisotropy Turbulent Spot Method (ATSM)) besides the CDRFG method are considered

to see how are thier performance for wind engineering application. These methods' performance are evaluated by plotting velocity spectrum at the inlet and building location and pressure over time at building location. The inlet velocity spectrum is compared with Von Karman spectrum (which is the real wind velocity spectrum based on the field measurment) to see how well the inflow method is capble to produce real turbulent wind flow. Then, velocity spectrum at the inlet is compared to velocity spectrum at the building location to how well energy is carried from the inlet to building location. The more we have similar velocity spectrum at the inlet and building location, the fewer error we have in our numerical model, and the more accurate peak pressure results we have. It is observed that all methods have a sharp decline in energy in the frequency less than f_{grid} in the building location. ATSML and DFSEM velocity spectrum at the inlet have lower amplitude compared to the Von Karman spectrum, so they produced the field with lower energy than real wind turbulent flow. Moreover, in most methods, spurious pressures are observed except in SEM-G, CDRFG, and ATSML. From concurrent comparison of velocity spectrum at the inlet and building location and pressure coefficient plots over time, we can see when the velocity spectrum at the inlet is close to the velocity spectrum at the building location, spurious pressure does not occur in the domain.

As the CDRFG method with maximum frequency of f_{grid} and SEM-G method produced the most comparable velocity spectrum at the inlet and building location and it does not have spurious pressure, they are considered for the second step of evaluation. In this step, their performance in wind load estimations is evaluated by comparing CFD peak pressure results to wind tunnel measurements reported by Moravej (2018). For the SEM-G and CDRFG method, the peak pressure is calculated over the centerline of the TTU building and compared to WT measurements. According to this evaluation, the SEM-G method has fewer error in computed peak and mean

pressure results compared to the CDRFG method. The SEM-G method has a maximum 30% error in CFD peak pressure results compared to WT6 measurements at windward.

5.6.Contribution

Existing popular methods are taken to evaluate their performance for wind engineering applications. The considered methods are a) Consistent Discrete Random Flow Generator method (CDRFG) under RFG, b) Digital filter methods (DFM), and c) Synthetic Eddy Method (SEM) with three different shape functions (i.e., Gaussian (SEM-G), Tent (SEM-T), and Step (SEM-S) shape functions) d) Divergence Free Synthetic Eddy Method (DFSEM), and e) two types (i.e., R and L) of Anisotropy Turbulent Spot Method (ATSM).

The CDRFG MATLAB code is modified to the produced inflow turbulence field can be used in our-house Fortran code.

A clear definition of spurious pressure in the FDM method is introduced and the reason behind the spurious pressure production is provided for RFG methods.

The effects of spurious pressure on peak and mean pressure results are presented.

I worked with SimCenter to learn and implement different inflow methods (i.e., DFM, SEM-G, SEM-T, SEM-S, DFSEM, ATSMR, and ATSML) in the OpenFOAM. These case files cannot run in the regular OpenFOAM and this needs to be modified to run. The modification steps are provided in Appendix A.

Finally, the following procedures are formulated to evaluate the inflow turbulence methods for wind engineering applications:

1. Comparing the velocity spectrum at the inlet location and building location with the Von Karman spectrum to evaluate different inflow methods' performance to produce the real turbulent wind flow at the inlet and their capability to carry energy from the inlet to the building location.
2. Identifying spurious pressures and a remedy (i.e., using the determined maximum frequency based on the grid spacing size) to reduce them.

5.7.Conclusion and Future Work

The CDRFG inflow method based on RFG can be controlled for the maximum and minimum frequencies. By selecting the proper maximum frequency with respect to the largest grid spacing size used in the computational domain, spurious pressures and subsequently peak pressure errors can be reduced. However, still, there are errors in computed peak pressures due to violation of maximum wave numbers in the process of satisfying the conservation of mass. The violation of maximum wave numbers occurs when wavenumbers beyond the grid wave numbers are introduced in the domain. Furthermore, CDRFG does not respect Taylor's hypothesis. These are challenges that need to be eliminated in future research. These issues led to significant errors in peak pressures on the windward and leeward sides of the building. On the roof, the peak pressures are reasonable in comparison to WT measurement.

The DFM method produced spurious pressures and has several other issues as discussed in the previous chapter and this method is not applicable in wind engineering applications.

The DFSEM method cannot produce the velocity spectrum close to the real wind spectrum, also it introduces spurious pressures in the domain, so this method is not proper for wind engineering applications.

The ATSM method has two types L and R. Although the ASTML method does not produce spurious pressures, it cannot produce the velocity spectrum close to the real wind spectrum. Furthermore, the ASTMR method introduces spurious pressures in the domain. Hence, the ATSM method is not proper for wind engineering applications.

SEM with Tent (SEM-T) and Step (SEM-S) shape functions cannot produce a comparable velocity spectrum at the inlet and building location, as well as, they introduce spurious pressures in the domain. Hence, these methods are not proper for wind engineering applications.

At this time SEM-G (with the Gaussian shape function) method has fewer errors in CFD peak and mean pressures compared to other methods and it can be stated that the computed pressures are comparable to the WT measurement.

In the case of SEM, DFSEM, and ATSM methods, the effects of input variables like six Reynolds stresses and nine integral length scales are not clear. For some methods like SEM-G, the divergence-free condition is violated at this time. In future research, the effects of input variables and divergence-free condition violation should be studied.

Appendices

7.A. Installation of Ubuntu Alongside Windows

1. Rufus should be downloaded to create bootable USB drives from the below link:

https://rufus.ie/

2. Ubuntu should be downloaded from the below link:

https://ubuntu.com/download/desktop

3. In this part, Rufus should be opened, and then from the select bottom, the flash memory card (on which Ubuntu saved) should be selected, and then press start (Fig. 7.A.1).
4. At that point, firstly, the partition, which Ubuntu can be installed on, should be selected, and then to change the NFTS format, the shrink volume should be chosen using right-click on that.

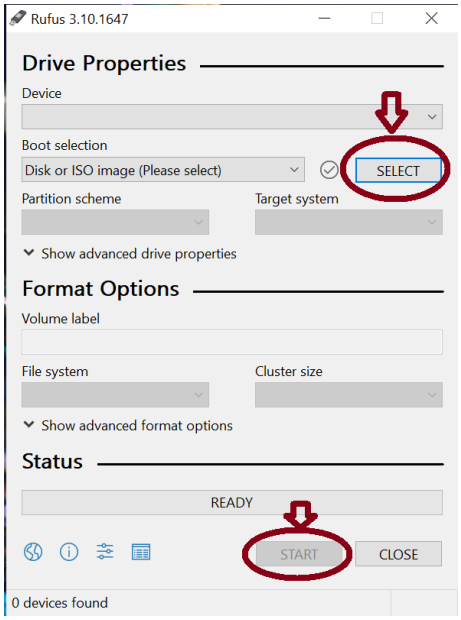

Fig. 7.A.1. Rufus Software Environment

5. Flash memory card should be booted by powering off pc and turning on. To boot PC, while the PC is turning on F1 to F10 should be pressed depending on your PC type. Then under the Boot section, you should bring your flash name in the first number to boot it.

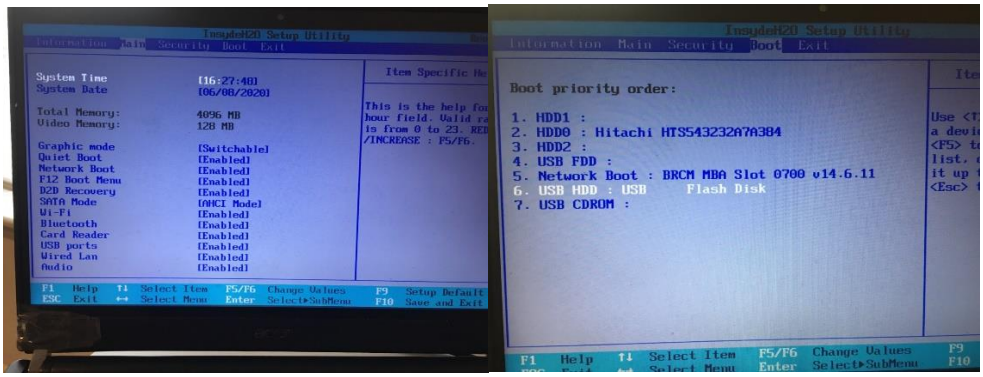

Fig. 7.A.2. Making boot the flash memory card

6. After that just you should follow the procedure of installing, and just in one step, you should choose to install Ubuntu alongside your windows (Fig. 7.A.3).

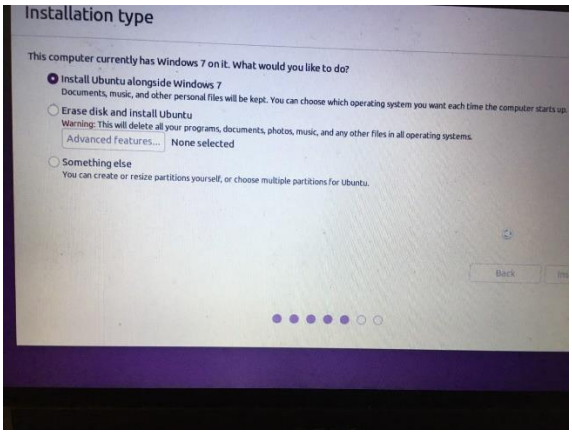

Fig. 7.A.3. Choosing “Install Ubuntu alongside Windows” option while installing Ubuntu

7. When you installed Ubuntu, it wants to restart your system, please be sure that before restarting take off your flash memory card.

When you installed Ubuntu, you need to restart it and you can choose the window or Ubuntu. (Fig. 7.A.4)

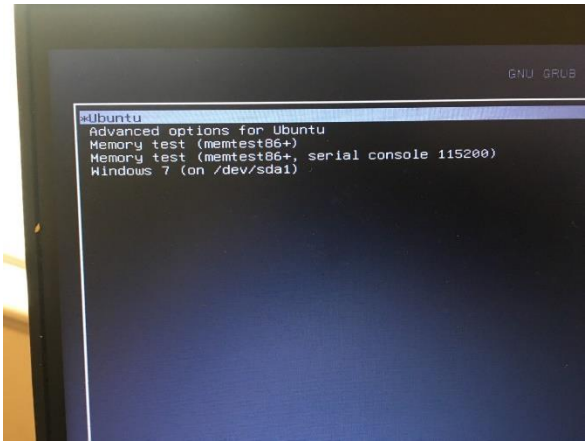

Fig. 7.A.4. Having two options concurrently, i.e., Ubuntu or Windows 7, on your device

Below you can find how you can install OpenFOAM on your Ubuntu.

7.B. Installation OpenFOAM on Ubuntu

OpenFOAM-dev can be simply installed using the apt package management tool. The user will need to provide superuser password authentication when executing the following commands with sudo.

1. If not already present, add (a) the public key (gpg.key) for the repository to enable package signatures to be verified and (b) the main repository at dl.openfoam.org. The key and main repository will be present if the user has already installed another pack, e.g., openfoam7.

- sudo sh -c "wget -O - http://dl.openfoam.org/gpg.key | apt-key add -"
- sudo add-apt-repository http://dl.openfoam.org/ubuntu

Note: This only needs to be done once for a given system

2. Copy and paste the following in a terminal prompt (Applications → Accessories → Terminal) to add dl.openfoam.org dev to the list of software repositories for apt to search.

- sudo add-apt-repository "http://dl.openfoam.org/ubuntu dev"

Note: This only needs to be done once for a given system

3. Update the apt package list to account for the new download repository location

- sudo apt-get update

4. Install OpenFOAM-dev which also installs paraviewopenfoam56 as a dependency if it is not already installed.

- sudo apt-get -y install openfoam-dev

OpenFOAM-dev is now installed in the /opt directory.

7.C. Needed Modification to Use TInF Tools

The modifications should be done in three main steps as follows:

7.C.1. Primary Modification

The primary steps to add the required library to OpenFOAM libraries are:

a) "TurbulenceInflowTool" file should be downloaded from SimCenter and stored in the same directory of case files.
b) The openFOAM_code under "TurbulenceInflowTool" and the code.zip and boundaryConditions_OpenFOAM7.zip files should be extracted.
c) Then in the two above-mentioned files, where the "Make" folder is located, a terminal should be opened and the command of $wmake should be used to produce the "platform" folder in the main folder.
d) Furthermore, the "libturbulentInflow.so" under the "platform" folder should be copied to the library file of OpenFoam 7 (can be found in opt).

7.C.2. Using TInF

To use TInF, by pressing 'Locate', the source file including '0', 'constant', and 'system' files should be chosen. Afterward, the 'inlet' face should be chosen in the 'select what boundary to modify' which is shown in Fig. 7.C.1.

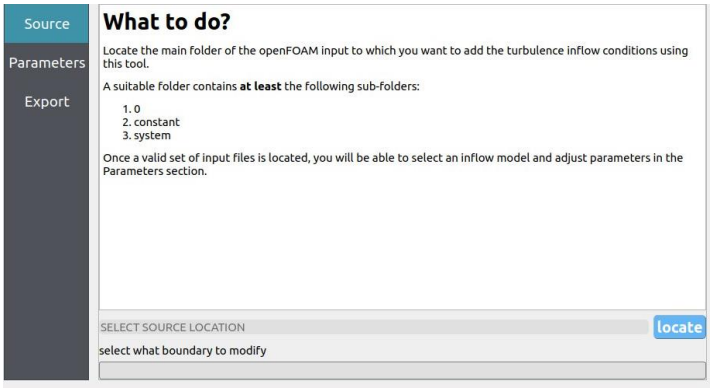

Fig. 7.C.1. The source section of TInF tools.

Based on Table 7.C.1, parameters should be inserted in the parameter section, which is indicated in Fig. 7.C.2.

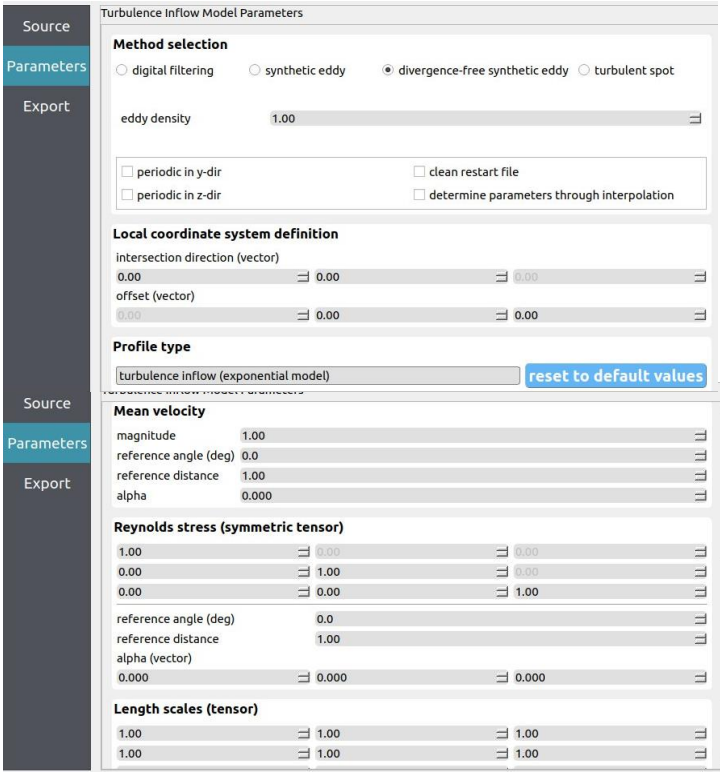

Fig. 7.C.2. The parameters section of TInF tools.

Finally, the ‘inlet’ face should be chosen in the ‘select what boundary to modify’ in the ‘Export’ section. Then the ‘Export’ key should be pressed to modify files (Fig. 7.C.3).

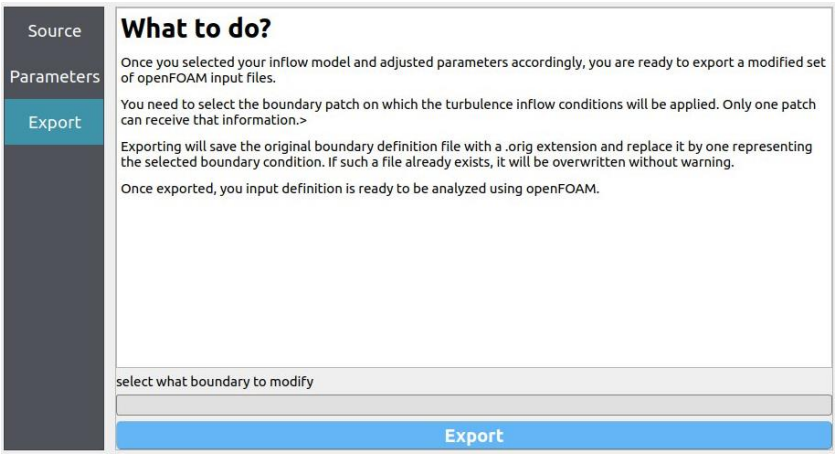

Fig. 7.C.3. The source section of TInF tools.

7.C.3. Final Modification

Below modification is done by running TInF or the case file can be directly modified. It should be noted that the modified case file using TInF should be checked before running the case file. Required steps to modify case files to implement different inflow methods in OpenFOAM:

a) In the control file, the following lines should be added.

("libturbulentInflow.so");

b) It should be noted that the solver should be chosen as pisoFoam in the control file.

c) Under “0” folder, in “U” file the inflow methods and its parameters should be defined at the inlet boundary condition as follows:

```
Inlet
 {type            turbulentSEMInlet;
  eddyType       gaussian;
  density         1;
  perodicInY       false;
```

perodicInZ false;

cleanRestart false;

calculateU true;

calculateL true;

calculateR true;

value uniform (19.48 0 0);}

d) Under "constant" folder, the "inflowProperties" file should be created. In "inflowProperties" we input the initial conditions for each inflow turbulence generator method. This file included the below information such as velocity profile, length scales, and Reynolds stresses.

Table 7.C.1. Turbulent Characteristics for the TTU Building (Mooneghi et al., 2016; Aboshosha et al., 2015).

Test Characteristics	**WT 1:6 Model**
Reference height	$H = 0.66\,m$
Reference wind velocity	$U_H = 19.48\,m/s$
Mean velocity	$\boldsymbol{U_{ave} = U_H \left(\frac{z}{H}\right)^{\alpha} m/s, \alpha = 0.326}$
Turbulent lengh scale *L*	$L_j = L_{1j} \left(\frac{z}{H}\right)^{dj} m$ $L_{11} = 0.43, L_{12} = 0.2\ and\ L_{13} = 0.13\,m$ $dj = 0.473, 0.881, 1.539$ in the u, v and w directions $L_{21} = 0.2L_{11} = L_{22} = L_{23}, \qquad L_{31} = 0.3L_{11} = L_{32} = L_{33}$
Reynolds stresses	R_{11}=4.3, R_{22}=3.6, R_{33}=3.5, R_{12}=1.8, R_{23}=1.8, R_{13}=1.8

$$R_{ij} = R_{ij}\left(\frac{z}{H}\right)^{dj}$$

$dj = 1.034, 0.898, 0.662$ in the u, v and w directions

```
// mean velocity
UDict
{  referenceValue        19.48;
   profile              exponential;
   referenceAngl         0;
   referenceDist        0.66;
   alpha                0.326;}
// Reynolds stress
RDict
{  referenceValue        (4.3  1.8  1.8  3.6  1.8  3.5);
   profile              exponential;
   referenceAngl         0;
   referenceDist        0.66;
   alpha                (1.034  0.898  0.662);}
// integral length scale
LDict
{ referenceValue        0.43
   profile              exponential;
   referenceAngl         0;
```

referenceDist 0.66;

alpha 0.473 }

Case files are provided for readers and engineers on the Github-webpage, https://github.com/MansouriZ/InflowMethods.git.

7.D. OpenFoam Case File - “0” folder

Under the “0” folder there should be located different files such as “U”, “P”, “nut” to define boundary and initial condition.

7.D.1. “U” file

In U file, after header, front dimension, the SI unites should be defined as [0 1 -1 0 0 0 0] which means for examples:

Kg to power 0

meter to power 1

second to power -1

After that we need to initialize all domain as a vector and not scaler, because velocity is as a vector.

(19.48 0 0)

-Then we have boundary fields:

Ground and Building boundary condition is defined as noSlip boundary condition.

Sides and Top boundary condition is defined as symmetry boundary condition.

Outlet boundary condition is defined as pressure outlet velocity with uniform value (0 0 0)

Inlet boundary condition is defined differently for each inflow generator method as below:

7.D.1.1. DFM Method Inlet Boundary Condition

```
Inlet
  {
    type            turbulentDFMInlet;
    filterType      exponential;
```

```
    filterFactor       4;
    gridFactor         1;
    perodicInY         false;
    perodicInZ         false;
    cleanRestart       false;
    calculateU         true;
    calculateL         true;
    calculateR         true;
    value    uniform (19.48 0 0);
  }
```

7.D.1.2. SEM-G Method Inlet Boundary Condition

```
  Inlet
  {
    type              turbulentSEMInlet;
    eddyType        gaussian;
    density           1;
    perodicInY         false;
    perodicInZ         false;
    cleanRestart       false;
    calculateU         true;
    calculateL         true;
    calculateR         true;
    value    uniform (19.48 0 0);
```

```
}
```

7.D.1.3. SEM-S Method Inlet Boundary Condition

```
Inlet
{
    type            turbulentSEMInlet;
    eddyType        step;
    density         1;
    perodicInY      false;
    perodicInZ      false;
    cleanRestart    false;
    calculateU      true;
    calculateL      true;
    calculateR      true;
    value    uniform (19.48 0 0);
}
```

7.D.1.4. SEM-T Method Inlet Boundary Condition

```
Inlet
{
    type            turbulentSEMInlet;
    eddyType        tent;
    density         1;
    perodicInY      false;
    perodicInZ      false;
```

```
    cleanRestart       false;
    calculateU         true;
    calculateL         true;
    calculateR         true;
    value    uniform (19.48 0 0);
  }
```

7.D.1.5. DFSEM Method Inlet Boundary Condition

```
  Inlet
  {
    type              turbulentDFSEMInlet;
    delta             3.3;
    density           1;
    perodicInY        false;
    perodicInZ        false;
    cleanRestart      false;
    calculateU        true;
    calculateL        true;
    calculateR        true;
    value    uniform (19.48 0 0);
  }
```

7.D.1.6. ATSML Method Inlet Boundary Condition

```
  Inlet
  {
```

```
    type              turbulentATSMInlet;
    vortonType        typeL;
    density           1;
       delta               3.3;
    perodicInY        false;
    perodicInZ        false;
    cleanRestart      false;
    calculateU        true;
    calculateL        true;
    calculateR        true;
    value    uniform (19.48 0 0);
  }
```

7.D.1.7. ATSMR Method Inlet Boundary Condition

```
Inlet
  {
    type              turbulentATSMInlet;
    vortonType        typeR;
    density           1;
       delta               3.3;
    perodicInY        false;
    perodicInZ        false;
    cleanRestart      false;
    calculateU        true;
```

```
        calculateL        true;
        calculateR        true;
        value    uniform (19.48 0 0);
    }
```

7.D.1.8. Example of "U" file, which is for ASTML inflow method:

```
/*--------------------------------*- C++ -*----------------------------------*\
  =========                 |
  \\      /  F ield         | OpenFOAM: The Open Source CFD Toolbox
   \\    /   O peration     | Website:  https://openfoam.org
    \\  /    A nd           | Version:  7
     \\/     M anipulation  |
\*---------------------------------------------------------------------------*/
FoamFile
{
    version     2.0;
    format      ascii;
    class       volVectorField;
    location    "1";
    object      U;
}
// * * * * * * * * * * * * * * * * * * * * * * * * * * * * * * * * * * * * * //

dimensions      [0 1 -1 0 0 0 0];
```

```
internalField   uniform (19.48 0 0);

boundaryField
{
    Ground
    {
     type    noSlip;
    }

    Inlet
    {
        type              turbulentATSMInlet;
        vortonType        typeL;
        density           1;
           delta                3.3;
        perodicInY        false;
        perodicInZ        false;
        cleanRestart      false;
        calculateU        true;
        calculateL        true;
        calculateR        true;
        value    uniform (19.48 0 0);
```

```
    }
    Outlet
    {
        type    pressureInletOutletVelocity;
        value    uniform (0 0 0);
    }
    Sides
    {
        type    symmetry;
    }
}
// ************************************************************************* //
```

7.D.2. “P” file

In p file, it should be noted that the pressure is not the actual pressure, it is divided by density.

In “p” file, after header, front dimension, the SI unites should be defined as [0 2 -2 0 0 0 0] which means for examples:

Kg to power 0

meter to power 2

second to power -2

After that we need to initialize all domain as Zero.

-Then we have boundary fields:

Ground, Building, and Inlet boundary condition is defined as zeroGradient boundary condition.

Sides and Top boundary condition is defined as symmetry boundary condition.

Outlet boundary condition is defined as fixed uniform value 0.

7.D.2.1. The example of "p" file is provided as follows"

```
/*--------------------------------*- C++ -*----------------------------------*\
  =========                 |
  \\      /  F ield         | OpenFOAM: The Open Source CFD Toolbox
   \\    /   O peration     | Website:  https://openfoam.org
    \\  /    A nd           | Version:  7
     \\/     M anipulation  |
\*---------------------------------------------------------------------------*/
FoamFile
{
    version     2.0;
    format      ascii;
    class       volScalarField;
    location    "1";
    object      p;
}
// * * * * * * * * * * * * * * * * * * * * * * * * * * * * * * * * * * * * * //
dimensions      [0 2 -2 0 0 0 0];
internalField   uniform 0;
boundaryField
{
```

```
    Inlet
    {
        type            zeroGradient;
    }
    Outlet
    {
        type            fixedValue;
        value           uniform 0;
    }
    Sides
    {
        type            symmetry;
    }
    Ground
    {
        type            zeroGradient;
    }
}
// ************************************************************************* //
```

7.D.3. “nut” file:

In “p” file, after header, front dimension, the SI unites should be defined as [0 2 -1 0 0 0 0] which means for examples:

Kg to power 0

meter to power 2

second to power -1

After that we need to initialize all domain as Zero.

-Then we have boundary fields:

Sides and Top boundary condition is defined as symmetry boundary condition.

Inlet and Outlet boundary condition is defined as calculated with the initial uniform value of 0.

Ground and Building boundary condition is defined as standard wall function boundary condition.

In OpenFOAM, different wall functions are provided. In the current study, the nutkWallFunction is implemented at walls. To apply wall function, in the nut file under '0' folder, the wall function should be specified for walls boundary condition as follows:

```
Wall
{
type            nutkWallFunction;
value           uniform 0;
}
```

7.D.3.1. The example of "nut" file is provided as follows"

```
/*--------------------------------*- C++ -*----------------------------------*\
  =========                 |
  \\      /  F ield         | OpenFOAM: The Open Source CFD Toolbox
   \\    /   O peration     | Website:  https://openfoam.org
    \\  /    A nd           | Version:  7
     \\/     M anipulation  |
```

```
\*---------------------------------------------------------------------------*/
FoamFile
{
    version     2.0;
    format      ascii;
    class       volScalarField;
    location    "1";
    object      nut;
}
// * * * * * * * * * * * * * * * * * * * * * * * * * * * * * * * * * * * * * * * * * * * * //
dimensions      [0 2 -1 0 0 0 0];
internalField   uniform 0;
boundaryField
{
    Inlet
    {
        type            calculated;
        value           uniform 0;
    }
    Outlet
    {
        type            calculated;
        value           uniform 0;
```

```
    }
    Sides
    {
        type            symmetry;
    }
    Ground
    {
        type nutkWallFunction;
        value           uniform 0;
    }
}
// ************************************************************************* //
```

7.E. OpenFoam Case File- “constant” folder

In constant folder we have, “polyMesh” folder, “transportProperties”, “turbulenceProperties”, and “inflowProperties”.

7.E.1. “transportProperties” file

In “transportProperties” we input the amount for nu= kinematic viscosity=1.5e-05. After header, front dimension, the SI unites and amount of nu should be defined as [0 2 -1 0 0 0 0] 1.5e-05 which means for examples:

Kg to power 0

meter to power 2

second to power -1

nu= kinematic viscosity=1.5e-05

7.E.1.1. The example of “transportProperties” file is provided as follows”

```
/*--------------------------------*- C++ -*----------------------------------*\
  =========                 |
  \\      /  F ield         | OpenFOAM: The Open Source CFD Toolbox
   \\    /   O peration     | Website:  https://openfoam.org
    \\  /    A nd           | Version:  7
     \\/     M anipulation  |
\*---------------------------------------------------------------------------*/
FoamFile
{
    version     2.0;
```

```
    format      ascii;
    class       dictionary;
    object      transportProperties;
}
// * * * * * * * * * * * * * * * * * * * * * * * * * * * * * * * * * * * * * * * * * * * * //
transportModel  Newtonian;
nu              [0 2 -1 0 0 0 0] 1.5e-05;
// ************************************************************************* //
```

7.E.2. turbulenceProperties

In "turbulenceProperties" we input the information related to turbulence modeling method. In this study, large eddy simulation (LES) with Wall Adapting Local Eddy-viscosity (WALE) sub grid scale model is used.

In this model, the below constants are considered:

$C_e = 1.048$

$C_k = 0.094$

$C_w = 0.325$

7.E.2.1. The example of "turbulenceProperties" file is provided as follows"

```
/*---------------------------------*- C++ -*----------------------------------*\
  =========                 |
  \\      /  F ield         | OpenFOAM: The Open Source CFD Toolbox
```

```
  \\    /   O peration     | Website:  https://openfoam.org
   \\  /    A nd           | Version:  7
    \\/     M anipulation  |
\*---------------------------------------------------------------------------*/
FoamFile
  {version     2.0;
   format      ascii;
   class       dictionary;
   location    "constant";
   object      turbulenceProperties;}
// * * * * * * * * * * * * * * * * * * * * * * * * * * * * * * * * * * * * * * * * //
simulationType LES;
LES
{
   LESModel        WALE;
   turbulence      on;
   printCoeffs     on;
   delta           vanDriest;
   cubeRootVolCoeffs
   {
      deltaCoeff      1;
   }
   PrandtlCoeffs
```

```
{
    delta           cubeRootVol;
    cubeRootVolCoeffs
    {
        deltaCoeff      1;
    }
    smoothCoeffs
    {
        delta           cubeRootVol;
        cubeRootVolCoeffs
        {
            deltaCoeff      1;
        }
        maxDeltaRatio   1.1;
    }
    Cdelta          0.158;
}
vanDriestCoeffs
{
    delta           cubeRootVol;
    cubeRootVolCoeffs
    {
        deltaCoeff      1;
```

```
        }
        smoothCoeffs
        {
            delta          cubeRootVol;
            cubeRootVolCoeffs
            {
                deltaCoeff      1;
            }
            maxDeltaRatio   1.1;
        }
        Aplus          26;
        Cdelta         0.158;
    }
    smoothCoeffs
    {
        delta          cubeRootVol;
        cubeRootVolCoeffs
        {
            deltaCoeff      1;
        }
        maxDeltaRatio   1.1;
    }
}// ************************************************************************* //
```

7.E.3. inflowProperties

In “inflowProperties” we input the initial conditions for each inflow turbulence generator method. This file included the below information such as velocity profile, length scales, and Reynolds stresses based on Table 7.C.1.

7.E.3.1. The example of “inflowProperties inflowProperties”

```
/*--------------------------------*- C++ -*----------------------------------*\
  =========                 |
  \      /  F ield         | OpenFOAM: The Open Source CFD Toolbox
   \    /   O peration     | Website:  https://openfoam.org
    \  /    A nd           | Version:  6
     \/     M anipulation  |
\*---------------------------------------------------------------------------*/
FoamFile
{
    version     2.0;
    format      ascii;
    class       dictionary;
    location    "constant";
    object      inflowProperties;
}
// * * * * * * * * * * * * * * * * * * * * * * * * * * * * * * * * * * * * * //
Naxis       ( 0 0 0 );
offset      ( 0 0 0 );
```

```
// mean velocity
UDict
{
    referenceValue        19.48;
    profile               exponential;
    referenceAngl         0;
    referenceDist         0.66;
    alpha                 0.326;
}
// Reynolds stress
RDict
{
    referenceValue        (4.3  1.8  1.8  3.6  1.8  3.5);
    profile               exponential;
    referenceAngl         0;
    referenceDist         0.66;
    alpha                 (1.034  0.898  0.662);
}
// integral length scale
LDict
{
    referenceValue        (0.43  0.13  0.2);
    profile               exponential;
```

```
    referenceAngl          0;
    referenceDist          0.66;
    alpha                  (0.473  0.473  0.473);
}
// ************************************************************************
```

7.F. CDRFG Code and Initial Parameters:

For the CDRFG MATLAB code, first it is needed to create a csv file named “inlet_co.csv” with two columns which has coordinate of inlet cross section in Y and Z direction as below.

Table 7.F.1. Example of inlet cross section coordinate in Y and Z direction in “inlet_co.csv” file.

Subtract: inlet: Direction [0,1,0] (m)	Subtract: inlet: Direction [0,0,1] (m)
0.00	0.00
0.25	0.00
0.50	0.00
0.75	0.00
1.00	0.00
0.00	0.25
0.25	0.25
0.50	0.25
0.75	0.25
1.00	0.25

7.F.1. Input Parameters for CDRFG

The input parameters in CDRFG are listed as below:

% h0u Reference height for the mean velocity

% Uh Mean velocity at h0u

% alphau Power low exponent of the mean velocity

% h0I Reference height for the turbulent intensity

% Iuh Longitudinal turbulent intensity at h0I

% Ivh Transverse turbulent intensity at h0I

% Iwh Vertical turbulent intensity at h0I

% dIu Power low exponent of the longitudinal turbulent intensity

% dIv Power low exponent of the longitudinal turbulent intensity

% dIw Power low exponent of the longitudinal turbulent intensity

% h0L Reference height for the length scale

% Luh Longitudinal length scale at h0L

% Lvh Transverse length scale at h0L

% Lwh Vertical length scale at h0L

% dLu Power low exponent of the longitudinal length scale

% dLv Power low exponent of the longitudinal length scale

% dLw Power low exponent of the longitudinal length scale

% Cxyz Coherency decay constants in x, y and z directions [1x3] matrix

% DGamma Characteristic length used to maintain the coherency

% nf Number of random frequencies in one segment

% nm Number of frequency segments

% fmax   Maximum frequency

% dt   Time step

% n   Number of time steps

% M   Matrix of the inflow coordinates [x y z]

7.F.2. Output Parameters for CDRFG

The output of CDRFG is three files (i.e. inletdata_U, inletdata_V and inletdata_W) that have the generated velocity records compatible with Tfdm (inhouse code).

7.F.3. Example on using the CDRFG_2015 Function

Below you can see the example of CDRFG case file that are input parameter inserted based on the Table. 4.1. and section 7.F.1.

%%%%%%%%%%%%%%%%%%%%%%%%%%%%%%%%%%%%%%

CDRFG_2015 Inputs

h0u=3.96;alphau=0.3264;Uh=7.66;

h0I=3.96;

Iuh=0.216;Ivh=0.207;Iwh=0.12;

dIu=-0.1914;dIv=-0.1228;dIw=-0.0048;

h0L=3.96;

Luh=35;Lvh=10.5;Lwh=7;

dLu=0.473;dLv=0.8813;dLw=1.5390;

```
Cxyz=[10 10 10];DGamma=0.3;

nf=100;nm=50;fmax=20;

dt=0.001;nt=4000;

% M=[zeros(5000,1) zeros(5000,1) (0.0002:0.0002:1)']; % Sample coordinate matrix

M = csvread('inlet_co.csv',1,0);

M(:,3)=M(:,2);

M(:,2)=M(:,1);

M(:,1)=0;

tic

CDRFG_2015(h0u,alphau,Uh,h0I,Iuh,Ivh,Iwh,dIu,dIv,dIw,h0L,Luh,Lvh,Iwh,...

dLu,dLv,dLw,Cxyz,DGamma,nf,nm,fmax,dt,nt,M)

toc
```

CDRFG_2015 Function

```
function CDRFG_2015(h0u,alphau,Uh,h0I,Iuh,Ivh,Iwh,dIu,dIv,dIw,h0L,...

Luh,Lvh,Lwh,dLu,dLv,dLw,Cxyz,DGamma,nf,nm,fmax,dt,nt,M)

% Consistent Discrete Random Flow Generation Function By Aboshosha et al. (2015)

%%%%%%%%%%%%%%%%%%%%%%%%%%%%%%%%%%%%%%%%%%%%%%%%%%%%%%%%

X=M(:,1);Y=M(:,2); Z=M(:,3); % x and y coordinates vector at the inflow plane
```

```
nd=size(X,1);                    % overall no of points

fmin=0.2;                % Min Freqency

df=(fmax-fmin)/(nm-1);       % Frequency step

fm=fmin:df:fmax;                % Frequency vector

tt=dt*(0:(nt-1));                % time vector

%% Prepare the output file accrding to the format required by STAR CCM+

%%%%%%%%%%%%%%%%%%%%%%%%%%%%%%%%%%%%%%%%%%%%%%%%%%%%

fid2 = fopen('inletdata_U.txt', 'w');

fid3 = fopen('inletdata_V.txt', 'w');

fid4 = fopen('inletdata_W.txt', 'w');

fid5 = fopen('Variables.csv', 'w');

fid6 = fopen('Wavenumbers.plt','w');

%csv='X,Y,Z,';

%fprintf(fid2,csv); fprintf(fid2,'ux(m/s)[t=%es],',tt);

%fprintf(fid3,csv); fprintf(fid3,'vx(m/s)[t=%es],',tt);

%fprintf(fid4,csv); fprintf(fid4,'wx(m/s)[t=%es],',tt);

fprintf(fid5,'Wn,Kx,Ky,Kz,Px,Py,Pz,Qx,Qy,Qz');

%% Calculate the average velocity, turbulent Intensity, and length scale profiles
```

```
%%%%%%%%%%%%%%%%%%%%%%%%%%%%%%%%%%%%%%%%%%%%%%%%%%%%%%%%%%%%%%%%%%%%%%%%%%%%%%%%%%%%%%%

Uav=Uh*(Z/h0u).^alphau; Iu=Iuh*(Z/h0I).^dIu;  Iv=Ivh*(Z/h0I).^dIv;

Iw=Iwh*(Z/h0I).^dIw;     Lu=Luh*(Z/h0L).^dLu; Lv=Lvh*(Z/h0L).^dLv;

Lw=Lwh*(Z/h0L).^dLw;

%% Generate Wn (nf x nm) matrix, wn has 2.pi.fm mean and rms=2.pi.df

%%%%%%%%%%%%%%%%%%%%%%%%%%%%%%%%%%%%%%%%%%%%%%%%%%%%%%%%%%%%%%%%%%%%%

wn=randn(nf,nm)*2*pi*df;

for nmi=1:nm

wn(:,nmi)=wn(:,nmi)-mean(wn(:,nmi));

wn(:,nmi)=wn(:,nmi)/std(wn(:,nmi))*2*pi*df;

wn(:,nmi)=wn(:,nmi)+fm(nmi)*2*pi;

end

 %% Calcualte the spectrum matrices

%%%%%%%%%%%%%%%%%%%%%%%%%%%%%%%%%%%%%%%

Su=zeros(nm,nd);Sv=zeros(nm,nd);Sw=zeros(nm,nd);         fms=(-
0.5:0.05:0.5)*df;nfsm=size(fms,2)/2+0.5;nfs=size(fms,2);

for i=1:nd

    for j=1:nm

         fmjs=fm(j)+fms;if j==1;fmjs=fm(j)+fms(nfsm:nfs);end
```

```
        Su(j,i) =mean(4*(Iu(i)*Uav(i))^2*(Lu(i)/Uav(i))./ ...
                    (1+70.8*(fmjs*Lu(i)/Uav(i)).^2).^(5/6));
        Sv(j,i) =mean(4*(Iv(i)*Uav(i))^2*(Lv(i)/Uav(i))*(1+188.4*...
                   (2*fmjs*Lv(i)/Uav(i)).^2)./(1+70.8*(2*fmjs*Lv(i) ...
                   /Uav(i)).^2).^(11/6));
        Sw(j,i) =mean(4*(Iw(i)*Uav(i))^2*(Lw(i)/Uav(i))*(1+188.4*(2*fmjs* ...
                     Lw(i)/Uav(i)).^2)./(1+70.8*(2*fmjs*Lw(i)/Uav(i)).^2).^(11/6));
    end
end
UavLs=mean(Uav); % mean longitudinal velocity which is used to identify the turbulent L Scale
 %% Generate of Matrices P,Q,K
%%%%%%%%%%%%%%%%%
K=zeros(nf,3,nm);
r=randn(nf,3,nm);
P=r./abs(r).*sqrt(1/nf*(r).^2./(1+r.^2));
Q=r./abs(r).*sqrt(1/nf*(1).^2./(1+r.^2));
Ls=zeros(nm,3,nd);
for nmi=1:nm
```

```
    for nyi=1:nd;
        Beta=10*DGamma/Lu(nyi);if Beta>6;Gammai=2.1;
        else Gammai=3.7*Beta^-.3;end
        Ls(nmi,:,nyi)=Uav(nyi)/fm(nmi)./Cxyz/Gammai;
    end
    K(:,:,nmi)=RandSampleSphere(nf);
    for i=1:nf
        XX=K(i,:,nmi)';
        myfun=@(xx) mapp(xx,P(i,:,nmi),Q(i,:,nmi));
        K(i,:,nmi) = (fsolve(myfun,XX))';
    end
end
%% Generate the Velocity Vectors
%%%%%%%%%%%%%%%%%%%%%%%%%%%%%%%%%%%%%%
U=zeros(nd,nt);V=zeros(nd,nt);W=zeros(nd,nt);
parfor_progress(nd); % Initialize
parfor inxyi=1:nd
        for nmi=1:nm;
```

```
        xjbar=1./Ls(nmi,:,inxyi).*[X(inxyi) Y(inxyi) Z(inxyi)];
        kjxj=(xjbar(1)*K(:,1,nmi)+xjbar(2)*K(:,2,nmi)+xjbar(3)*K(:,3,nmi));
        U(inxyi,:)=U(inxyi,:)+sum(sqrt(Su(nmi,inxyi)*df*2)*(P(:,1,nmi)* ...
          ones(1,nt)).*cos(wn(:,nmi)*tt+kjxj*ones(1,nt))+sqrt(Su(nmi,inxyi)*df*2) ...
          *(Q(:,1,nmi)*ones(1,nt)).*sin(wn(:,nmi)*tt+kjxj*ones(1,nt)));
        V(inxyi,:)=V(inxyi,:)+sum(sqrt(Sv(nmi,inxyi)*df*2)*(P(:,2,nmi)* ...
          ones(1,nt)).*cos(wn(:,nmi)*tt+kjxj*ones(1,nt))+sqrt(Sv(nmi,inxyi)* ...
          df*2)*(Q(:,2,nmi)*ones(1,nt)).*sin(wn(:,nmi)*tt+kjxj*ones(1,nt)));
        W(inxyi,:)=W(inxyi,:)+sum(sqrt(Sw(nmi,inxyi)*df*2)*(P(:,3,nmi)* ...
          ones(1,nt)).*cos(wn(:,nmi)*tt+kjxj*ones(1,nt))+sqrt(Sw(nmi,inxyi)*df*2) ...
          *(Q(:,3,nmi)*ones(1,nt)).*sin(wn(:,nmi)*tt+kjxj*ones(1,nt)));
    end
    U(inxyi,:)=U(inxyi,:)+Uav(inxyi); % Add the mean velocity
  parfor_progress; % Count
end
parfor_progress(0); % Clean up
%% Print the velocity vectors
%%%%%%%%%%%%%%
```

```
Tu=[U]; Tv=[V]; Tw=[W];

TableU=Tu'; TableV=Tv'; TableW=Tw'; jm=226;

TableU(:,1:jm)=0;

TableV(:,1:jm)=0;

TableW(:,1:jm)=0;

TableWn=reshape(wn,[],1);

KR1=K(:,1,:);

TableK1=reshape(KR1,[],1);

KR2=K(:,2,:);

TableK2=reshape(KR2,[],1);

KR3=K(:,3,:);

TableK3=reshape(KR3,[],1);

PR1=P(:,1,:);

TableP1=reshape(PR1,[],1);

PR2=P(:,2,:);

TableP2=reshape(PR2,[],1);

PR3=P(:,3,:);

TableP3=reshape(PR3,[],1);
```

```
QR1=Q(:,1,:);

TableQ1=reshape(QR1,[],1);

QR2=Q(:,2,:);

TableQ2=reshape(QR2,[],1);

QR3=Q(:,3,:);

TableQ3=reshape(QR3,[],1);

TableVar=[TableWn,TableK1,TableK2,TableK3,TableP1,TableP2,TableP3,TableQ1,TableQ2,T
ableQ3];

TableA=[abs(TableWn./(2*pi)),abs(2.74.*TableWn.*TableK1./(2*pi)),abs(2.74.*TableWn.*Tabl
eK2./(2*pi)),abs(2.74.*TableWn.*TableK3./(2*pi))];

for i=1:size(TableU,1)

   j=1:size(TableU,2);    fprintf(fid2,'%12.6f ',TableU(i,j)); fprintf(fid2,'\r\n');

end

for i=1:size(TableV,1)

   j=1:size(TableV,2);    fprintf(fid3,'%12.6f ',TableV(i,j)); fprintf(fid3,'\r\n');

end

for i=1:size(TableW,1)

   j=1:size(TableW,2);    fprintf(fid4,'%12.6f ',TableW(i,j)); fprintf(fid4,'\r\n');

end
```

```
for i=1:size(TableVar,1)

   fprintf(fid5,'\r\n');    j=1:size(TableVar,2);    fprintf(fid5,'%e,',TableVar(i,j));

end

fprintf(fid6,' VARIABLES = "f","kx","ky","kz"');

fprintf(fid6,'\r\n');

for i=1:size(TableA,1)

 j=1:size(TableA,2);  fprintf(fid6,'%e  ',TableA(i,j)); fprintf(fid6,'\r\n');

end

fclose(fid2);fclose(fid3);fclose(fid4);fclose(fid5);fclose(fid6);

end
```